

SO(5) multicriticality in two-dimensional quantum magnets

Jun Takahashi^{†,1} Hui Shao^{†,2} Bowen Zhao,³ Wenan Guo,⁴ and Anders W. Sandvik^{3,5,*}

¹*Center for Quantum Information and Control, University of New Mexico, Albuquerque, NM 87131, USA*

²*Center for Advanced Quantum Studies, Department of Physics,
Beijing Normal University, Beijing 100875, China*

³*Department of Physics, Boston University, 590 Commonwealth Avenue, Boston, Massachusetts 02215*

⁴*Department of Physics, Beijing Normal University, Beijing 100875, China*

⁵*Beijing National Laboratory for Condensed Matter Physics,
Institute of Physics, Chinese Academy of Sciences, Beijing 100190, China*

(Dated: May 13, 2024)

We resolve the long-standing problem of the nature of the quantum phase transition between a Néel antiferromagnet and a spontaneously dimerized valence-bond solid in two-dimensional spin-1/2 magnets. We study a class of J - Q models, in which the standard Heisenberg exchange J competes with multi-spin interactions Q_n formed by products of n singlet projectors on adjacent parallel links of the lattice. Using large-scale quantum Monte Carlo (QMC) calculations, we provide unambiguous evidence for first-order transitions in these models, with the strength of the discontinuities increasing with n . In the case of the widely studied $n = 2$ and $n = 3$ models, the first-order signatures are very weak, but observable in correlation functions on large lattices. On intermediate length scales (up to hundreds of lattice constants, depending on the observable) we can extract well-defined scaling dimensions (critical exponents) that are common to the models with small n , indicating close proximity to a universal quantum critical point. By combining two different Q terms, specifically we consider the J - Q_2 - Q_6 model, the transition can be continuously tuned from weak to more strongly first-order. In the plane (Q_2, Q_6) , with $J = 1 - Q_2$, the two coexisting order parameters on the first-order line scale with an unusually large exponent $\beta \approx 0.85$. This exponent and others coincide closely with known rigorous bounds for an SO(5) symmetric conformal field theory (CFT), but, in contrast to prevailing scenarios, the leading SO(5) singlet operator is relevant and responsible for the first-order transition ending at a fine-tuned multicritical point. We quantitatively characterize the emergent SO(5) symmetry by computing the scaling dimensions of its leading irrelevant perturbations. The large β value and a large correlation length exponent, $\nu \approx 1.4$, partially explain why the transition remains near-critical on the first-order line even quite far away from the critical point and in many different models without fine-tuning. In addition, we find that few-spin lattice operators are dominated by their content of the SO(5) violating field (the traceless symmetric tensor), and interactions involving many spins are required to observe strong effects of the relevant SO(5) singlet that brings the system into the coexistence line. Beyond the scaling dimensions that can be directly explained by the CFT, the exponent that had previously been identified with the divergent correlation length when crossing between the two phases does not have a corresponding level in the CFT spectrum. We explain this emergent “pseudocritical” length scale by a mechanism relying on a dangerously irrelevant SO(5) perturbation in combination with repulsive interactions between the two order parameters. This length scale is reflected in crossover behaviors of observables when traversing the weak first-order line. We argue that the multicritical point is also most likely the top of a gapless spin liquid phase recently discovered in frustrated Heisenberg models, into which the J - Q models can be continuously deformed. Our results are at variance with the conventional scenario of generic deconfined quantum critical points, including the complex CFT proposal. The multicritical point should exist within real Hamiltonians, though perhaps only outside the regime amenable to sign-free QMC simulations.

CONTENTS

I. Introduction	2	III. Overview of findings	12
II. The DQCP enigma	6	A. Quantum Monte Carlo methods	12
A. AFM–VBS transition and putative DQCP	7	B. Results and insights	13
B. Simulations of lattice models	8	IV. Order parameters	15
C. Conformal bootstrap method and the		A. Correlation functions and exponents	15
complex CFT scenario	10	B. Phase coexistence in J - Q_n models	16
D. Multicriticality scenario	11	C. Scaling dimension of the order parameters	18
		1. Correlation functions and derivatives	19
		2. Scaling corrections from descendants	21
		V. Relevant perturbations	24
		A. Fully symmetric operator	26
		B. Conserved current operator	27

* Corresponding author. E-mail: sandvik@bu.edu

C. Pseudo scaling dimension	28
VI. Scaling on the AFM-VBS coexistence line	30
VII. Emergent symmetries	35
A. \mathbb{Z}_4 perturbation and U(1) crossover	35
1. Scaling dimension Δ_4	36
2. Emergent U(1) scale in the VBS phase	37
B. Irrelevant SO(5) perturbations	38
C. SO(5) finite-size window	40
VIII. Pseudocritical scaling	43
A. Emergent length scale	43
B. Scaling crossover	45
C. Tests of the correlation length	45
D. Crossover scaling of the transition point	47
IX. Anomalous finite-size scaling	48
A. Extended finite-size scaling hypothesis	49
B. Spin stiffness	50
X. Discussion	51
Acknowledgments	52
References	52

I. INTRODUCTION

Quantum phase transitions out of the two-dimensional (2D) Néel antiferromagnetic (AFM) state have been of central interest in condensed matter physics since the early days of high- T_c superconductivity in the cuprates [1–5], and soon thereafter also in the context of frustrated quantum magnetism [6]. Two classes of non-magnetic states have been of particular interest; quantum spin liquids (QSLs) [7–9], which have no conventional long-range order (but should have topological order), and crystalline valence-bond-solid (VBS) states [3, 10–12] in which lattice symmetries are spontaneously broken by the formation of some pattern of modulated singlet density on the lattice links. Theories of quantum magnets often place AFM, QSL, and VBS ground states within the same phase diagram [13–22], but it has proven difficult to understand precisely how these states of matter relate to each other in specific quantum spin models and materials, and what the nature is of the quantum phase transitions between the phases.

In particular, theories involving the hypothesized deconfined quantum critical point (DQCP) [23–26] as a “beyond Landau” scenario for the generic AFM–VBS transition have remained unsettled and controversial. Monte Carlo studies of 2D quantum spin Hamiltonians [27] and related 3D classical systems [28, 29] have identified some tantalizing signatures of the DQCP, e.g., emergent symmetries [27, 29–35], exponents for $SU(N)$ symmetric models agreeing with field theory calculations for large N [37–40], and apparent manifestations of deconfined

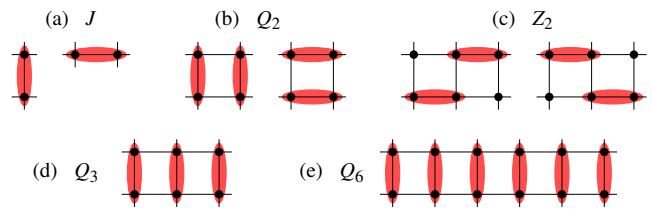


FIG. 1. Interactions between $S = 1/2$ spins on the square lattice. Red ellipses indicate singlet projectors ($\mathbf{S}_i \cdot \mathbf{S}_j - 1/4$), and two or more ellipses in the same lattice cell correspond to products. The original J - Q (here referred to as J - Q_2) model [27] combines the conventional AFM Heisenberg exchange in (a) at strength J with the four-spin interaction in (b) at strength Q_2 . Other arrangement of the projectors can also be considered, such as the Z_2 operator in (c). Interactions Q_n have n projectors forming columns, e.g., $n = 3$ in (d), while Z_n has n projectors in a staircase formation. The largest interaction considered here is the twelve-spin case in (e). In (c)-(e), the 90° rotated interaction patterns are also included in the summation over the full lattice, so that all square-lattice symmetries are preserved. In addition to the J - Q_n models, we also consider Hamiltonians with three different couplings; J - Q_2 - Z_2 , J - Q_2 - Z_3 , and J - Q_2 - Q_6 .

spinon excitations [41, 42]. Other observed features appear to be at odds with a true DQCP, e.g., scaling violations that have been interpreted either as a weak first-order transition [33, 43–45] or anomalies not originally anticipated at the DQCP [28, 41, 46]. These counter-indicators may require only minor modifications of the original theory, e.g., the non-unitary conformal field theory (CFT) scenario, which has dominated the theoretical discourse during the past several years [47–52]. Alternatively, a more drastic overhaul of the theory of AFM–VBS transitions will be required, e.g., if a continuous transition is realized only as a fine-tuned multi-critical point [53–55]. A resolution of the problem is pressing, considering also that experimental platforms targeting DQCP physics are under active development [56–58].

Here we will present unambiguous evidence for a line of first-order AFM–VBS transitions ending at a multi-critical point with emergent SO(5) symmetry. We apply quantum Monte Carlo (QMC) methods to study ground states of a class of spin-1/2 J - Q models (those introduced in Refs. [27, 34] as well as generalizations not studied previously), in which multi-spin interactions favoring locally correlated singlets on the 2D square lattice are added to the conventional Heisenberg two-spin exchange J . The models are illustrated and further explained in Fig. 1.

The J - Q models and their generalizations permit QMC studies of the transition between the AFM state and a spontaneously dimerized columnar VBS state in great detail without approximations other than well controlled small statistical errors and finite lattice size. In some cases we here take the linear size as large as $L = 1024$, which is unprecedented in ground state simulations. We consider several different Q terms, with multi-spin interactions Q_n consisting of n singlet projectors on adjacent

parallel lattice links, i.e., forming columns of length or height n , as illustrated for some cases in Fig. 1. Focusing on the AFM–VBS transition, we compare results for several of these J - Q_n models, anticipating strongly first-order transitions for large n [32]. For $n = 2$ and $n = 3$ we find first-order transitions with very small ordered moments of the coexistence state. There is a significant range of length scales on which the systems exhibit robust quantum critical scaling, which we study using a wide range of correlation functions and observables probing emergent symmetries.

We also investigate a model combining two different Q terms, in order to realize an entire line of AFM–VBS transitions in a phase diagram with two axes. Specifically, we use a J - Q_2 - Q_6 model to access a line of AFM–VBS transitions in the plane of Q_2 and Q_6 (with $Q_2 + J = 1$). Here we observe critical scaling of the growth of the coexisting order parameters upon moving further into the first-order line. We also study the first-order line with the J - Q_2 - Z_2 and J - Q_2 - Z_3 model, where the Z_2 interaction, illustrated in Fig. 1(c), has a staircase arrangement of two singlet projectors and Z_3 is an extension to three projectors. Comparisons of the different models provide information on the relevant (continuum field) operator content of the lattice interactions.

Our multi-faceted analysis the AFM–VBS transition in the J - Q models and new theoretical insights allow us to tie together many analytical and numerical results that previously appeared to be in conflict with each other. The perceived discrepancies are largely consequences of intricate scaling behaviors for a system not located exactly at the critical point but hosting a near-critical ground state with coexisting weak AFM and VBS orders. We completely resolve the nature of the phase transition, demonstrating a line of first-order transitions terminating at an SO(5) multicritical point. We determine several scaling dimensions of this critical point, including relevant ones (i.e., those related to the conventional critical exponents) as well as some irrelevant ones; specifically, those characterizing the leading perturbations of the SO(5) symmetry.

As shown in Table I, both relevant and irrelevant scaling dimensions agree reasonably well with recent results for a multicritical SO(5) conformal field theory (CFT) [55], obtained using a variant of the numerical bootstrap method [60]. Strictly speaking, the bootstrap results in this case reflect only bounds on the scaling dimensions, some of which had been obtained previously [61, 62]. In $O(N)$ models, the true scaling dimensions typically fall exactly on the boundary of the CFT allowed region of scaling dimensions, and in general it is believed that they must at least be close to the boundary. The small discrepancies between our values and those of Ref. 55 likely stem from the input value in the bootstrap calculation, the scaling dimension Δ_ϕ of the order parameters, that was not known precisely and to some extent impacts the output values of the other scaling dimensions. Our refined value of Δ_ϕ in Table I differs slightly from the previously

TABLE I. Scaling dimensions obtained here from the J - Q models compared with values reported for the SO(5) multicritical CFT [55] and exact diagonalization on the fuzzy sphere with 10 electronic orbitals (from Table II of Ref. [59]). The subscripts correspond to the order parameter (Δ_ϕ), the relevant SO(5) singlet operator (Δ_s), the traceless symmetric tensor (Δ_t), the conserved current operator (Δ_j), and the leading irrelevant SO(5) perturbation (Δ_4). Star superscripts indicate necessary or assumed values; $\Delta_\phi = 0.63$ was used as input in the CFT numerical bootstrap calculation [55] and the other exponents depend to some (yet unknown) extent on this value, while $\Delta_j = 2$ must hold in the CFT and was imposed for calibration of the level spectrum in the fuzzy sphere calculation [59]. Our convention for statistical errors here and henceforth is that the digit(s) within () correspond to the one standard deviation error of the preceding digit, i.e., 3.723(11) means 3.723 ± 0.011 .

	Δ_ϕ	Δ_s	Δ_t	Δ_j	Δ_4
This work	0.607(4)	2.273(4)	1.417(7)	2.01(3)	3.723(11)
SO(5) CFT	0.630*	2.359	1.519	2*	3.884
Fuzzy sphere	0.585	2.831	1.458	2*	3.895

best estimate and using it in the bootstrap calculation indeed improves the agreement with all the other values [63]. Our values of Δ_ϕ , Δ_t , and Δ_s , coincide at a level of uncertainty of only 1 – 2% with the CFT permissible boundaries (which are believed to be at or very close to the actual scaling dimensions [55?]) in the planes (Δ_ϕ, Δ_t) and (Δ_ϕ, Δ_s) computed previously [62].

Concrete evidence for a multi-critical point in the context of the DQCP was to our knowledge first proposed in Ref. 53 by three of us (though with, in hindsight, a misidentification of one of the scaling dimensions), and attempts to construct a corresponding field theory were made in Ref. [54]. The good agreement with the CFT calculations [55, 62], in particular showing the relevance of a singlet operator, firmly establishes the existence of the multicritical point. This scenario is not specific to the J - Q models studied here, but should be universal for quantum magnets with AFM–VBS transitions as well as other systems with analogous order parameters.

The CFT calculations did not address the nature of the phase diagram in any particular microscopic model. The phases and transitions generated when subjecting the SO(5) CFT to a specific relevant microscopic perturbation are not automatically known. The critical point was assumed to be of the tricritical variant [55], though the scaling dimensions alone cannot rule out a bicritical point. Three putative phase diagrams relevant to generic 2D quantum magnets are presented schematically in a space of two scaling fields in Fig. 2. Our J - Q results are in principle consistent with both the cases depicted in Fig. 2(a) and 2(b), where a first-order line terminates at the multicritical point; tricritical in (a) and bicritical in (b). In Fig. 2(a) there is a generic line of DQCP transitions below the multicritical point, which corresponds to the original DQCP scenario [23–25] with no relevant sin-

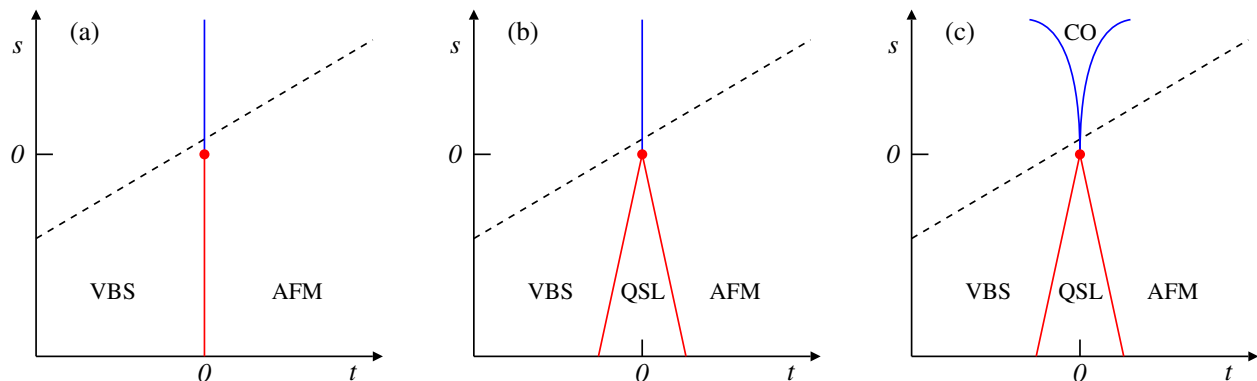


FIG. 2. Schematic phase diagrams containing transitions between VBS and AFM phases in a space of two scaling fields (s, t), corresponding to the relevant singlet and traceless symmetric tensor in the multicritical $SO(5)$ CFT [55]. The red circles indicate a multicritical point in all three phase diagram, classified as tricritical in (a), bicritical in (b), and tetracritical in (c). The blue vertical lines in (a) and (b) indicate first-order transitions ending at the multicritical point, below which there is a line of continuous DQCP transitions in (a) and a QSL phase intervening between the VBS and AFM phases in (b). The blue curves in (c) are the phase boundaries of an extended AFM–VBS coexistence phase ending at the tetracritical point, which is also the tip of a QSL phase as in (b). The slanted dashed lines show a possible path taken with the models studied here when a single parameter is tuned, e.g., the ratio J/Q_n in a $J-Q_n$ model. The field t changes the symmetry of the order parameter from \mathbb{Z}_4 in the VBS [with emergent $U(1)$ symmetry close to criticality] to $SO(3)$ in the AFM, while s does not violate the $SO(5)$ symmetry of the multicritical point. Case (a) corresponds to the conventional DQCP scenario, where a QSL phase (not shown) may also in principle connect to a lower end point of the generic continuous transition. Both (a) and (b) with multicritical points hosting emergent $SO(5)$ symmetry are consistent with our results, though when including other arguments (b) is more likely. We can positively exclude the coexistence phase in (c). The placement of the dashed lines is in accord with the $J-Q$ models in the regime without QMC sign problem, where only the first-order line can be crossed—though sufficiently close to the multicritical point so that its scaling dimensions can be reliably determined.

glet (and where the nature of a putative end point of the critical line was not addressed). In contrast, in Fig. 2(b), the multicritical point is also the tip of a gapless QSL phase.

Figure 2(c) depicts a tetracritical point scenario, which within a Landau-type theory would require effectively attractive interactions between the AFM and VBS order parameters [64]. Studying the way in which the $SO(5)$ symmetry is violated for large system sizes on the first-order line, we can conclude that the interactions actually must be repulsive, thus excluding an extended coexistence phase.

While we only directly study the first-order line, both in extreme proximity to the multicritical point and further away from it, several recent works [65–73] have pointed to a QSL phase intervening between AFM and VBS phases in frustrated quantum magnets. Many of these models can in principle be continuously deformed into the $J-Q$ models studied here by adding Q terms [70] (which has not yet been done). Given the first-order line that we examine in detail here, the most natural scenario when introducing additional frustrating (sign problematic) terms is indeed that a disordered QSL phase opens on the other side of the multicritical point, in analogy with the paramagnetic phase above the critical temperature in a classical $O(N)$ model. This analogy would be very close indeed with a model in which $O(3)$ and $O(2)$ transitions meet at a fine-tuned point with emergent $O(5)$ symmetry, except for the fact that emergent $O(N_1 + N_2)$

symmetry is possible in conventional classical spin models only for $N_1 = N_2 = 1$ [74, 75]. The QSL phase also should have non-trivial topological properties, unlike a conventional classical paramagnet.

Because of the remaining uncertainty on the nature of the phase diagram, Fig. 2(a) or 2(b) or some more exotic scenario, we will refer to the critical point as multicritical. However, we regard Fig. 2(b) as the most plausible, considering the existence of QSLs in frustrated models as well as an apparently disordered phase in the fuzzy sphere calculation with added $SO(5)$ violating terms [79].

As shown in Table I, the scaling dimensions that we determine within the $J-Q$ models also agree approximately with values extracted from the spectrum of an electronic $SO(5)$ model on a “fuzzy sphere” [59], though the results of the latter are likely not yet fully converged with respect to the number of orbitals. The interpretation of the fuzzy sphere results—in particular Δ_s flowing to more relevant values versus the number of orbitals—was that of a DQCP described by a non-unitary (complex) CFT [59], where the $SO(5)$ singlet of the underlying complex CFT is presumed irrelevant.

In our opinion, the non-unitary CFT scenario, in which the true DQCP only exists below (but presumably close to) 2+1 dimensions [47–51], is superfluous in light of the close agreement between the $SO(5)$ multicritical unitary CFT and our findings here (though the non-unitary scenario may in principle apply to other situations). Fig. 2(b) resembles the phase diagram of a different fuzzy

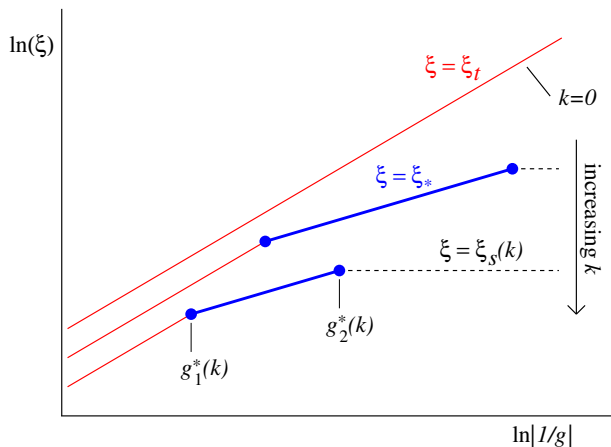


FIG. 3. Illustration of crossover from the conventional correlation length $\xi_t(g, k)$ (governed by the traceless symmetric tensor, with scaling dimension Δ_t in Table I) to a slower growing bubble size $\xi_*(g, k)$ when the weak first-order transition is approached in a model parameter space (g, k) . Here changing g at fixed k corresponds to moving on the dashed line in the space of relevant CFT operators (s, t) in Fig. 2(b), and increasing $k \geq 0$ corresponds to shifting the line higher in s . The critical point is at $g = k = 0$ (where also $s = t = 0$), where the correlation length $\xi = \xi_t$ applies all the way to $g = 0$. For $k > 0$, the crossover to the slower growing bubble length $\xi = \xi_*$ occurs at $g = g_1^*(k)$ and persists until $g = g_2^*(k)$, which is close to the first-order transition where ξ saturates in the coexistence state (in a way controlled by the relevant singlet with scaling dimension Δ_s in Table I). The crossover point $g_1^*(k)$ moves to the right as $k \rightarrow 0$, but the range of ξ_* (bubble sizes) still expands because of the strongly diverging $\xi_s(k \rightarrow 0)$. In reality the crossovers are smooth, without the sharp kinks drawn for simplicity here.

sphere calculation [79] including SO(5) breaking terms. Scaling dimensions were not determined precisely there, but a third phase was found to emerge from a point that, in light of Ref. 55 and our present work, should be the SO(5) multicritical point.

Our results not only establish beyond doubt a first-order line ending at a multicritical SO(5) point, but we also have obtained new insights into the nature of the weak first-order transition, including the key question of why many models seem to almost automatically harbor such transitions without fine-tuning. A major reason for the latter is that the exponent β governing the growth of the order parameters on the coexistence line is unusually large, $\beta \approx 0.85$, and the exponent controlling the correlation length is likewise large; $\nu_s \approx 1.4$ (both these exponents are related to the scaling dimensions in Table I in the standard way). Thus, the order parameters are small and the correlation length is large on the first-order line even quite far away from the critical point. A typical model will therefore have a transition inside the near-critical window, and its ordered coexistence state will emerge clearly only on large length scales. A different, but related, interpretation is that typical lattice

interactions are dominated by the CFT operator with scaling dimension Δ_t , since Δ_s is significantly larger. It is also likely that typical lattice operators overlap very weakly with the s field, thus necessitating the use of spatially extended Q_n operators with $q \geq 4$ (Fig. 1) to reach more strongly first-order transitions.

The impact of the weak first-order transition on various scaling behaviors is not merely a conventional crossover from nearly critical fluctuations to a coexistence state with long-range order, as would be expected in what are often called fluctuation driven first-order transitions. A new length scale appears that we interpret as the typical size of bubbles of the second phase inside one of the ordered phases, but, in contrast to a conventional fluctuation driven first-order transition near a critical point, the bubbles do not grow as rapidly as would be expected based on the value of the relevant scaling dimension of that critical point; here Δ_t of the traceless symmetric tensor (which is related to what is often called the crossover exponent in classical statistical physics [80]).

As illustrated in Fig. 3, on approaching the weak first-order transition from one of the ordered phases, the observed correlation length ξ is initially, relatively far from the transition, the conventional length ξ_t governed by the exponent $\nu_t = (3 - \Delta_t)^{-1}$, before crossing over to the slower growing bubble scale ξ_* governed the smaller emergent exponent ν_* . This type crossover of the correlation length was in fact observed, but not explained, in the 3D loop model by Nahum et al. [28], and was also in hindsight present in results for the J - Q model [41, 81]. Here we study the crossover in detail and explain it as an emergent pseudocritical phenomenon quantitatively related to the SO(5) CFT.

The crossover depends on the crossing distance s (i.e., when $t = 0$) to the critical point, which in a model is determined by a parameter that we denote by k in Fig. 3; the crossover takes place versus the tuning parameter g (with fixed k) at $g_1^*(k)$. The closer the system is to the critical point, the longer the conventional correlation length persists, i.e., $g_1^*(k) \rightarrow 0$ when $k \rightarrow 0$. When crossing the first-order line, the bubbles can grow only up to a size that is also dictated by the distance $s \sim k$ to the critical point (through the singlet dimension Δ_s). Thus, there is a second crossover to an essentially saturated bubble size at $g_2^*(k)$ and this size diverges when $k \rightarrow 0$. We will argue that the range of bubble sizes between $g_1^*(k)$ and $g_2^*(k)$ diverges when $k \rightarrow 0$. Thus, the pseudocritical length scale is a completely well defined critical property at the AFM-VBS transition, even though the exponent ν_* does not correspond to any operator in the CFT spectrum.

We will argue that the root cause of the emergence of a scale different from the conventional correlation length is effectively repulsive interactions between the AFM and VBS order parameters (which we demonstrate explicitly using QMC results) in combination with an irrelevant perturbation of the critical SO(5) symmetry (whose scaling dimension we have also computed) that becomes rel-

evant on the coexistence line and leads to the slower correlation length (bubble size) as the first-order transition is approached. We derive and numerically confirm a relationship between the exponent ν_* and the CFT scaling dimensions. The underlying mechanism differs from that of the conventional symmetry crossovers caused by “dangerously irrelevant” operators [82–87], though the scaling dimension Δ_4 (Table I) of such an operator (generated by the square lattice) does play an important role in fixing the value of ν_* .

The emergent length scale is most directly visible in the way the emergent SO(5) symmetry is violated in the neighborhood of the critical point, and we use finite-size scaling of a quantity characterizing the deviations from perfect SO(5) symmetry to extract a precise value of the exponent ν_* . This exponent can account very well for the growth of the correlation length after the crossover (to the right of g_1^* in Fig. 3), as well as scaling behaviors with crossovers of many other physical observables.

Though we are not aware of any previous discussion of the emergent pseudocritical length scale, our derivations are inspired by the case of attractive order-parameter interactions, which lead to an coexistence phase extending out from a tetracritical point, as in Fig. 2(c). If the tetracritical point has emergent O(N) symmetry, the boundaries of the coexistence phase are also in part governed by the scaling dimension of the leading irrelevant perturbation of the symmetry [64]. In analogy, at the AFM–VBS transition the associated repulsive order parameter interactions induce a region of influence that is very similar, in a scaling sense, to the coexistence phase. Results of Ref. 64 can therefore be adapted to the present case.

Our conclusions point to what appears, at first sight, a rather conventional Landau picture of the AFM–VBS transition. However, there are still exotic non-classical “beyond Landau” phenomena associated with it. As already mentioned, the emergent higher continuous symmetry is not possible classically at a point where O(N_1) and an O(N_2) transitions meet, since there are relevant perturbations to the O($N_1 + N_2$) critical point for $N_1 + N_2 > 2$ [74, 75]. The emergent SO(5) symmetry at the AFM–VBS transition must therefore be a consequence of the topological θ term, which when added to the nonlinear σ -model gives the level $k = 1$ Wess-Zumino-Witten (WZW) CFT [26, 35, 47, 76–78]. The emergent symmetry, in turn, is responsible for the emergent pseudo critical length scale when crossing the weak first-order transition.

While the topological term has been expected for some time to be at the heart of the DQCP phenomenon [26, 35, 47, 76–78], the relevant SO(5) singlet operator is not part of the original scenario. Recent work on the WZW model with the fuzzy sphere regularization also indicated the possibility of a relevant singlet operator at the AFM–VBS transition [79]. Its presence also is a natural route to generating the QSL phase on the other side of the transition in Fig. 2(b), thus connecting the QSL in frustrated models and the first-order line in bipartite

systems such as the J - Q model [70]. The QSL, if it exists, would of course also be beyond the Landau framework.

The rest of the paper is organized as follows: In Sec. II we provide a more detailed account of the background and current status of the 2D AFM–VBS transition and its persistent controversies. In Sec. III we summarize our main results and how they resolve the current enigmatic state of affairs. In the following two sections, after showing evidence for increasing first-order discontinuities with increasing n in the J - Q_n models in Sec. IV B, we present detailed results and analysis leading to some of the relevant scaling dimensions in Table I. Order parameter correlations governed by Δ_ϕ are analyzed in Sec. IV C, while other correlation functions giving estimates of Δ_t , and Δ_j are presented in Sec. V. We proceed in Sec. IV to study lines of first-order transitions in the J - Q_2 - Z_2 , J - Q_2 - Z_3 , and J - Q_2 - Q_6 models. Detailed studies of the latter model, in particular, show that the growth of the coexisting order parameters with increasing Q_6 is fully compatible with the exponents of the multicritical point (the scaling dimensions Δ_ϕ and Δ_s in Table I). We present results for emergent SO(5) symmetry in Sec. VII, going beyond previous works [32, 35] by extracting irrelevant scaling dimensions of two different perturbations of the symmetry as well as the exponent ν_* . The results here also demonstrate the eventual violation of the SO(5) symmetry on the first-order line when L becomes large. All these results provide us with the necessary components for deriving and further testing the relationship Eq. (1) between ν_* and CFT exponents in Sec. VIII, which allows us to obtain the most precise value of Δ_* . Here we also discuss the roles played by the regular correlation length and the emergent length scale when crossing the weak first-order transitions—with scaling results supporting the picture outlined in Fig. 3. In Sec. IX we present a broader view of how all three exponents ν_t , ν_s , and ν_* impact scaling of physical observables, with the spin stiffness as a specific example. In Sec. X we further discuss our main results and their broader impact in the context of the DQCP phenomenon and beyond.

II. THE DQCP ENIGMA

Our current understanding of the AFM–VBS transition in 2D quantum magnets, as reported in this paper, builds on decades of work by a large number of researchers using many different theoretical and computational techniques. While the proliferation of ideas and results have in some cases been difficult to reconcile, in the end it is the synergistic combination of different results and approaches that has allowed us to reach a solid conclusion of the nature of the transition and its broader implications in quantum-many body physics. In this section we provide the relevant background to our present work, up to the rather confusing status of the field prior to the developments reported in this paper. We summarize our results and resolution of the previously puzzling

aspects of the transition in Sec. III.

A. AFM–VBS transition and putative DQCP

The AFM ground state of the 2D $S = 1/2$ Heisenberg model is well described by spin wave theory [4, 88]. Though there is no analytical proof (there is for $S = 1$ and higher [89, 90]), the numerical evidence, mainly from QMC simulations, of robust long-range order is overwhelming [91–94]. The very large ordered moment, about 60% of the value in the absence of quantum fluctuations, is also in the end the reason why spin wave theory works so well in this case.

Once the AFM order is reduced by some kind of competition between interactions (still keeping the spin rotational invariance) and the ordered moment is reduced, spin wave theory fails and all analytical descriptions become challenging when the amplitude fluctuations cannot be neglected [95]. However, the continuum field theory (the nonlinear σ -model) is well understood [2, 5] and can describe the quantum phase transition into a non-degenerate featureless (with no topological order) paramagnetic state through a Wilson-Fisher $O(3)$ [strictly speaking $SO(3)$] critical point. QMC simulations perform well, as exemplified by numerous studies of the transition in Heisenberg systems with imposed coupling patterns (mostly with dimers) [96–100].

Studies of VBS (spontaneously dimerized) ground states of deformed Heisenberg models (here again we limit the discussion to spin-rotationally invariant interactions) also have a long history. The discrete symmetry breaking associated with the formation of a pattern of varying singlet density turned out to be much more challenging than the AFM phase and its $SO(3)$ symmetry breaking. In quantum field theory, the VBS state on the lattice can be understood as the confined phase of certain topological defects of a compact $U(1)$ gauge field coupled to matter in the form of $S = 1/2$ objects (spinons) [10, 11, 101, 102].

In a more intuitive picture, the spinons in the ground state of a strongly ordered VBS are bound into short bipartite singlets—the valence bonds forming a four-fold degenerate columnar pattern on the square lattice. An $S = 1$ excitation of the VBS involves the presence of a triplet bond, or, in a basis of singlet bonds and unpaired spins, two bound $S^z = 1/2$ objects in a background of singlets. When the order is reduced, longer valence bonds are required to describe the ground state, which corresponds to a longer confinement scale. The energy required to excite one valence bond—the spin gap—should then be reduced as well. Spinon bound states can be directly observed in QMC simulations of J - Q models in the valence bond basis [103, 104].

In the simplistic picture based on valence bonds, a continuous transition at which the VBS melts would imply spinon proliferation and deconfinement by unbinding of spinon pairs when the distribution of valence-bond

lengths becomes very broad. The AFM phase forms on the other side of the DQCP by condensation of spinons. In the basis of valence bonds, the AFM ground state is also characterized by a broad distribution [118], with the probability of a bond of length l decaying as l^{-3} [119, 120], but here some fraction of the spinons have formed a condensate, reflecting the Néel order. Once the $SO(3)$ symmetry is broken, the singlet character of the (bipartite) valence bonds is lost [120] as the spins previously forming singlets now experience effectively opposite magnetic fields from the staggered magnetic order.

When elevating the symmetry of the spins from $SU(2)$ to $SU(N)$ (with a specific representation), the Heisenberg model spontaneously dimerizes into a four-fold degenerate columnar state for large N through a mean-field-like mechanism, and corrections have been studied with $1/N$ expansions [10, 11]. The value of N at which dimerization takes place, $N \approx 4.5$, has been confirmed by QMC simulations [105, 106]. However, it proved difficult to obtain reliable results for the dimerization (VBS) transition in the frustrated spin-1/2 $SU(2)$ Heisenberg Hamiltonians that were typically the focus of research in the field of quantum magnetism.

The main computational problem here is that QMC simulations are hindered by the “sign problem”, i.e., our inability to formulate the problem with positive definite sampling weights (except in special cases) [107, 108]. Early studies of frustrated Heisenberg models were therefore limited to small lattices accessible with exact diagonalization methods [3, 109–112] or series expansions around some solvable limit [113]. It is only recently that methods targeting larger systems, such as the density matrix renormalization group (DMRG) [65, 67, 114, 115] as well as more general matrix-product and tensor-product based methods [72], have been able to approach the necessary degree of reliability for 2D Hamiltonians with VBS (and also QSL) ground states. Machine learning is also making rapid inroads in its ability to produce good variational wave functions [69, 116]. Still, with all existing methods, it is difficult to reliably study quantum phase transitions in the traditional frustrated spin models.

The AFM–VBS transition in 2D quantum magnets came into renewed focus with the DQCP proposal, according to which the transition is generically continuous. In contrast, a generic first-order transition between two ordered phases is expected within the conventional Landau-Wilson-Ginzburg (LGW) framework, with continuous transitions realized only at fine-tuned multicritical points. The essential non-Landau aspect of the DQCP proposal is that the AFM and VBS order parameters are not the fundamental degrees of freedom in a low-energy description, but they emerge from the same spinon field by either confinement or condensation.

In the DQCP theory the spinons at the critical point are coupled to a non-compact (defect-free) $U(1)$ gauge field [23, 24, 117], originally in a CP^1 theory extended to CP^{N-1} for $SU(N)$ spins. Working with $SU(N)$ spinons [102], Senthil et al. showed that DQCPs are realized for

large N , and, motivated at least in part on prior suggestive numerical results for related lattice models [121, 122], conjectured that such non-LGW continuous transitions persist all the way to $N = 2$ [23, 24]. While subsequent numerical work for spin Hamiltonians with rather large values of N match well with results from $1/N$ expansions [38–40], the fate of the transition for small N , in particular $N = 2$, on which most of the work has focused has remained uncertain.

In principle, the putative DQCP universality class should also be accessible in 3D classical Heisenberg models (or the nonlinear σ -model in the continuum) with “hedgehog” defects suppressed, corresponding to the non-compact gauge field in the theory [117]. Though the symmetry of the order parameter is the same as in the conventional model, where hedgehogs proliferate at the phase transition, the absence of topological defects is believed to change the universality from that of the Wilson-Fisher $O(3)$ transition. Though encouraging results for unconventional critical exponents were obtained by Monte Carlo simulations of such a defect-suppressed model [117], in practice the complete suppression of defects on the lattice is difficult, as the singular nature of hedgehogs strictly appears only in the continuum.

Numerical results for quantum spin systems and other related lattice models, to be detailed below, have shown that the AFM–VBS transition in the $SU(2)$ case is associated with emergent $SO(5)$ symmetry of the combined order parameter with three AFM components and two VBS components. A DQCP theory building in a higher symmetry had already been proposed in the context of an XY (two-component) AFM order parameter, where the emergent symmetry is $O(4)$ [26]. The corresponding theory when the AFM order parameter is $SO(3)$ symmetric is the nonlinear sigma model with a topological θ term [26, 76, 77], corresponding to the WZW level $k = 1$ CFT. This is essentially a generalization to two spatial dimensions of the much better understood case of the WZW $k = 1$ theory in one space dimension, which describes the dimerization transition in spin chains with half-odd integer S [123]. A number of other $SO(5)$ field theories have also been proposed and investigated in the context of a proposed “web of dualities” that links seemingly different theories to the same critical points [47, 124]. Similar dualities have been demonstrated explicitly for low-energy theories of spin chains [125]). Whether or not these theories properly describe the 2D AFM–VBS transition, in lattice models as well as real materials [58], is a key question whose answer may have ramifications also for other proposed non-LGW transitions [126–129]. The only currently realistic way to answer this question is through unbiased numerical studies of lattice models.

B. Simulations of lattice models

To circumvent the numerical difficulties associated with traditional frustrated quantum magnets that may

harbor AFM–VBS transitions, the J - Q model was proposed specifically to study this transition without QMC sign problems on large lattices [27]. For negative coupling constants, the Q_n interaction terms illustrated in Fig. 1 clearly favor columnar alignment of singlets for large n . Even in the case of $n = 2$, which was studied first, there is a columnar VBS phase for large coupling Q_2 , with the transition into the AFM state taking place when adding the Heisenberg interaction at strength $J/Q_2 \approx 0.045$. The initial QMC results [27] indeed supported a continuous transition of the predicted DQCP type, e.g., with emergent $U(1)$ VBS order parameter and rather large values of the anomalous dimensions $\eta_{\text{AFM}} \approx \eta_{\text{VBS}} \approx 0.26$ —much larger than $\eta \approx 0.03$ at the $O(3)$ transition—and overall scaling behaviors at finite temperature similar to the large- N CP^{N-1} DQCP theory [36, 37].

Scaling anomalies on larger lattices were subsequently found in several works and were taken as evidence either of a rather conventional weak first-order transition [33, 45], unusually strong scaling corrections [46, 130], or behaviors influenced by two divergent length scales [41]. Similar scaling violations were also found in lattice versions of the proposed field theory [43, 44, 131], and later in a 3D classical loop model inspired by the J - Q models [28, 35]. Many results have also been reported for 3D classical dimer models [29, 132–136], which were argued to realize the same DQCP transition in the presence of appropriate interactions. Some exponents match reasonably well those obtained with J - Q and loop models [29, 136], though also in this case large scaling corrections were pointed out.

Fermion models with putative DQCP transitions have been studied extensively by determinant based QMC simulations [137–141], but the system sizes accessible here are much smaller, making it difficult to obtain reliable results for critical exponents or to reach the system sizes where the scaling anomalies become significant.

As mentioned, the predicted emergent $U(1)$ symmetry of the critical (and near-critical) VBS order parameter was found in early studies of J - Q models [27, 33, 34], and later $SO(5)$ symmetry was found in the 3D loop [35], dimer [29], and fermion [138] models. The close resemblance of the loop and J - Q models suggested that this higher symmetry should emerge also in J - Q models. Indeed, the very similar values that had already been found for AFM and VBS anomalous dimensions (which must be the same if the higher symmetry exists) [27] in hindsight had its explanation in emergent $SO(5)$ symmetry. Indications of the higher symmetry were also observed in emergent degeneracies of the excited level spectrum [142].

A version of the J - Q model with plaquette-singlet ground state (where the singlets form on units of four spins in a checker-board like pattern instead of the columnar dimers) was later constructed which exhibited $SO(5)$ symmetry on large length-scales despite the transition being clearly first-order [32]. The strong influence of the higher symmetry even rather far away from the presumed DQCP, which was also found in variants of the J - Q [30]

and loop [31] models with emergent $O(4)$ symmetry, suggests that the exponent governing the emergent $SO(5)$ symmetry must be very large. However, no quantitative results for such exponents were available.

The close connection between the 3D loop and J - Q models deserves further discussion. The similarity is apparent in the (2+1)D configuration space to which spin-1/2 models are mapped for the purpose of QMC simulations (for a review, see Ref. [145]), where efficient system updates are carried out by constructing space-time loops of spins [146, 147]. The spins can in fact be completely integrated out, which results in improved estimators for observables expressed solely with the system partitioned into a set of close-packed loops [93, 148, 149]. Thus, the J - Q model is mapped to a close-packed loop model, and the Q term corresponds closely to a tunable loop-loop interaction in the loop model [145]. The main difference between the J - Q and classical loop models is that the latter explicitly builds in space-time symmetry (as any of the three space dimension can be regarded as the time dimension), while in the J - Q model Lorentz invariance is emergent on large scales. A dynamic exponent $z = 1$ was found early on in the J - Q_2 model [27], and, given also the very similar scaling behaviors observed in the loop and J - Q model [28, 81] (and to some extent also the 3D dimer model [29, 132]), emergent Lorentz invariance in the J - Q model is not in doubt.

In general, for the different types of lattice models investigated, the anomalous dimension(s) extracted from spin and dimer correlation functions have been rather stable over time and across models, with already the first J - Q_2 study resulting in $\eta = 0.26(3)$ [27], common to both order parameters. Later, much larger systems still gave a compatible exponent, $\eta = 0.27(1)$ [150], from system size up to $L \approx 100$. The often cited best estimate up until now (prior to the results presented here) is from the 3D loop model, $\eta_{\text{AFM}} = 0.259(6)$ and $\eta_{\text{VBS}} = 0.25(3)$ [28], where system sizes up to $L = 512$ were studied. Results for the classical dimer model are consistent with these η values [136].

In contrast, estimates of the correlation length exponent ν in the J - Q model have changed over time, from $\nu = 0.78(3)$ in the first study [27] and then gradually decreasing over time [36, 39, 46, 130], to the most precise recent estimate $\nu = 0.455(2)$ [81]. In the 3D loop model, large drifts were observed as a function of the system size, with $\nu \approx 0.62$ holding over a range of moderate system sizes before drifting toward values $\nu \approx 0.46$ (consistent with the J - Q model) for the largest system sizes [28]—in a way very similar to what we have illustrated qualitatively in Fig. 3. Such drifts versus the system size were also previously observed in the J - Q model [41, 81], though the crossover was not analyzed extensively.

The larger exponent, $\nu \approx 0.62$, extracted for the loop model at the smaller length scales [35], also agrees with a rough estimate obtained from a short-distance correlation function producing $\Delta = 3 - 1/\nu$ in the same model [35]. The value is also in good agreement with

rather stable values of ν observed in the 3D dimer model [136] (where the system sizes were smaller and a potential crossover of the exponent may therefore not have been visible). These results raise the question as to why ν drifts so much with the system size and which value, $\nu \approx 0.62$ or $\nu \approx 0.45$, is correct (if any). Note that still smaller values of ν should result from finite-size scaling at a first-order transition, with $1/\nu \rightarrow d + z = 4$ (with $z = 2$ coming from the AFM long-range order at the transition) [30]. Thus, it appears that the observed behavior is in some way related to criticality, even if the flow eventually should tend to a different behavior characterizing the first-order transition.

Another puzzling finite-size drift that was pointed out early on in a study of the J - Q model was an anomalous behavior of the spin stiffness ρ_s , which should scale as $\rho \sim L^{-z}$ at a critical point with dynamic exponent z , here with $z = 1$. Instead, a slower decay was observed [33], but, as mentioned above, interpretations relying on $z \neq 1$ can be excluded (see also Ref. [151]). The anomalous behavior of ρ_s in the J - Q model [33] (and similar quantities in lattice field theories [43, 44]) had initially prompted suggestions of a first-order transition, spurring further work to demonstrate it more clearly [45]. However, the anomalous scaling can also in principle be caused by logarithmic corrections [46] or two competing length scales [41]. A weak first order transition was more recently indicated in simulations of J - Q models including appropriate order parameter fields, which make it easier to observe what appears to be discontinuities [152]—though perhaps still with some room for anomalous scaling.

The bipartite entanglement entropy of the J - Q_3 model for a corner-less bipartition is consistent with four Goldstone modes, as expected for an AFM–VBS coexistence state near an $SO(5)$ DQCP [143], while the corner contributions for a particular bipartition of the J - Q_2 model have a near-critical $SO(5)$ CFT form [144]. In contrast, another series of results on entanglement entropy in J - Q_2 and J - Q_3 models, using different bipartitions, were interpreted as a complete inconsistency with the CFT description [153–155]. The expected CFT behavior of the corner contributions was observed only for $SU(N)$ variants of the model [38] with $N \gtrsim 7$ [156]. The profound dependence on the way the entanglement subregion is defined [144] in this cases needs to be better understood.

As mentioned above, many different quantum field theories are believed to describe the DQCP through the web of dualities [47]. Though all theories may be equivalent, when treated within approximate schemes (e.g, mean-field theories) they are typically different. One approach then is to use lattice numerics to try to identify which theory within which approximation can best describe available data. One such example is Ref. 42, where dynamic spectral functions of a variant of the J - Q model were computed using stochastic analytic continuation [157] of QMC computed imaginary-time correlation functions. The resulting dispersion relation matches very well that of a parton mean field treatment (equiv-

alent to the square-lattice π -flux state) of four-fermion QED₃, and interactions included within the random-phase-approximation further improved the agreement with the QMC computed spectral functions. This result makes it clear that spinon deconfinement takes place at the AFM–VBS transition on very large length scales, despite the transition likely being ultimately first-order (as is now certain for all the J - Q_n models, as will be shown in Sec. IV B).

It appears clear that the AFM–VBS and related transitions in the lattice models are sufficiently close to a (possibly inaccessible) critical point for its scaling properties to be realized up to rather large length scales. However, it is not yet clear how reliable the so far extracted scaling dimensions are, i.e., to what degree their values have been affected by the ultimate crossover to first-order behavior.

C. Conformal bootstrap method and the complex CFT scenario

The numerical conformal bootstrap [60, 158] has emerged as a central method in studies of CFTs in three dimensions. Here the constraints imposed by conformal invariance, along with other applicable symmetries, are used to systematically exclude combinations of scaling dimensions, in some cases leading to small regions (“islands”) of possible scaling dimensions. After initial successes with Ising and $O(N)$ models [159], the method was applied to the DQCP [61], including the $SO(5)$ case [60, 62]. While the applied constraints were not sufficient to produce small islands in the space of scaling dimensions, useful bounds were found. The bound on the scaling dimension of the order parameter corresponds to $\eta \gtrsim 0.6$ [60, 62], far exceeding the numerically found value $\eta \approx 0.26$ (though $\eta \approx 0.6$ was found in one of the fermion models [139]). Moreover, the correlation length exponent $\nu \approx 0.45$ [28, 81] violates $\nu > 0.51$ [61]—a bound that is applicable to any CFT, including the presumed generic DQCP, with only a single relevant operator obeying all the symmetries of the Hamiltonian. It should be noted, however, that the larger value mentioned above, $\nu \approx 0.62$ obtained in some calculations or within ranges of smaller system sizes, does satisfy the bootstrap bound.

The discouraging conclusions of the bootstrap calculation, in combination with a prevailing perception that all the models studied had similar weak first-order transitions, spurred speculations that the DQCP must not be fundamentally reachable. Instead, it may exist only outside the physical three dimensional space [47], below some critical dimensionality. Specifically, based on ϵ -expansions for the level- k WZW nonlinear σ -model, $d_c < 3$ was found for all k by Nahum [51] and $d_c = 2.77$ was obtained for $k = 1$ (the case presumed to be applicable to the DQCP) by Ma and Wang [50]. A similar d_c value was found using the CFT bootstrap [52]. The critical dimensionality may then be sufficiently close to

$d = 3$ for “walking” behavior of a near-critical system to be observed [48, 49]. This type of slow evolution under renormalization group (RG) flow would then be responsible for the gradual drift of some of the critical exponents when the system slowly crosses over to the first-order fixed point.

Walking-type near-criticality can in some cases be described by a non-unitary CFT, with complex scaling dimensions. The perhaps most well studied case is the five-state Potts model in two dimensions, which has a phase transition where the correlation length is about 2500 lattice spacings [160]. There is no corresponding unitary CFT, and a real Hamiltonian with the 5-state full permutation symmetry maintained can never be driven to a continuous transition. A complex CFT can, however, describe observed crossover behaviors [49, 161]. Though there are no direct indications from the lattice calculations that this type of scenario can quantitatively explain any numerical data for the AFM–VBS transition, it has been widely accepted as the correct theory.

The bounds on scaling dimensions from the CFT bootstrap assumed a generic critical point, with only one relevant operator; in commonly used CFT language the traceless symmetric tensor, with field strength denoted by t on the vertical axes in Fig. 2. In classical statistical physics the corresponding exponent ν_t (or its inverse ratio with the conventional correlation exponent [80]) is often called the crossover exponent, as the transition involves an explicit change in symmetry of the Hamiltonian when crossing an $O(N)$ critical point by turning on perturbations of the form ϕ_i^2 of some of the components $i = 1, \dots, N$ of the order parameter. At the DQCP, the subset of these perturbations that take the system from the AFM to the VBS phase are still symmetric in the microscopic lattice Hamiltonian, e.g., in the J - Q models the symmetries of the Hamiltonian do not change when tuning coupling ratios. However, these perturbations are not symmetric under the putative emergent $SO(5)$ symmetry, since the order parameter changes from $SO(3)$ in the AFM phase to \mathbb{Z}_4 in the VBS phase, with the latter enlarged to $U(1)$ as the critical point is approached, then combining with the AFM order parameter to form the unified $SO(5)$ symmetric order parameter.

All fully symmetric perturbations—singlet operators under the $SO(5)$ symmetry—were assumed to be irrelevant at the DQCP [35, 47]. This is in sharp contrast to the classical $O(N)$ models, where changing the temperature from the critical T_c is the relevant symmetric perturbation that takes the system from a paramagnet above T_c to an ordered state with broken $O(N)$ symmetry below T_c . A generic $SO(5)$ DQCP transition would correspond to Fig. 2(a) below the special multicritical point, with the entire line consisting of AFM–VBS transitions in the same universality class, presumably satisfying the bounds on ν and η found in Refs. 60–62, unless the complex CFT description is necessary here.

The original DQCP scenario [23, 24], which did not involve an emergent $SO(5)$ symmetry, could in principle

also correspond to the phase diagram in Fig. 2(a) below the multicritical point. In that case s would be a redundant (or irrelevant) direction until the multicritical point is reached, but not one that preserves $SO(5)$ symmetry (which is not present). In either case, the critical line would still be expected to be supplanted by a first-order transition for some sufficiently large values of s , and a special (multicritical) point would then separate the two types of transitions. However, given the results of the numerical simulations discussed above, most recent theoretical works have assumed that the generic transition does have emergent $SO(5)$ symmetry, as observed numerically on rather large length scales [32, 35], though the transition ultimately becomes first-order according to the non-unitary $SO(5)$ CFT proposal. The scenario of a generic line of pseudocritical transitions, described by the WZW $k = 1$ CFT, is now widely accepted as the solution to the perceived fine-tuning problem [47]; the generic weak first-order transitions observed in many lattice models with a single tuning parameter.

The fuzzy sphere calculation [59, 163] involves an electronic model coupled to a central magnetic monopole, previously introduced by Haldane in the context of the quantum Hall effect [162]. The spherical symmetry is optimal for numerical studies of 3D CFTs, in the sense that the level spectrum of a Hamiltonian is directly related to the spectrum of scaling dimensions in an underlying low-energy CFT description. Remarkably, even with a very small number of electronic (Landau level) orbitals, of the order 10, a spectrum in very close agreement with the 3D Ising CFT was found in a model with \mathbb{Z}_2 (Ising ferromagnetic) symmetry breaking [163]. By subsequently studying a fermionic $SO(5)$ WZW theory [77], likewise regularized in the basis of Landau orbitals, Zhou et al. [59] found scaling dimensions (reproduced here in Table I) that are in approximate agreement with those of the multicritical CFT. However, the presence of a singlet operator that becomes relevant with increasing number of orbitals was interpreted as pseudocriticality, with an RG flow toward a first-order transition controlled by a complex CFT [59].

D. Multicriticality scenario

An order–order transition would normally be expected to be continuous only at fine-tuned multi-critical points. The conjecture that there is no relevant $SO(5)$ singlet operator is an important “beyond-Landau” aspect of the DQCP scenario, implying a generic continuous transition between the AFM and VBS states when an interaction implicitly violating the $SO(5)$ symmetry is tuned, favoring either the three AFM components or the two VBS components of the five-dimensional order parameter. However, there is now mounting evidence that the AFM–VBS transition in the lattice models studied so far actually is continuous only at a multicritical point. In Ref. 53, a scaling dimension that we now identify as Δ_t was found within the J - Q_2 model. Since it was

believed that the correlation length exponent $\nu \approx 0.45$ (in both the J - Q and loop models) should correspond to a relevant symmetric operator, the finding of another relevant operator associated with a different exponent, $\nu_t = (3 - \Delta_t)^{-1} \approx 0.62$, would imply a multi-critical point [53].

Though similar values of ν_t had also been found in some earlier works, as detailed in Sec. IIB above, the mismatch between ν and Δ_t , even within the same model (the loop model [28, 35]) had not been addressed previously. We now know (Sec. VIII) that the above exponent $\nu \approx 0.45$, which we will denote as ν_* henceforth (and for which we find a slightly smaller value, $\nu_* \approx 0.42$), does not control the conventional correlation length when approaching the critical point exactly, but only governs the slower growing bubble size when the weak first-order transition is approached; see Fig. 3. Nevertheless, the existence of two exponents ν and ν_* is not consistent with the generic DQCP scenario. Indeed, we will show in Sec. VIII that the exponent ν_* depends on both ν_s and ν_t , as well on the scaling dimension of the leading irrelevant $SO(5)$ perturbation.

Adding to the rise of the multi-criticality scenario, some years ago numerical evidence started to build for QSL phases located between AFM and VBS phases in frustrated spin-1/2 models [65–72] that can be continuously deformed into the J - Q models with direct AFM–VBS transitions. This potential to tune a model from a QSL to a direct AFM–VBS transition prompted the suggestion [71] that the generic phase diagram of frustrated models with QSL, AFM, and VBS phases is like that in Fig. 2(b). Subsequently, such a phase diagram was found in a J_1 - J_2 - J_3 Heisenberg model [73], though it is not clear, because of the numerical challenges for conventional frustrated spin models, whether the direct transition is always first-order (a generic continuous transition was suggested). Field theories to incorporate the QSL and $SO(5)$ multicriticality within the DQCP scenario are also now under active investigations [21, 22, 54, 72].

If the AFM–VBS transitions in the lattice models indeed is situated at, or very close to, a multicritical point, then the previous bounds on critical exponents from the CFT bootstrap are no longer of concern in this context [53]. Very recently, Chester and Su [55] applied the bootstrap method to the $SO(5)$ symmetric CFT in the manner of using one input scaling dimension, $\Delta_\phi = 0.63$ from lattice calculations, to predict other scaling dimensions, with the results listed in Table I. Contrary to the previous conjecture, this calculation actually indicated a relevant $SO(5)$ singlet operator, with a rather large scaling dimension $\Delta_s \approx 2.36$. The procedure actually corresponds to the identification of scaling dimensions located on the boundary of the CFT allowed region, and the boundaries had also previously been computed for the most important pairs of scaling dimensions; (Δ_ϕ, Δ_t) and (Δ_ϕ, Δ_s) . It is believed that the true scaling dimensions fall on or very close to the allowed boundaries, as is the case for the simpler $O(N)$ models [60]. The value $\Delta_s \approx 2.37$ [55]

(in our calculation slightly smaller, as seen in Table I) corresponds to a correlation function decaying with an exponent $2\Delta_s$, larger than 4.5, which may explain why it had remained undetected (or mistaken for a scaling correction) in the lattice calculations.

It would now appear that multicriticality is the simplest explanation of all the previous lattice numerics. In addition to the conformal bootstrap calculation supporting it, at face value the recent work on the fuzzy sphere also seems consistent with this conclusion, though the authors of Ref. 59 instead take their results as support of the non-unitary CFT scenario. In the multicritical scenario the singlet that switches from being irrelevant to weakly relevant versus the number of orbitals simply would reflect that this scaling dimension converges more slowly than some of the other scaling dimensions, eventually reaching a value close to (presumably) our result or the CFT bootstrap value in Table I. However, in the fuzzy sphere calculation it was argued that the specific dependence on the number of orbitals instead supports the complex CFT scenario [59].

The non-unitary CFT description was originally proposed [47] in order to try to reconcile the the generic DQCP scenario and interpretations of the numerical lattice data available at the time. With the current knowledge that a multicritical unitary CFT is possible [55, 62], the scenario of non-unitary CFT seems obsolete—violating the principle of Occam’s Razor. Indeed, in another application of the fuzzy sphere method [79], it was found that the CFT spectrum is only stable within a narrow range of an interaction parameter in the electronic model. The previous calculation had assumed that this parameter, which regulates the strength of a scalar operator, only tunes scaling corrections and that there is an optimal point at which these corrections are minimized, similar to classical models in which scaling behavior can be optimized by tuning away the leading scaling correction [164]. Moreover, by moving a way from the line of exact SO(5) symmetry, another phase between the AFM and VBS phases was found [79], thus potentially realizing a phase diagram such as the one in Fig. 2(b). All these developments make the multicritical SO(5) point and the phase diagram in Fig. 2(b) the most likely scenario for the AFM–VBS transition, setting the stage for our study producing comprehensive evidence for it and uncovering its broader consequences.

III. OVERVIEW OF FINDINGS

Given the length of the paper and the large number of interrelated results and insights, we here provide a concise summary of our methodology and conclusions. References are provided to the respective sections in which the supporting numerical results are presented and details of the theoretical arguments are given.

A. Quantum Monte Carlo methods

We study the J - Q models with two types of QMC simulation algorithms:

(1) Stochastic series expansion (SSE), where the partition function $Z = \text{Tr}\{e^{-\beta H}\}$ is sampled in the form of strings of the local operators of the Hamiltonian appearing in a series expansion of $e^{-\beta H}$, along with basis states—eigenstates of the S_i^z operators—to perform the trace operation stochastically. To obtain results suitable for finite-size scaling at a $z = 1$ quantum critical point, we take the inverse temperature as $\beta = aL$. Any factor of proportionality a works asymptotically for large L , and we use either $a = 1$ or (in the case of the J - Q_2 model) $a = 1/c$, where $c \approx 2.38$ is an estimated velocity of excitations [142].

(2) Depending on the quantity studied, it is some times more practical to instead project out the ground state from a translationally invariant singlet state $|\Psi\rangle$ (an amplitude-product state [118]), using either the operator $e^{-\beta H/2}$, which can be series expanded as in the SSE method, or $(-H)^{pN/2}$, where N is the total number of spins and $p \propto L$ should be expected for convergence (in the case of criticality with $z = 1$). The computational effort, which scales with the length of the operator string, is then similar to the expansion of the exponential, where $\beta \propto L$ is required for convergence to the ground state and the corresponding mean string length is $\propto \beta N$.

Though a singlet state $|\Psi\rangle$ is used as the “trial state”, the sampling of the normalization of the projected state, $\langle\Psi|e^{-\beta H}|\Psi\rangle$ or $\langle\Psi|(-H)^{pN}|\Psi\rangle$, is still carried out in the S^z basis. The implementation of this projector QMC (PQMC) method is overall very similar to the SSE method—essentially the two methods only use different boundary conditions in imaginary time. However, the computational effort to completely reach the ground state can be less, given that only singlet states at zero momentum are included in the sampling space, thus eliminating many of the low-lying excitations that affect the $T \rightarrow 0$ convergence of the $T > 0$ QMC method. Moreover, operator expectation values can be conveniently expressed using transition graphs [118] of valence-bond configurations, i.e., when measuring observables the basis is switched back to that of valence bonds, which is an essentially trivial task. To converge to the ground state the parameter β or p typically must only be small multiple of L , and we have checked for full convergence of all results presented here.

Both the above QMC methods are well established, and for implementation details we refer to Ref. 145 for SSE and Ref. 93 for PQMC. Some useful PQMC operator estimators are further discussed in Refs. 149 and 169. The methods are both exact in the sense that, for a given system size, there are no approximations beyond statistical errors.

B. Results and insights

The scenario that we have arrived at for the AFM–VBS transition consists of many separate parts and concepts that are difficult to discuss in a linear manner, as they all depend on each other in some way and the complete picture emerges only when all the components are put together. We therefore often refer to concepts and results that have not yet been discussed in detail but that motivate our numerical analysis in the different sections. The main numerical work is roughly organized in the order of the conventional relevant scaling dimensions first, then concepts and numerical results pertaining to the emergent SO(5) symmetry, followed by results on the first-order line. It is only after all these aspects of the transition have been discussed that the the pseudocritical scaling and crossover when approaching the first-order line can be fully appreciated and explained, which we do with the aid of results obtained and insights gained in the preceding sections.

In Sec. IV B we study the spin and dimer correlation functions, corresponding to the AFM and VBS order parameters, of several J - Q_n models and establish beyond doubt that all these models have first-order AFM–VBS transitions. Nevertheless, for $n = 2$ and $n = 3$ the coexistence states are sufficiently weakly ordered for the properties of the nearby critical point to be well established; specifically, two-point correlation functions of many operators exhibit stable power laws up to distances of 100 lattices spacings or more. The exponents are common to the J - Q_2 and J - Q_3 models, and in some cases the J - Q_4 model also produce very similar power law decays, though its first-order tendencies are much stronger. The scaling dimensions listed in Table I are mostly based on the J - Q_2 model, though we present many consistency checks with J - Q_3 results as well.

In Sec. IV C we use the standard spin and dimer (singlet) correlations corresponding to the AFM and VBS order parameters to extract the scaling dimension Δ_ϕ to unprecedented precision. We use the trick of taking the distance (r) derivative $C'(r)$ of a correlation function $C(r)$ as a “filter” [28] to minimize the impact of the eventual long-range order at the weak first-order transitions. With the PQMC method we have converged such calculations to the ground state for system sizes up to $L = 1024$, where critical scaling is observed up to distances close to 200. We also fit an appropriate function directly to $C(r)$ for L up to 512, with scaling corrections included, and the results of this approach also agree well with those from the derivatives. All these results lead us to the firm conclusion that Δ_ϕ is about 4% smaller than previously believed (see Table I), which may appear to be a small difference but an important one when it comes to establishing agreement with the SO(5) CFT. The individual values for Δ_ϕ obtained from spin and dimer correlations agree with each to within a statistical error of about 1% and we therefore assume that they really are the same, as required by the SO(5) CFT description.

We use a symmetric multi-spin (singlet) correlator not containing the order parameters in attempts to extract the scaling dimensions Δ_t and Δ_s of the two relevant symmetric perturbations of the critical point. However, while the value of Δ_t is relatively easy to extract from the asymptotic decay, giving the value listed in Table I, it turns out to be impossible to distinguish Δ_s from the expected contributions to the correlation function from the first descendant of the t field, since Δ_s and $\Delta_t + 1$ are rather close to each other. We obtain Δ_s in other ways, as explained further below.

We also argue that a spatial bond (J -term) modulation used to induce a helical VBS phase in Ref. 53 contains the conserved current operator, which allows us to extract its scaling dimension Δ_j . This scaling dimension was already obtained approximately in Ref. 53, but without noting the role of the conserved current operator and with a numerical value 1.90(2); five error bars off the expected value 2. With improved results for the corresponding correlation function, we now find a value consistent with the general requirement $\Delta_j = 2$ for a Noether current operator. This result is important in that it demonstrates explicitly that a scaling dimension with a known CFT value can be extracted despite the fact that the systems we study cannot reach the critical point exactly.

The most natural scenario for a multicritical point is that it is attached a first-order line on which the relevant singlet field s is varying and the SO(5) violating field vanishes ($t = 0$), as in either of the scenarios in Fig. 2(a) and Fig. 2(b). To study such a first-order line in a 2D parameter space, we use the J - Q_2 - Q_6 model, keeping $J + Q_2 = 1$ and extracting transition values Q_{2c} for several values of Q_6 . As expected, we find that the transition for increasing Q_6 develops gradually stronger first-order signatures, which we use to further test the multicriticality scenario.

Using finite-size scaling (data collapse) of Binder a cumulant, we show consistency with the value in Table I of the correlation-length exponent ν_s pertaining to the first-order line. Moreover, we extrapolate the order parameters to infinite size, using the common value $m^2(L)$ of the two squared order parameters where they cross each other, to ensure that the system is properly in the coexistence state for each L . We find power-law scaling of the form $m^2 \sim (Q_6 - Q_{6c})^{2\beta}$ with $\beta \approx 0.87(5)$, which agrees with the value computed from the scaling dimensions in Table I; $\beta = \Delta_\phi / (3 - \Delta_s) \approx 0.84$. The fitted critical Q_6 value is negative, $Q_{6c} = -0.07(2)$, and cannot be studied directly with sign-free QMC simulations. However, there is now no reason to doubt that this multicritical point exists in the real model space, in contrast to the common view that only a critical point described by a complex CFT is possible [47, 50–52, 59].

A similar analysis of the first-order line of the J - Q_2 - Z_2 and J - Q_2 - Z_3 models reveal no detectable changes in the order parameters when Z_2 or Z_3 is increased, even though the transition point evolves considerably. This behavior

implies that the Z_2 and Z_3 operators are dominated by their t field content, which points to one plausible reason why many models show weak first-order AFM-VBS transitions (beyond the fact that the critical exponents β and ν_s imply large critical scaling regions): the overlap of the s field with typical lattice interactions is small, for reasons that we do not know. Extreme operators such as Q_6 are required to shift the transition significantly into the coexistence line (increasing the s field).

In addition to the scaling dimensions of the relevant CFT operators, we also extract scaling dimensions of leading irrelevant perturbations of the $SO(5)$ symmetry. The finite-size decay of the Z_4 deformation of the critical VBS order parameter delivers the exponent denoted Δ_4 in Table I. Surprisingly, we find that the inherent deformation (i.e., arising from a perturbation present in the lattice Hamiltonian) of the $SO(5)$ symmetry in the subspace of one AFM (M_z) and one VBS (D_x) component is not governed by Δ_4 but by $\Delta_{4'} = \Delta_4 + 1$, which we detect in the probability distribution $P(M_z, D_x)$. This weaker finite-size deformation of $P(M_z, D_x)$ than $P(D_x, D_y)$ shows that the primary $SO(5)$ deformation in the models is caused by the lattice, as expected. However, the effect on the other dimensions of the $SO(5)$ sphere is secondary (derivative) and governed by the first descendant operator of the lattice perturbation. Inherent primary perturbations affecting the symmetry between the AFM and VBS components should also exist but must have scaling dimensions larger than $\Delta_{4'}$.

If an external perturbation is imposed that breaks the symmetry between components of the order parameter belonging to the AFM and VBS sectors, the applicable scaling dimension would of course still be Δ_4 . The weaker intrinsic symmetry deformation is important here because it governs the value of the emergent exponent ν_* of the pseudocritical (bubble) scale.

As discussed above in Sec. IIB, a glaring inconsistency between previous results for J - Q and loop models and potential CFT descriptions of the DQCP phenomenon has been the anomalously small correlation length extracted from various quantities, e.g., Binder cumulants [28, 81]. The value, $\nu \approx 0.45$, violates a generic CFT bound $\nu = 0.51$ under the assumption of only one relevant perturbation that maintains all the symmetries of the Hamiltonian, i.e., the absence of relevant $SO(5)$ singlet operators [61]. This bound is no longer of concern if there is a relevant singlet in the CFT spectrum, in which case the transition is fine tuned as proposed in Ref. [53]. However, as seen in Table I, there is no scaling dimension $\Delta_* = 3 - 1/\nu \approx 0.80$ of the right symmetry in the CFT spectrum computed in Ref. [55] and also no operator close to this value in the fuzzy sphere calculation [59].

In Ref. 81 an apparent scaling dimension $\Delta_* \approx 0.80$ was identified in the form of a particular correlation function decaying as $1/r^{2\Delta_*}$. This value of Δ_* matched very well the correlation length exponent, as it was understood to be at the time, $\nu_* \approx 0.45$, through the stan-

dard relationship $1/\nu_* = 3 - \Delta_* \approx 2.2$. However, we now have a better way of estimating the pseudocritical exponent, from a scaling behavior of the emergent $SO(5)$ away from the transition investigated in Sec. VIIB, finding $1/\nu_* \approx 2.40$. We believe that Δ_* (whose value stays close to 0.80 in the improved analysis here) is also associated in some way with the phenomenon of pseudocriticality, but we do not know the exact relationship between Δ_* and ν_* . Presumably, a perturbation theory of the $SO(5)$ CFT on the weak first-order line could answer this question, but this undertaking is beyond the scope of the present paper.

A major result of our work is that ν_* can be derived from a generalization of results for a classical tetracritical point with emergent $O(N)$ symmetry by Bruce and Aharony [64]. They showed that the shape of phase boundaries of the coexistence phase of two order parameters, schematically drawn in Fig. 2(c), is given by a combination of the crossover exponent, ν_t in the present context, and the scaling dimension of the leading irrelevant perturbation of the $O(N)$ symmetry, here $\Delta_{4'} = \Delta_4 + 1$, where Δ_4 is the scaling dimension of the irrelevant lattice perturbation of the $SO(5)$ critical point (Table I). We show that the dangerously irrelevant perturbation that becomes relevant on the first-order line, breaking the symmetry between the AFM and VBS components of the order parameter, is the descendant of the primary lattice induced perturbation.

There is no coexistence phase in the J - Q model, which we have been able to demonstrate explicitly from a quantity detecting effectively repulsive interactions between the AFM and VBS order parameters. The tetracritical point with its adjacent coexistence phase instead forms in Landau theory as a result of attractive interactions between two order parameters [64]. We will argue that, while there is no new phase induced by repulsive interactions, an associated crossover region nevertheless surrounds the first-order transition. This region is associated with a length scale that we can derive by starting from scaling arguments previously developed for the attractive case. In Sec. VIII we arrive at the following expression relating the exponents ν_* to ν_t , ν_s , and Δ_4 :

$$\frac{1}{\nu_*} = \frac{1}{\nu_s} \left(\frac{1}{\nu_t} + |y_{4'}| \right), \quad (1)$$

where $y_{4'} = 3 - \Delta_{4'} = 2 - \Delta_4$.

By studying the way in which the $SO(5)$ symmetry is violated upon moving away from the transition point, in Sec. VIIB we also obtain a very precise independent estimate for the pseudocritical exponent

$$\frac{1}{\nu_*} = 2.402(6). \quad (2)$$

By using this value in Eq. (1), together with our estimates for ν_t and $y_{4'}$, we can solve for $1/\nu_s = 3 - \Delta_s$, which leads to our value of Δ_s in Table I. The value is close to the predicted CFT bootstrap value in Table I and, in

combination with our values of Δ_ϕ and Δ_t , falls very close to previously computed SO(5) CFT bounds [62] (which are believed to be close to the true exponents [55]). In Sec. VI we show that our Δ_s value is also compatible with the growth of the coexisting order parameters when moving along the first-order line of the J - Q_2 - Q_6 model.

In Secs. VIII B and VIII C we show that a detailed understanding of the correlation length requires all the relevant length scales, i.e., the three exponents ν_t , ν_s , and ν_* . We further explain how the scaling crossover of the correlation length, schematically illustrated in Fig. 3, varies as the first-order line is crossed at different distances from the multicritical point, using the J - Q_2 - Q_6 model with different values of Q_6 (corresponding to k in Fig. 3). The impact of the length scale governed by ν_* fades away as the critical point is approached, becoming truly extinct at the critical point.

The three length scales governed by ν_t , ν_s , and ν_* impact also other physical observables that intrinsically are related to the correlation length. In Sec. IX we discuss the previous ansatz with two length scales (corresponding to ν_t and ν_*) [41] in light of our present understanding, which implies a reinterpretation of the physical nature of the length scales assumed in Ref. 41 (but with the same scaling forms). While ν_t and ν_* often dominate scaling properties, to account for the full finite-size dependence of many observables also requires that ν_s is taken into account when the transition is crossed as in Figs. 2(a) and 2(b), where both the fields s and t are varied. We demonstrate the resulting intricate behavior using the spin stiffness ρ_s .

IV. ORDER PARAMETERS

In Sec. IV B we present PQMC results for spin and dimer correlations at distance $r = L/2$ on lattices of size up to $L = 384$ for the J - Q_2 model and somewhat smaller, $L = 320$, for the J - Q_3 and J - Q_4 models. The main result here is that the J - Q_2 model undergoes a very weak first-order transition, which is clearly detectable in the correlation functions of the order parameters only with high-quality data (small error bars) for large lattices. For increasing n , the J - Q_n models host transitions of increasing first-order character, as seen in the magnitude of the coexisting AFM and VBS order parameters.

In Sec. IV C, we examine the distance dependence of the correlation functions $C_{s,d}(r)$ and their r derivatives, the latter of which shows power-law behaviors over longer distances and is useful for extracting the scaling dimension Δ_ϕ , as was previously found with the 3D loop model [28]. In the case of the J - Q_2 model, we present ground-state converged PQMC results for distances up to $r = 256$ for a system as large as $L = 1024$. To complement and confirm the validity of this approach, we also analyze the correlation functions themselves with scaling corrections included, using system sizes up to $L = 512$, which is the largest size for which the correlations are

well converged to the ground state—the derivatives converge faster, as we will explain. The two approaches deliver compatible results for the common AFM and VBS value of Δ_ϕ . The individual scaling dimensions are the same to within statistical errors of less than 1%. Our best estimate of the common value is $\Delta_\phi = 0.607(5)$.

A. Correlation functions and exponents

We define the staggered spin correlation functions as

$$C_s(\mathbf{r}) = \langle \mathbf{S}_0 \cdot \mathbf{S}_\mathbf{r} \rangle \epsilon_{0\mathbf{r}}, \quad (3)$$

where $\epsilon_{\mathbf{r}} = (-1)^{r_x+r_y}$ is the AFM phase factor for the spin at $\mathbf{r} = (r_x, r_y)$. The dimer correlation function is defined as

$$C_d(\mathbf{r}) = [(\langle \mathbf{S}_0 \cdot \mathbf{S}_{\hat{x}} \rangle \langle \mathbf{S}_\mathbf{r} \cdot \mathbf{S}_{\mathbf{r}+\hat{x}} \rangle) - \langle \mathbf{S}_0 \cdot \mathbf{S}_{\hat{x}} \rangle^2] \theta_0 \theta_\mathbf{r} \quad (4)$$

where $\hat{x} = (1, 0)$ is the lattice vector in the x direction and $\theta_\mathbf{r} = (-1)^{r_x}$ is the appropriate phase factor for a columnar dimer pattern in the ordered state, corresponding to the wave-vector of the dominant critical fluctuations; $q = (\pi, 0)$ and $(0, \pi)$ (the latter with $x \leftrightarrow y$). In all cases, we average translationally over the reference spin “0” and also use the reflection and rotation symmetries of the square lattice as appropriate.

In a system with long-range order of a given kind, the corresponding long-distance correlation function should converge to a non-zero value representing the square of the ordered moment, while in a critical system a power law decay of the form

$$C(r) \propto r^{-2\Delta_\phi} = r^{-(1+\eta_\phi)} \quad (5)$$

should be observed asymptotically. Here Δ_ϕ is the scaling dimension of the order parameter considered, and its indicated relationship to the critical exponent η_ϕ (the anomalous dimension) is the simplified form of

$$2\Delta_\phi = d + z - 2 + \eta_\phi \quad (6)$$

for spatial dimensionality $d = 2$ and dynamic exponent $z = 1$. Evidence for $z = 1$ was presented already in the first study of the J - Q_2 model [27] and later, e.g., in Ref. [142]. The similarities between the J - Q_2 model and the manifestly space-time invariant classical 3D loop model [28, 35] also supports $z = 1$, as we already discussed in Sec. II B.

Below we will show both the spin and dimer correlations only for separations along the line $\mathbf{r} = (r, 0)$. We have also computed the correlations along the lines (r_x, r_x) and $(0, r)$, the latter of which is not equivalent to $(r, 0)$ in the case of the dimer correlations for x -oriented dimers. We find the same type of behavior (including the decay exponent that we extract) in all cases in both spin and dimer correlations.

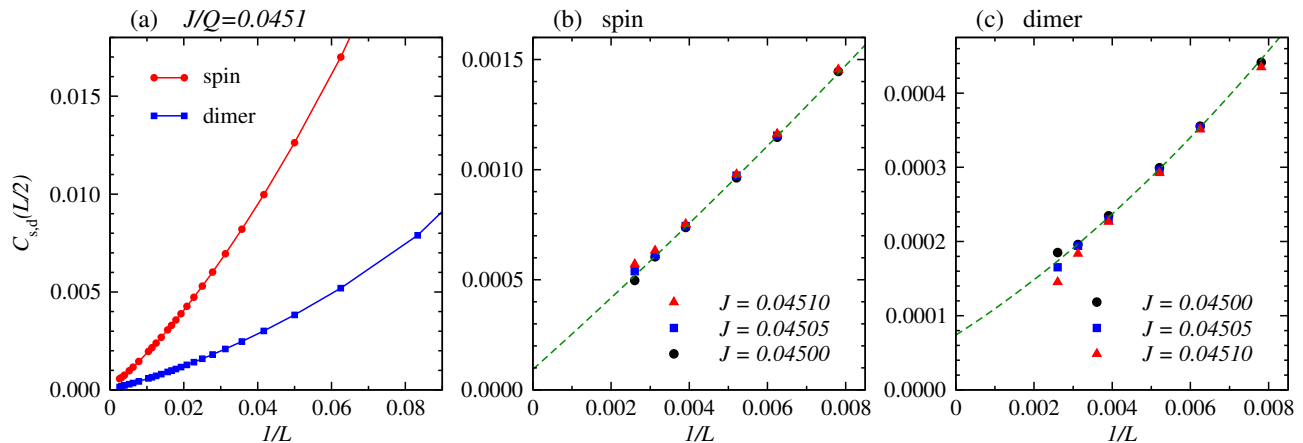


FIG. 4. Spin and dimer correlation functions at distance $L/2$ vs the inverse system size in the near-critical J - Q_2 model, obtained with ground-state converged PQMC calculations. In (a), both correlation functions are shown vs $1/L$, with L from 16 (spin) or 12 (dimer) up to $L = 384$. In (b) and (c) the correlation functions at three values of the coupling J (at fixed $Q_2 = 1$) are zoomed in to the points for $L = 128, 160, 192, 256, 320$, and 384. The error bars for the largest system in (c) are about half the symbol size, while for all other cases they are much smaller. The green dashed curves are cubic collective fits to the data for $J = 0.04500$ and $J = 0.04505$ (with several smaller system sizes also included in the fitting).

B. Phase coexistence in J - Q_n models

Long-distance correlation functions in finite systems can be studied either by considering distances $r \ll L$ for large L or by taking one of the longest distances in a periodic system, e.g., $r = L/2$. The former approach delivers the true correlation function in the thermodynamic limit, while $C(L/2)$ for large L extrapolates to the correct squared order parameter in a system with long-range order. For a critical system, the same scaling exponent governs the correlations versus r and versus L , while the overall factor is different because of boundary enhancements when $r \approx L/2$. For the purpose of detecting weak long-range order, investigating $C(L/2)$ versus L is preferable, as only the behavior versus the single parameter L has to be monitored.

Figure 4(a) shows both spin and dimer correlations at $r = L/2$ versus $1/L$ at the value of the critical coupling ratio of the J - Q_2 model obtained from Binder cumulant crossings in Ref. [81]. It is certainly clear that any non-zero values for $L \rightarrow \infty$ must be very small, suggesting a critical point or very nearly critical ground state. For system sizes up to about $L = 100$, power laws can describe the behaviors reasonably well, e.g., in Ref. [150] the exponent $1 + \eta \approx 1.27$ was found this way for both spin and dimer correlations. However, the exponent drifts significantly for larger systems. For the 3D loop model, system sizes up to $L \approx 500$ were considered [28] and it was found that η extracted under the assumption of the critical form Eq. (5) eventually tends toward negative values, while for shorter distances η matches well the value in the J - Q model. Such drifting behavior is also found with the present results in Fig. 4(a).

In Figs. 4(b) and 4(c) we zoom in on the largest system sizes for three different values of J (here keeping $Q = 1$)

close to the transition point. Comparing the variations in the spin and dimer correlations in this small window of couplings leaves little doubt that there is one value of J , or possibly a small range of values, for which both order parameters extrapolate to non-zero values. Thus, instead of a critical ground state, AFM and VBS long-range orders coexist, as expected at a first-order transition or in a coexistence phase. We will later, in Sec. VII B, provide strong evidence for there being no finite coexistence phase, only a first-order AFM–VBS coexistence line (on which we will move by adjusting another coupling in Sec. VI). The present data indicate that the transition value of J is between the values 0.04500 and 0.04505; slightly lower than the estimate in Ref. [81] but close to an older estimate based on correlation lengths in Ref. [145].

The dashed curves Figs. 4(b) and 4(c) are cubic polynomial fits to the data at both $J = 0.04500$ and 0.04505 (i.e., one function was collectively fitted to two data sets) in order for the curve to roughly correspond to the behavior at the transition point. While these curves likely provide reasonably good estimates for the coexistence state located between these two couplings, they are here intended only to illustrate the main qualitative trends. More detailed analysis of the non-zero $L \rightarrow \infty$ order parameters will be deferred to Sec. VI, where we move further into the first-order coexistence state by introducing a third tunable interaction (Q_6).

A leading linear correction in $1/L$ of the order parameter is expected in general for a system breaking $O(N > 1)$ symmetry, reflecting gapless Goldstone modes with their associated transverse correlations decaying as $1/r$ in two spatial dimensions. The AFM order parameter is $O(3)$ symmetric [strictly speaking $SO(3)$, but the lack of reflection symmetry of the AFM state is irrelevant here] and

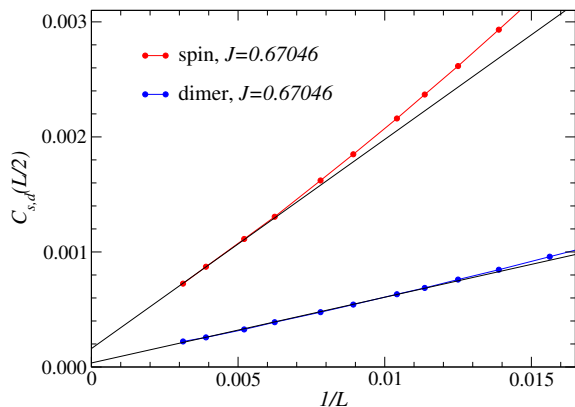


FIG. 5. Long-distance ($r = L/2$) spin and dimer correlations vs the inverse system size in the J - Q_3 model close to its AFM-VBS transition point (with $Q_3 = 1$ in all cases). The results for the largest system sizes in each case fall on almost straight lines with non-zero intercept, indicating a first-order transition with coexisting AFM and VBS long-range orders (located at J slightly above the value used here).

the ultimately \mathbb{Z}_4 symmetric VBS order parameter has emergent U(1) symmetry up to some length scale (as discussed further in Sec. VII A) in a near-critical VBS phase. Moreover, the two order parameters form an emergent SO(5) symmetry (discussed in Sec. VII B), and so the $1/L$ behavior with corrections in the form of higher powers in Figs. 4(b) and 4(c) is expected for both order parameters over some range of system sizes, both inside the phases and at the transition point. Ultimately, as will be shown in detail in Sec. IV C, the distance dependence of the correlations is characterized by a crossover from critical power-law decay to the non-zero squared ordered moment of the coexistence state.

In Fig. 5 we show results for the J - Q_3 model close to its AFM-VBS transition. Here we only draw straight lines in $1/L$ through the data points for the largest systems. We note that the dimer correlation for the largest size ($L = 320$) deviates slightly upward from the linear behavior, and there is also a less apparent downtrend in the spin correlation. These behaviors suggest that the value of J used here is marginally inside the VBS phase. Focusing on the AFM order parameter, where a linear behavior exactly at the transition should persist when $L \rightarrow \infty$ both inside the AFM phase and on the coexistence line (which is in practice close enough to the J value used here), we see that the extrapolated correlation function is roughly twice that of the J - Q_2 model in Fig. 4(b), i.e., the first-order discontinuity is stronger in the J - Q_3 model, though not very dramatically so.

Moving on to the J - Q_4 model, in Fig. 6 we show data for values of the Q coupling (here with $J + Q = 1$) close to the transition as well as further inside the ordered phases. The roughly extrapolated order parameters of the coexistence state are clearly significantly higher than those of the J - Q_2 and J - Q_3 models.

In Fig. 6(b) we observe non-monotonic behavior of the

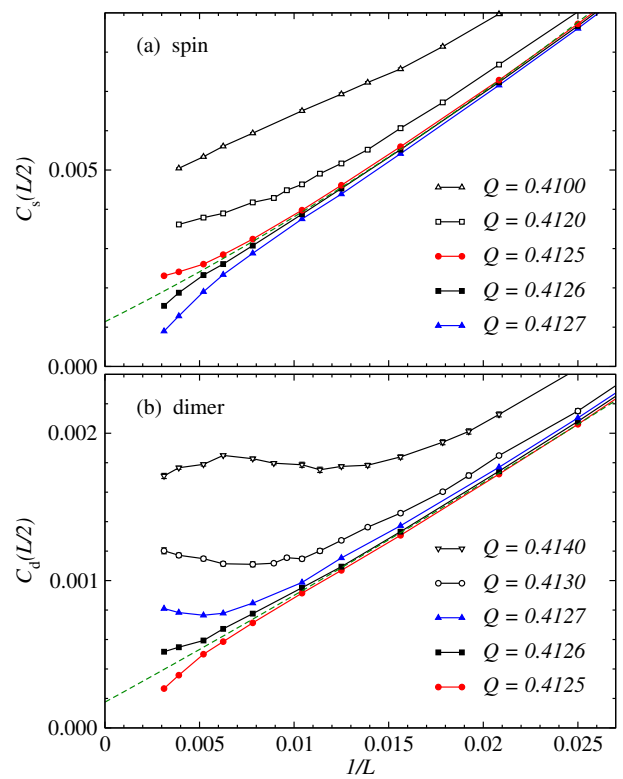


FIG. 6. Spin (a) and dimer (b) correlation functions in the J - Q_4 model at distance $L/2$ vs the inverse system. Results in both (a) and (b) are shown with red, blue, and black solid symbols for values of the coupling Q (with $J + Q = 1$) close to the transition point. Other values of Q (open black symbols) correspond to systems further inside the AFM phase in (a) and the VBS phase in (b). Error bars are at most of the order of the symbol size. The green dashed curves are cubic collective fits to the data for $Q = 0.41251$ and $Q = 0.41260$, but do not necessarily extrapolate reliable to infinite size because of possible crossover behavior for systems larger than available here.

dimer order parameter inside the VBS phase, close to the transition point. Such behavior is natural in the neighborhood of a first-order transition (another example was discussed in Ref. [165]), where a small system effectively is in the coexistence state and the order parameter that eventually is stabilized is averaged together with its much small value pertaining when the system fluctuates into the other phase. Once the system is large enough, it no longer fluctuates between the two phases, and the computed order parameter therefore represents, in the limit of infinite system size, the actual value in the ordered phase. The non-monotonic behavior is only completely observable in Fig. 6(b) at $Q = 0.4140$, but the upward trend is clear also at $Q = 0.4130$ and $Q = 0.4127$. A precursor to the increasing behavior is seen at $Q = 0.4126$. The maximum seen at $L \approx 150$ at $Q = 0.4140$ gradually diminishes as Q is increased further and eventually (data not shown here) a completely monotonic behavior sets in, with $C_d(L/2)$ rapidly approaching (on account of

the gapped VBS state with finite correlation length) its $L \rightarrow \infty$ value from above.

In Fig. 6(a) the spin correlations do not exhibit non-monotonicity for the available system sizes, though likely a maximum followed by convergence from above would also set in here for larger system sizes. Precursors similar to those preceding the upturn with increasing L in Fig. 6(b) are seen, and the same arguments for non-monotonicity apply in the AFM phase as well. The less pronounced non-monotonic behavior here should follow because the AFM order parameter has three components with exact SO(3) symmetry, representing a larger phase space compared to the eventually discrete four-fold degenerate VBS pattern. The fluctuations out of the AFM phase, even relatively close to the transition point, will therefore be weaker.

Clearly, in both phases, the non-monotonic behaviors will shift to larger systems upon moving closer to the transition point, and exactly at the transition the crossover out of the coexistence phase never takes place; thus a monotonic behavior is expected at the transition point. It is very difficult (computationally expensive) to locate the transition point to sufficient precision to follow the coexisting order parameters for large L . The transition window shrinks rapidly with increasing system size—in classical d -dimensional systems as L^{-d} and, correspondingly in quantum systems as L^{-d-z} , where z is the dynamic exponent (which likely should be taken as $d = 2$ for order parameters with continuous symmetry [30]). The relative probability of either of the two phases changes smoothly from close to 0 to close to 1 when traversing this narrow window.

The curves fitted in Fig. 6 can represent the size dependence when the coexisting order parameters have developed the emergent SO(5) symmetry. This symmetry must eventually break down (as discussed further in Sec. VII B), which should be accompanied by a crossover of the order parameters versus $1/L$ also at the transition point. The SO(3) symmetric AFM order parameter should still approach its infinite-size limit as $1/L$, but with a different constant of proportionality. Due to its ultimate discrete nature, the VBS order parameter will asymptotically converge exponentially. Such crossovers, which require very large sizes to be observed in these models, make it essentially impossible to extract the discontinuities in the order parameters at the transition. For scaling purposes, we have nevertheless found a practically useful method for extrapolating the strength of the coexisting order parameters, which we do on the first-order line of the J - Q_2 - Q_6 model in Sec. VI.

C. Scaling dimension of the order parameters

In the first study of the J - Q_2 model [27], using system sizes up to $L = 32$ it was found that the critical decay of the AFM and VBS order parameters was similar, with an exponent $\eta = 0.26(3)$, or $\Delta_\phi \approx 0.630(15)$ by Eq. (5).

Later studies for larger lattices by many groups found consistent results for larger lattices, e.g., in Ref. 150 the value $\eta \approx 0.27$ described both order parameters for L up to 96. These results were based on the distance integrated correlation functions, which scales with the system size in the same way as the $r \ll L$ correlator with r . For a generic correlation function $C(r)$ the squared size-normalized order parameter is

$$m^2 = \frac{1}{N} \sum_{\mathbf{r}} |C(\mathbf{r})|, \quad (7)$$

and if $C(r) \sim r^{-2\Delta_\phi}$ then $m^2(L) \sim L^{-2\Delta_\phi}$.

In the 3D loop model [28], a study of much larger system sizes revealed that η extracted from correlation functions at $r = L/2$ drifts toward smaller values with increasing L , eventually turning negative. For small to moderate values of r , up to $r \approx 20$, the above quoted values of η still describe the behavior, however, in support of the loop and J - Q models hosting the same kind of critical fluctuations. The behavior of η turning negative (with $1 + \eta$ eventually tending to 0 at the first-order transition that is now without doubt) can clearly be understood as arising from the small ordered moment of a coexistence state, which dominates the correlation function for large distances; $C(r) \rightarrow m^2$ for $r \rightarrow \infty$, while not affecting much the critical fluctuations for small r .

Nahum et al. [28] further made a very interesting and useful observation: the first discrete r derivative of the correlation functions exhibited good power-law scaling, $C'(r) \sim r^{-2-\eta}$, up to much larger distances than $C(r) \sim r^{-1-\eta}$. For $L = 512$, power law decays were observed for distances up to $r \approx 200$, with $\eta_s = 0.256(6)$ and $\eta_d = 0.25(3)$, respectively, for the AFM and VBS correlations (with the larger error bar on the VBS result explained by much larger statistical errors of the dimer correlations). This much extended scaling behavior of the derivatives can be explained by writing the correlation function (spin or dimer) for a finite system as

$$C(r, L) = C_1(r) + C_2(L) + C_3(r, L), \quad (8)$$

which clearly can always be done. In the case at hand, one would suspect that $C_1(r)$ is close to the critical power law described by the exponent $1 + \eta$ and $C_2(L)$ is essentially the small size dependent magnetization squared, i.e., a function similar to $C_{s,d}(L/2)$ in Figs. 4, 5, and 6. The mixed term $C_3(r, L)$ can of course not completely vanish, but if it is relatively small until r approaches $L/2$, then $C'(r, L) = \partial C(r, L)/\partial r$ will be close to $dC_1(r)/dr$, which, in turn, should be close to the critical form $\propto r^{-2-\eta}$. The results of Ref. 28 clearly showed this to be the case for the AFM and VBS correlation functions of the 3D loop model.

We here test the derivative method for the J - Q models. We also fit the correlation function itself to a form including appropriate scaling corrections. Both methods produce compatible values of the scaling dimension, $\Delta_\phi \approx 0.61$ from both spin and dimer correlations, slightly

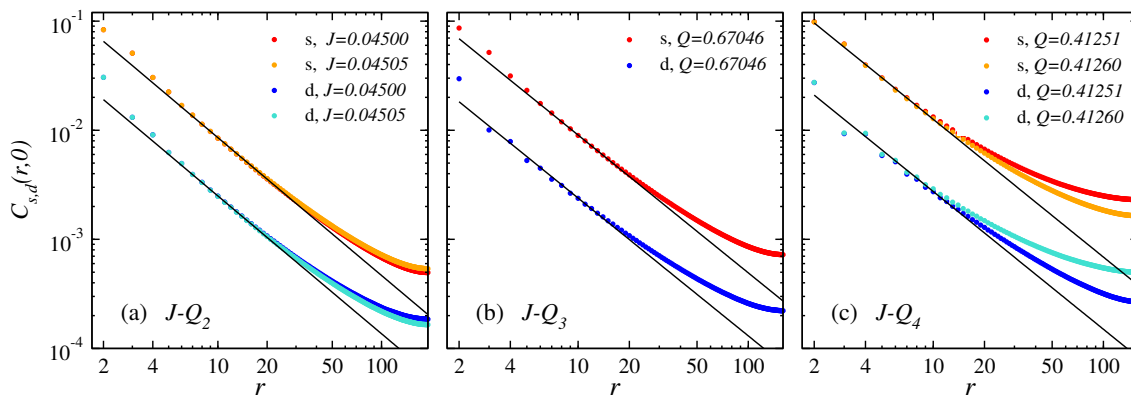


FIG. 7. Spin and dimer correlations of the $J-Q_2$ (a), $J-Q_3$ (b), and $J-Q_4$ (c) model at points close to their respective AFM–VBS transition points. The lines correspond to the critical form $C_{s,d} \propto x^{-2\Delta_\phi}$, where $\Delta_\phi = 0.63$ and the amplitude has been adjusted for good fits for $x \approx [5, 20]$ in the $J-Q_2$ model and smaller ranges in the other two models. The system size is $L = 384$ and (a) and 320 in (b) and (c).

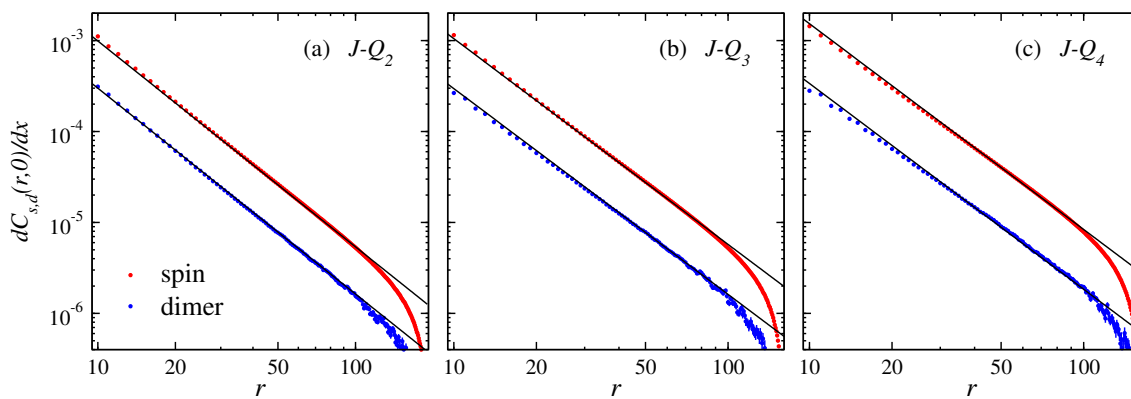


FIG. 8. First derivative, based on Eq. (9), of the spin (red symbols) and dimer (blue symbols) correlation functions of the $J-Q_2$ (a), $J-Q_3$ (b), and $J-Q_4$ (c) model. In (a) and (c), the results represent averages of the two couplings states in Figs. 7(a) and 7(c). The black lines all have slope -2.26 and have been adjusted for best fit to the data in the range $x \approx [30, 80]$. The system size is $L = 384$ and (a) and 320 in (b) and (c).

smaller than most previous estimates—in particular the $\text{SO}(5)$ CFT value in Table I.

1. Correlation functions and derivatives

We first examine the r dependent spin and dimer correlation functions on relatively large systems, $L = 384$ for the $J-Q_2$ model and $L = 320$ for the $J-Q_3$ and $J-Q_4$ models. Ground state results for $C_{s,d}(r)$ from PQMC simulations are shown in Fig. 7. For the $J-Q_2$ model the two couplings that we previously determined as brackets of transition point (Fig. 4) are used in Fig. 7(a). The results are indistinguishable in the plot for short distances but split off from each other for larger distances. The lines show the decay expected for a critical system with the scaling dimension $\Delta_\phi = 0.63$ assumed in the CFT bootstrap calculation [55], which is within the error bars of the value obtained with the loop model [28] and is also consistent with earlier results for the $J-Q$ model [27, 150].

The form indeed describes reasonably well both the AFM and VBS data up to $r \approx 20$, though some small corrections are also clearly present. It is not possible to determine a reliable exponent from these results from a fit to a single power law, primarily because of the crossover to a much slower decaying form reflecting the weak long-range order, but also because of the short-distance corrections. The results overall look very similar to those for the 3D loop model [35].

For the $J-Q_3$ model, in Fig. 7(b) we show results for the same near-critical coupling as in Fig. 4. Again the short-distance behaviors, beyond the regime where corrections are apparent, are reasonably well described by a common exponent $\Delta_\phi = 0.63$. This behavior applies up to somewhat shorter distances than for the $J-Q_2$ model, which again indicates a slightly more ordered coexistence state. The same trend of diminishing range of the critical decay, due to more pronounced long-range order, is seen for the the $J-Q_4$ model in Fig. 7(c), where we show results for the two couplings bracketing the transition point

according to Fig. 6.

Next we study the derivatives. To minimize discretization errors, we use the fourth-order approximant of the first r derivative and define $C'(r)$ with an overall minus sign in order to have a positive quantity;

$$C'(r) = \frac{2}{3} [C(r-1) - C(r+1)] - \frac{1}{12} [C(r-2) - C(r+2)]. \quad (9)$$

Results for all three models and the same lattices sizes as above are shown in Fig. 8. The derivatives are not as sensitive as the correlation functions themselves to the exact value of the coupling in the neighborhood of the transition point. To reduce the statistical errors further, we have therefore taken the average over two couplings used in Fig. 7(a) and Fig. 7(c) for the J - Q_2 and J - Q_3 model, respectively, which also corresponds to an interpolation with the two data sets to a value closer to the transition point than the two individual values.

For all three models, we find a very substantial range of distances over which the decay is closely described by $\propto r^{-1-2\Delta_\phi}$, with $\Delta_\phi \approx 0.63$. The behavior is very similar to that in the 3D loop model [28]. It is remarkable that even the J - Q_4 model exhibits this critical behavior up to distances $r \approx 100$, though with larger corrections than the J - Q_2 and J - Q_3 models. This critical behavior is manifested even though the model has a clearly ordered coexistence state according to the size dependent correlation functions in Fig. 6—with the AFM correlations extrapolating to a value about 10 times larger than in the J - Q_2 model in Fig. 4. The good agreement between these results for all three J - Q_n models, as well as the previously studied 3D loop model [28], should leave no doubt that the behavior reflects universal scaling originating from a nearby critical point.

We use the J - Q_2 model, the transition of which is the closest to the critical point, to extract the most reliable value of Δ_ϕ . Based on just the results for $L = 384$ in Fig. 8(a), it appears that the data agree with the previous estimates of the scaling dimension, $\Delta_\phi \approx 0.63$. However, the indicated scaling behavior is statistically good only over distance windows of a few tens of lattice spacings, and the best exponent also depends to some extent on how the window is chosen. We therefore proceed to study the evolution of the derivatives $C'_{s,d}(r)$ with increasing system size and also take corrections to the leading power law behavior into account in fits to $C_{s,d}(r)$.

As we have seen, the derivatives show much better scaling than the correlation functions themselves, for reasons that can be understood based on Eq. (8) when there is weak long-range order. We have observed a related favorable aspect of the PQMC simulation algorithm: the derivatives converge significantly faster with the projection power than the long-distance correlations. The variant of the PQMC method used here (Sec. III A) samples contributions to the normalization of the ground state projected out of a singlet state, $\langle \Psi | (-H)^{pN} | \Psi \rangle$, where p

typically has to be larger than the system length L for complete convergence to the ground state (we often use $p = 2L$). In contrast, the derivatives of the spin correlations are well converged already for $p \approx L/2$, which allows us to reach larger system sizes when targeting the derivative $C'(r)$, even though $C(r)$ is not yet fully converged to the ground state. The derivative of the dimer correlation function appears to converge somewhat slower and is also noisier. We therefore only analyze the derivative of the spin correlation function here, using system sizes up to $L = 1024$.

The faster convergence of $C'(r)$ can also likely be traced to the role of the long-range ordered component of $C(r)$. The value of the ordered moment, which affects $C_2(L)$ in Eq. (8), converges relatively slowly, while the power-law contribution dominating $C_1(r)$ at the transition converges faster. In Fig. 9 we show results for system sizes $L = 256, 512$, and 1024 , in each case with the projection parameter $p = L/16, L/8, L/4$, and $L/2$. In the case of $L = 1024$, the largest p is slightly smaller, $p = 500$ instead of 512 , because this is the largest value of p for which our implementation of the PQMC method works with four-byte integers; with an address space of 2^{32} elements of a linked list of vertices (see Refs. 145 and 93 for technical details on the sampling procedures). For $L = 256$ and $L = 512$ we also include results for $p = 2L$, where also $C(r)$ is fully converged. In Fig. 9 we have multiplied the derivatives by $r^{2.26}$, which would give r independent values (over some range of distances) if the scaling dimension takes the previously assumed value $\Delta_\phi = 0.63$.

For $L = 256$ and $L = 512$, already $p = L/4$ gives well converged results for $C'(r)$. For 1024 , there are still some differences between the results for $p = 256$ and 500 . For $L = 512$, convergence is explicitly confirmed by the essentially perfect agreement between the results for $p = L/2$ and $p = 2L$. Given that reasonably good convergence is also seen for $L = 512$ already with $p = L/4$ and the rather small differences between $p = L/4$ and $p \approx L/2$ for $L = 1024$, the latter should also be well converged within error bars.

These results for three large system sizes allows us to refine the value of Δ_ϕ . We have fitted power laws to a range of distances where such behavior appears to hold. Though the range of distances with approximative power-law behavior is limited, it grows with increasing system size and an effective size dependent scaling dimension can be defined to within a rather small level of uncertainty.

In Fig. 9(a), we see that the effective scaling dimension is larger than 0.63 , i.e., the power-law decay is faster than $r^{-2.26}$. However, for both $L = 512$ and $L = 1024$ the decay for large distances is slightly slower, corresponding to Δ_ϕ smaller than 0.63 . The decay exponent adjusted by the multiplier $r^{2.26}$ is in the range $[2.236, 2.240]$ for $L = 512$ and $[2.218, 2.224]$ for $L = 1024$, suggesting a rather rapid convergence for these larger systems and a scaling dimension $\Delta_\phi \approx 0.61$. However, it should also be noted that the window of apparent power law behavior

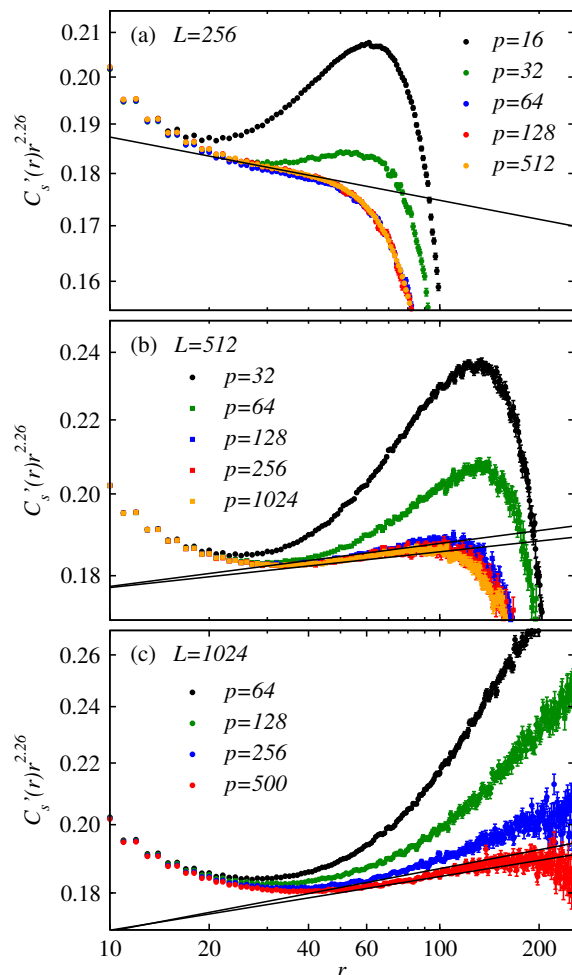


FIG. 9. Discrete derivative, Eq. (9), of the spin correlation function in the near-critical J - Q_2 model on lattices of size $L = 256$ (a), 512 (b), and 1024 (c). The results were obtained by PQMC simulations with a total of Np operators in the string, with p ranging from $L/16$ to $2L$ for $L = 256$ and $L = 512$, and up to $p = 500 \approx L/2$ for $L = 1024$. The results have been multiplied by $r^{2.26}$, so that the previously presumed scaling dimension $\Delta_\phi = 0.63$ would give an asymptotically flat behavior for a large critical system. Lines are drawn in the regions of approximate power-law behavior to provide size dependent estimates of Δ_ϕ . In (a), the single line has slope -0.030 , corresponding to $\Delta_\phi = 0.645$ for $L = 256$. In (b) and (c), the two lines correspond to $\Delta_\phi \in [0.618, 0.620]$ for $L = 512$ and $\Delta_\phi \in [0.609, 0.612]$ for $L = 1024$.

shifts to larger distances with increasing L , which shows that the corrections to the leading power law continue to play some role and may still affect the effective exponent even for $L = 1024$.

2. Scaling corrections from descendants

To further investigate the stability of the value of Δ_ϕ , we also perform an analysis including scaling corrections,

using fully converged $C(r)$ results for $L = 256, 384$, and 512 . In order to properly account for the enhancement of the slowly decaying correlations close to (and even quite far away from) $r = L/2$, because of the periodic boundary conditions, we should not just fit to a sum of power laws but use a form that respects the necessary condition $C(r) = C(L - r)$. For a quantum system in one spatial dimension, the proper CFT geometry is a periodic chain (a ring), where the conformal distance for a system of length L is given by

$$x = (L/2) \sin(r\pi/L), \quad (10)$$

for lattice distances $r = 0, 1, \dots, L - 1$. In two spatial dimensions, the proper conformal geometry is a sphere. On the torus, we still find it useful to define the distance x as above with r on the line $(r, 0)$, which guarantees reflection symmetry about $r = L/2$ of whatever function is fitted for $x \in [0, L/2]$. In the context of our 2D system, we will refer to x as the proxy conformal distance.

We assume that the dominant corrections to the asymptotic critical form $C(x) \sim x^{-2\Delta_\phi}$ arise from the descendant of the order parameter. Including two such terms in addition to the constant reflecting the nonzero squared ordered moment, we fit the correlation functions to the form

$$C(x) = \frac{a}{x^{2\Delta_\phi}} + \frac{b}{x^{2\Delta_\phi+2}} + \frac{c}{x^{2\Delta_\phi+4}} + m^2. \quad (11)$$

Though this form has five adjustable parameters, a, b, c, m^2 , and Δ_ϕ , it is clearly also highly constrained by the relationship between the three exponents $2\Delta_\phi, 2\Delta_\phi + 2$, and $2\Delta_\phi + 4$ from the expected primary operator and two leading descendants. The proposed function is therefore unlikely to cause overfitting.

Equation (11) cannot be completely correct, not just because of neglected higher-order terms or corrections arising from potential other operators besides the order parameter (which should have larger scaling dimensions), but because of additional terms expected in the ordered coexistence state. Given that the system at the transition point has emergent $SO(5)$ symmetry, we should expect contributions to the correlation functions from the four associated Goldstone modes, up to some large system size beyond which the $SO(5)$ symmetry is violated due to perturbations that are irrelevant at the critical point but relevant in the ordered coexistence state (often referred to as dangerously irrelevant operators). Even after this crossover, the AFM component of the coexistence state has exact $SO(3)$ symmetry and two associated Goldstone modes. The leading Goldstone contributions decay as $1/r$, i.e., *slower* than the critical correlations that we have assumed to be dominant above. The Goldstone contributions arise from the transverse fluctuations of the order parameter and its amplitude should be of the order of the stiffness constant (helicity modulus) of the $SO(5)$ or $SO(3)$ order parameter.

We analyze the spin stiffness ρ_s at the transition point in Sec. IX B and find a very small value in the thermo-

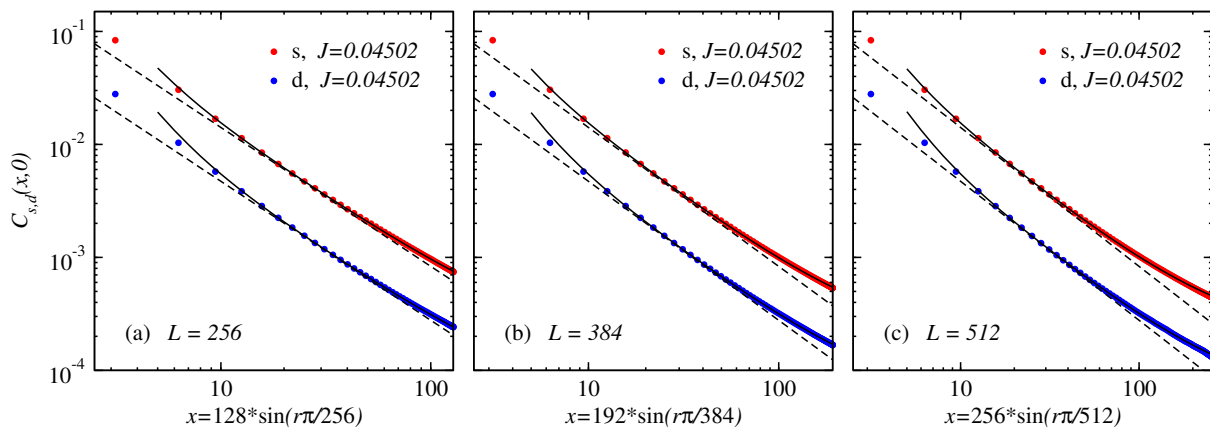


FIG. 10. Spin and dimer correlation functions graphed versus the proxy conformal distance, Eq. (10), for three different system sizes; (a) $L = 256$, (b) $L = 384$, and (c) $L = 512$. The solid curves are fits to Eq. (11) with $\Delta_\phi = 0.61$ and $c = 0$ (i.e., excluding the second descendant term) in all cases. The dashed lines indicate the slope corresponding to the leading term $\propto x^{-2\Delta_\phi}$.

dynamic limit; as expected given the small ordered moment of the coexistence state. We therefore assume that the Goldstone contribution will not significantly impact the fitted value of Δ_ϕ as long as we restrict the fit to relatively short distances. Indeed, given that the single independent decay parameter Δ_ϕ also controls the corrections in Eq. (11), we should not have to fit the correlation functions at very long distances. Thus, provided that the fitting form indeed is appropriate, we can at least to some extent avoid the complications arising from the crossover into the likely complicated large- r behavior.

The second descendant term in Eq. (11) decays very rapidly but we still include it in some cases in order to be able to fit data also at short distances, where the statistical errors of $C(x)$ are very small. The constant m^2 in Eq. (11) is necessary in order to obtain good fits even with only short-distance data included. It should be interpreted as a way to approximately include the effects of the long-range order at short to intermediate distances. We have also investigated an additional $1/x$ term and will further comment on it below.

We first discuss fits including also the longest distances. With only the leading correction and constant included, we can obtain visually good fits with Eq. (11) for all $r \geq 10$ ($x \gtrsim 15$), as shown in Fig. 10 for both spin and dimer correlations and system sizes $L = 256, 384$, and 512 . The proxy conformal distance indeed works very well, suggesting that Eq. (10) should be close to an ideal distance definition also in two spatial dimensions. All of these fits deliver values of the scaling dimension Δ_ϕ close to 0.61 , and for the fits shown we fixed said value in all cases. Deviations from Eq. (11) when this function is extended below the shortest distance included in the fitting procedure are obvious, but all the data points can be fitted well once the second correction is included (fits not shown here). The value of Δ_ϕ changes only marginally when the second correction is included.

While the fits in Fig. 10 look good, they are actually of very poor statistical quality. Because data at different

distances are highly correlated, it is necessary to compute the full covariance matrix and use it in the definition of the goodness of the fit χ^2 . The dominant source of covariance—the eigenvector corresponding to the largest eigenvalue—is a common, almost uniform fluctuation. The eigenvalue of this mode is typically (for large systems) more than an order of magnitude larger than the second largest eigenvalue. Therefore, even a statistically substandard fit can look visually good, with the fitted function falling very close to the center of the data points, as in Fig. 10, even though there are statistically significant deviations when covariance is properly taken into account.

In Fig. 11 we use smaller ranges of distances in order to eliminate distortions by potential shortcomings of the functional form Eq. (11) at both short and long distances. Here we also include the second correction, and in all cases we still obtain $\Delta_\phi \approx 0.61$. However, in the case of the spin correlations, where we use the range of lattice distances $r \in [10, 40]$ in Fig. 11(a), the statistical quality of the fits is still not good, having reduced χ^2 values close to 50 for $L = 256$ and 384 and about 8 for $L = 512$, despite the fact that the relative deviation of the fitted function from the data points is typically less than 10^{-4} , as shown in the inset of Fig. 11(a). These remarkably small deviations are an order of magnitude below the naive statistical errors of the data points, defined using only the diagonal elements of the covariance matrix. The deviations versus x show very similar patterns for all three system sizes, demonstrating that they are not purely statistical in nature but arise from additional corrections (most likely of higher order) not taken into account by Eq. (11). In an absolute sense, these deviations are very small and do not appreciably affect the extracted value of Δ_ϕ , but they still cause poor χ^2 values because they are large on a scale set by the very small eigenvalues of the covariance matrix (beyond the largest eigenvalue corresponding to the unison fluctuation).

The dimer correlations, shown in Fig. 11(b) for dis-

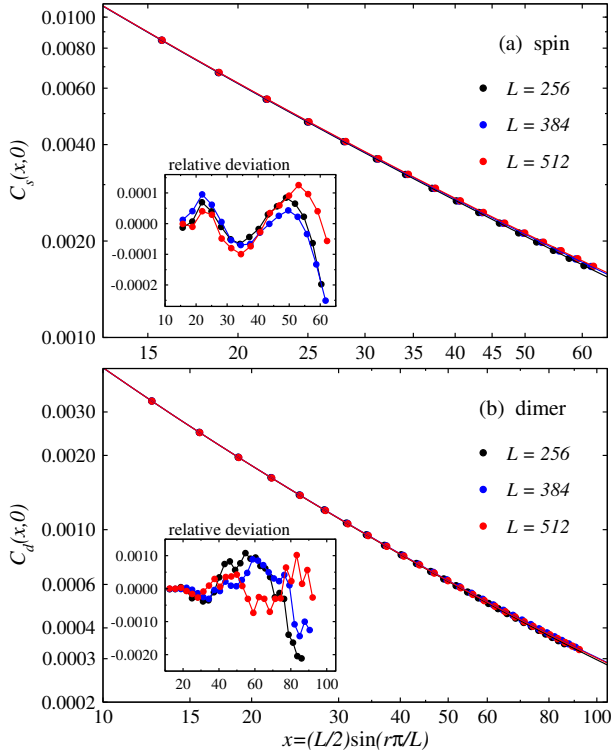


FIG. 11. Spin (a) and dimer (b) correlation function vs the proxy conformal distance x for the same system sizes as in Fig. 10 but for limited ranges of distances where the fitting function Eq. (11) can reproduce the QMC data very closely. In (a) the spin correlations are shown for $r \in [10, 40]$, where fits to the full Eq. (11) have relative deviations $(C_{\text{QMC}} - C_{\text{fit}})/C_{\text{fit}}$ from the data points of order $\approx 10^{-4}$ or less, as shown in the inset. The best-fit scaling dimensions are $\Delta_\phi = 0.601$ for $L = 256$, 0.605 for $L = 384$, and 0.606 for $L = 512$. In (b), the dimer correlations are shown for $r \in [10, 60]$, where the relative deviations from the fitted functions (inset) are typically 10^{-3} or less. The scaling dimensions here are $\Delta_\phi = 0.592$ for $L = 256$, 0.606 for $L = 384$, and 0.607 for $L = 512$.

tances $r \in [10, 60]$, have larger overall statistical errors and show less effects of neglected higher-order corrections. The χ^2 values are good for all system sizes. While the deviations of the data from the fit have some similarities for small x , and also for larger x in the case of $L = 256$ and $L = 384$, they look quite different for $L = 512$ at larger x , where the statistical errors are larger and the systematic deviations are therefore likely masked by the noise. For a given L , the deviations are still not independent for different x values, because of the covariance effects. Repeating the fitting procedure many times with Gaussian noise added to the data transformed to the eigenbasis of the covariance matrix (with the magnitude of the noise set by each eigenvalue), we can also obtain statistical errors (one standard deviation) on the scaling dimension. The final results from the dimer correlations with $r \in [10, 60]$ are $\Delta_\phi = 0.592(2)$ for $L = 256$, $0.606(3)$ for $L = 384$, and $0.607(5)$ for $L = 512$.

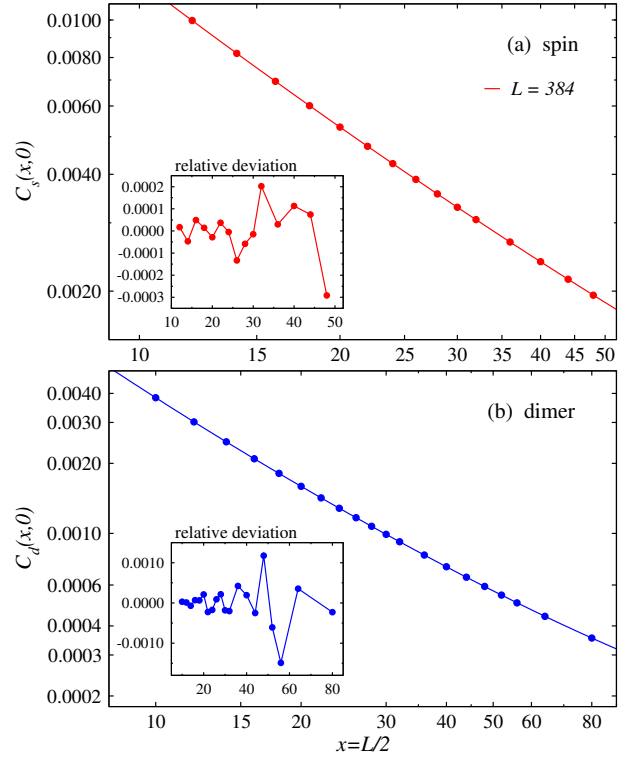


FIG. 12. Spin (a) and dimer (b) correlation functions vs distance $r = L/2$ along with fits to Eq. (11) with $x = L/2$. The ranges of data correspond to windows of L in which statistically good fits are obtained. The relative deviations from the fitted form, shown in the insets, are of the order of the statistical errors. The scaling dimensions extracted from these fits are $\Delta_\phi = 0.606(3)$ in (a) and $0.613(3)$ in (b).

In the case of the spin correlations, to achieve statistically good fits and compute meaningful error bars, we further reduce the range of distances to $r \in [14, 28]$, i.e., using only eight data points in the fit to the five-parameter form Eq. (11). While the number of degrees of freedom is very small (3), the fits are now statistically sound and deliver the following values of the scaling dimension: $\Delta_\phi = 0.601(2)$ for $L = 256$, $0.605(2)$ for $L = 384$, and $0.606(5)$ for $L = 512$, all of which are consistent with the results obtained for the larger range $r \in [10, 40]$ in Fig. 10. Overall, the statistical errors of Δ_ϕ are very similar to those above from the dimer correlations. Though the raw dimer correlations have significantly larger statistical errors, these errors are compensated by the fact that a wider range of points can be included in fits with acceptable χ^2 values. In fact, the range of the dimer correlations can be further extended and still allow good fits with only marginal changes in Δ_ϕ , but to stay on the safe side in light of potential Goldstone effects we restrict the analysis to $r \in [8, 60]$ in Fig. 11(b).

The four scaling dimensions extracted from the spin and dimer correlations for $L = 384$ and 512 are mutually consistent, while they are slightly smaller for $L = 256$.

The size dependence is much weaker than what is observed in the derivative of the spin correlation function versus the original lattice distance r in Fig. 9. The Δ_ϕ value estimated from the $L = 1024$ derivative in Fig. 9(c) is fully consistent with the results from the correlation functions at shorter distances for $L = 384$ and 512 .

If a term e/x is added to the fitting form Eq (11), the amplitude e in the unconstrained six-parameter fit becomes unrealistically large (given the small ordered moment and associated ρ_s value) and the scaling dimension Δ_ϕ becomes much larger, above 2, to compensate for the large $1/x$ contribution. With our extracted value $\Delta_\phi \approx 0.61$, the forms $1/x$ and $1/x^{2\Delta_\phi}$ are very close to each other, and it is not surprising that they cannot be separated in an unconstrained fit. We can also add the e/x term while keeping $\Delta_\phi \approx 0.61$ and fitting only at long distances. Then the amplitude of a of $1/x^{2\Delta_\phi}$ becomes smaller to compensate for a rather large e (with $e/a \approx 0.5$ in the case of the spin correlations). However, this kind of fit may not be meaningful, because the $1/x$ term is only one aspect of the Goldstone effects. Higher powers of $1/x$ are also expected [91, 93] and the crossover between the critical form and the asymptotic form in the presence of long-range order is likely complicated and beyond quantitative analysis with the present data and understanding. Fitting to a single power law plus a constant, $C(x) = a/x^{1+\eta} + m^2$, for large systems we find that η approaches 0 from above when the fitting window is moved to larger x values, as also found previously for the loop model [28]. We find similar behavior with $x = L/2$, and for large L such data can also be fitted to a polynomial with leading $1/L$ behavior, as in Fig 4.

The restriction of x to rather short distances in our final analysis should ensure negligible impact of the Goldstone modes and crossover effects, and this conclusion is also supported by the derivatives in Figs. 9(a) and 9(b) for larger distances. In further support of not including the $1/x$ term, in Fig. 6 there are no significant changes in the approximate power-law behaviors for the three different models up to $r \approx 100$, even though the $J-Q_4$ model has much larger ordered moments. Thus, we conclude that the Goldstone contributions must only play a significant role in the correlation functions of all the $J-Q_2$ model for distances beyond those used in Figs. 10 and 11.

To complete the analysis, we next study the correlation functions at distance $r = L/2$ for a range of moderate system sizes L , where the critical correlations dominate. In this case, we may also expect corrections of the form $L^{-|y|}$ from irrelevant operators with scaling dimension $\Delta > 3$ and $y = 3 - \Delta$. Surprisingly, we do not find any significant effects of leaving these out, obtaining good fits to Eq. (11) with $x = L/2$. The value of the scaling dimension Δ_ϕ is also close to the results of the previous fits for $r \ll L$, where the irrelevant scaling corrections should be absent for large L (which is supported by the very small differences between results for $L = 256, 384, \text{ and } 512$). In this case the data for differ-

ent L are of course statistically independent and χ^2 is defined with only the individual standard deviations. In Fig. 12 we show results for spin and dimer correlations obtained with windows of $r = L/2$ where good χ^2 values can be obtained. The deviations from the fitted function in this case are naturally of the order of the error bars of the data points (on average about one standard deviation, corresponding to a statistically good χ^2 value). The resulting scaling dimensions are $\Delta_\phi = 0.606(3)$ and $0.613(3)$ from spin and dimer correlations, respectively.

The suitability of the fitting form Eq. (11) is clearly supported by the stability of our results for Δ_ϕ with respect to different system sizes and fitting windows, and also by the good agreement between results obtained with $r = L/2$ and $r \ll L$. The fact that the results obtained from spin and dimer correlations are statistically indistinguishable at the level below 1% also lends further credibility to the SO(5) scenario, according to which Δ_ϕ must be the common scaling dimension for the AFM and VBS order parameters.

We have obtained several different estimates of Δ_ϕ that are mutually consistent statistically. In principle we could produce a weighted average of all of these estimates as our final result for Δ_ϕ . However, given that the results obtained with $r = L/2$ may to some extent be affected by neglected L dependent scaling corrections, we instead just take the average of the spin and dimer based results for $L = 512$ as our final result; $\Delta_\phi = 0.607(4)$, which is also statistically consistent with the two values from the $r = L/2$ fits. The difference between our final value and the input value $\Delta_\phi = 0.63$ used in the CFT bootstrap calculation [55] could very plausibly account for the other minor discrepancies between the exponents seen in Table I. It is also interesting to note that our Δ_ϕ value is reasonably close to that obtained in the fuzzy sphere calculation, where this scaling dimension is rather stable as a function of the number of orbitals [59].

V. RELEVANT PERTURBATIONS

Here we present results for correlation functions of operators that deliver the scaling dimensions Δ_t and Δ_j in Table I. In addition, we will present results for the ‘‘pseudo dimension’’ Δ_* , which is not part of the CFT spectrum but presumably is a manifestation of the perturbed CFT slightly inside the first-order line. In principle, we should also be able to extract the singlet dimension Δ_s from the same correlation function that gives Δ_t . However, it is difficult to separate the contribution of Δ_s from that of the first descendant of the t field, because $\Delta_t + 1$ is close to Δ_s . The value of Δ_s in Table I is instead extracted from the predicted pseudocritical relationship Eq. (1), which we motivate further in Sec. VIII A. The values of $y_{4'}$ and ν_* needed to solve for ν_s are extracted in Sec. VIII B.

Given a critical Hamiltonian H_c , we are interested in the stability of the fixed point to perturbations. We here

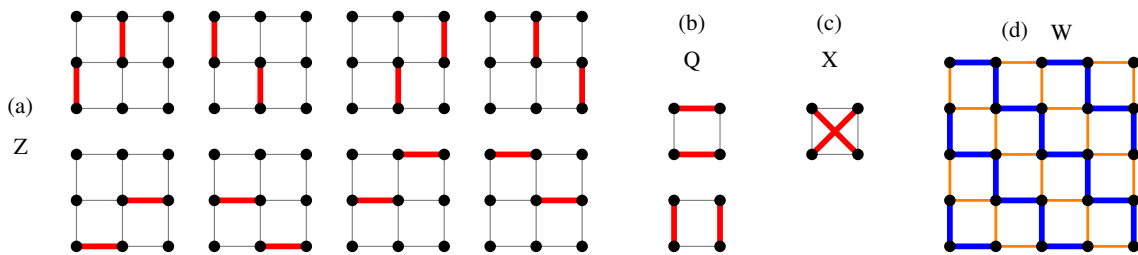


FIG. 13. Operators used in correlation functions for extracting relevant scaling dimensions [53]. In (a), (b), and (c), red thick bars represent bond operators $\mathbf{S}_i \cdot \mathbf{S}_j$ with i and j nearest neighbor sites. The Z and Q operators are defined as sums of products of two of these bond operators within 3×3 (a) and 2×2 (b) spin cells. The X operator in (c) is a single product of the bond operators on the diagonals of a plaquette. In (d), the W operator is defined in a cell of 5×5 spins, with thick blue and thin orange lines representing individual nearest-neighbor operators $\pm \mathbf{S}_i \cdot \mathbf{S}_j$, which are summed over the 5×5 cell.

denote a generic extensive perturbing operator by

$$V = \sum_r \epsilon_r V_r, \quad (12)$$

where V_r are local operators on individual spins, or groups of spins centered at lattice position r , and ϵ_r are phases that typically would be all unity or correspond to some regular pattern or “wave”. Upon adding V to H_c at small strength λ , $H \rightarrow H_c + \lambda V$, the system can either remain critical or flow (here with increasing system size) to some other fixed point. Whether or not the perturbation is irrelevant or relevant in this sense depends on its scaling dimension Δ_V , or, equivalently, the corresponding exponent (which corresponds to an eigenvalue in an RG transformation),

$$y_V = d + z - \Delta_V = 3 - \Delta_V \quad (13)$$

that controls the flow of the strength of the perturbation with the length scale.

In finite-size scaling, the length scale is the system size L and the scaling function (of some quantity exhibiting critical scaling when $\lambda = 0$) contains an argument λL^{y_V} , which can be interpreted as the renormalized (coarse grained) strength of the perturbation at length scale L [179–181]. Thus, the perturbation is relevant (the argument grows with L) if $y_V > 0$ and irrelevant (the argument approaches zero in the thermodynamic limit) if $y_V < 0$. The length scale corresponding to a relevant perturbation diverges upon approaching the critical point as $\xi_V \sim \lambda^{-\nu_V}$, with $\nu_V = y_V^{-1}$.

The most direct way to numerically extract a scaling dimension Δ_V in the absence of the perturbation ($\lambda = 0$) is to compute the two-point correlation function $C_V(r) = \langle V_0 V_r \rangle$ of the local operator V_r . The asymptotic power-law decay $C(r) \sim r^{-2\Delta_V}$ is governed by the (leading) scaling dimension, as previously stated for the order parameters in Eq. (5). Here the correlation function should be considered in combination with the phase factors ϵ_r in Eq. (12), and what matters in the relationship to y_V in Eq. (13) is $C(r)\epsilon_r$ integrated over space (and imaginary time, which when $z = 1$ just gives one more factor of L). When considering spatially uniform

perturbations, i.e., $\epsilon_r = 1 \forall r$, we are targeting the uniform component of the corresponding correlation function. The previously studied critical order parameters are associated with phases taken into account in Eqs. (3).

In this section we will study correlation functions of the operators illustrated in Fig. 13. The Z , X , and W operators were previously studied in Ref. 53 and the Q operator was studied in Ref. 81 (with a slightly different definition in terms of singlet projectors instead of just $\mathbf{S}_i \cdot \mathbf{S}_j$). Here we provide more extensive analysis with improved PQMC data and discuss the results in light of the scaling dimensions recently obtained within the CFT bootstrap calculation [55] and the fuzzy sphere [59].

A given lattice operator will in general contain all the CFT operators consistent with its symmetries. For a system with a CFT description, the correlation function should therefore be an infinite sum of algebraic decays $a_i r^{-2\Delta_i}$ (and possible phases ϵ_i that we leave out here), with the amplitudes a_i corresponding to the particular lattice operators chosen. The CFT operators are orthogonal and cross terms of the form $r^{-(\Delta_i + \Delta_j)}$ do not appear. Despite the possibility of several power laws appearing in a numerically computed lattice correlation function, in general one would expect the decay corresponding to the smallest CFT scaling dimension to be clearly observable and in some cases it may be possible to also extract additional larger scaling dimensions from the corrections to the leading form. In this section we will focus on relevant operators, leaving the case of irrelevant perturbations of the $SO(5)$ symmetry to Sec. VII, where we will use techniques not relying on correlation functions.

The models we study cannot be brought exactly to the critical point, and we observed large effects of the long-range ordered coexistence state in Sec. IV C. We were able to reduce these effects by taking the derivative. However, we will find here that correlation functions of operators not directly related to the order parameter are much less impacted, which is natural since they do not approach non-zero constants at large distances.

A. Fully symmetric operator

In the multicritical point scenario, the two tuning parameters required to reach the critical point of a lattice model must both control operators with the same microscopic symmetries as the Hamiltonian; no explicitly symmetry-breaking operators should be introduced. The previously studied correlation function of the Z cell operator in Fig. 13(a) exhibited a leading decay $C_Z \sim r^{-2\Delta_Z}$ with $\Delta_Z \approx 1.40$ [53] that we can now identify as the scaling dimension of the CFT t operator; $\Delta_Z = \Delta_t$.

All previous works had assumed that standard analysis of Binder cumulants or data collapse of the order parameters would deliver the exponent $\nu = \nu_t$ corresponding to the single correlation length expected within the original DQCP scenario. As already summarized in Sec. IIB, large finite-size drifts had been observed in this exponent in many different works, but the two most extensive studies, of the J - Q model [81] and the 3D classical loop model [35], both achieved apparent convergence toward $\nu \approx 0.45$, or $\Delta = 3 - 1/\nu \approx 0.80$. A power law decay consistent with this value of Δ was further obtained [81] from the correlation function of an interaction energy (similar to that of the Q operator studied below in Sec. VC). It was therefore natural to assume that $\Delta_Q \approx 0.80$ and $\Delta_Z \approx 1.40$ reflected a CFT with two relevant symmetric operators, and, under the assumption of emergent $SO(5)$ symmetry, that Δ_Q and Δ_Z should be identified as Δ_t and Δ_s , respectively. However, in light of the CFT bootstrap calculation [55], it now seems more plausible that $\Delta_Z \approx 1.40$ is actually Δ_t , while the anomalous scaling dimension extracted from C_Q (which also contains the VBS order parameter) is the pseudoscaling dimension that we call Δ_* and for which we obtain an improved value in Sec. VC.

Given the very large value $\Delta_s \approx 2.36$ of the relevant $SO(5)$ singlet in the CFT [55] and our slightly smaller value in Table I, it is not surprising that it could have been missed in previous lattice calculations. If indeed the Z operator also contains this operator, it should produce a $1/r^{2\Delta_s}$ correction to the slower $1/r^{2\Delta_t}$ decay of the Z - Z correlation function. However, we also expect a correction from the first descendant of the t field, of the form $1/r^{2\Delta_t+2}$. Since $2\Delta_t + 2 \approx 4.8$ is very close to the independent estimate $2\Delta_s \approx 4.6$ obtained in Sec. VIIB, it will unfortunately not be possible to separate these two contributions by fitting QMC data for C_Z . We will here only be able to demonstrate that the second exponent is close to these two values. Analyzing both J - Q_2 and J - Q_3 data, we further reinforce the universal value of the scaling dimension $\Delta_t \approx 1.42$. Since the boundary enhancements of the Z correlation function is not significant, and also because we focus our quantitative analysis on $r = L/2$, there is no need to use the proxy conformal distance Eq. (10) here.

The definition of a 3×3 lattice cell containing eight four-spin operator (two singlet projectors) in a staircase arrangement was used in order for the Z correlation func-

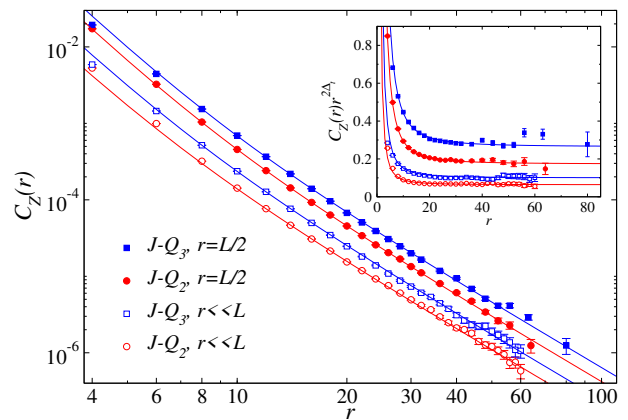


FIG. 14. Correlation function of the Z operator illustrated in Fig. 13. Red circles and blue squares show results for the near-critical J - Q_2 and J - Q_3 models, respectively, and in both cases results are shown for distances r much shorter than the system size (results averaged over lattices with $L \geq 256$) and for $r = L/2$ for a range of system sizes L . The curves show fits to Eq. (14) with fixed $\Delta_Z = 1.417$ and $\Gamma_Z = 2.417$ in all cases, with only the coefficients a and b optimized. The inset shows the results multiplied by $r^{-2\Delta_Z}$.

tion to not contain any potential contamination from scaling dimensions corresponding to symmetry-breaking singlet patterns [81]. We use the same definition of the Z correlator here, as illustrated in Fig. 13. Fig. 14 shows results for both the J - Q_2 and J - Q_3 models versus the separation r between the cells, in either cases for $r \ll L$ (lattices much larger than the maximum separation beyond which the results become too noisy) and also at $r = L/2$ for several system sizes up to $L \approx 100$. In the case of $r \ll L$, to improve the statistics we have averaged results for different lattice sizes $L \geq 256$ that do not show any differences beyond statistical errors. All these data sets indeed exhibit asymptotic decay with an exponent close to 2.8 and a secondary power law with exponent close to 4.8.

The data points for $r = L/2$ in Fig. 14 represent independent stochastic outcomes, unlike the correlated r points for the $r \ll L$ sets, and we therefore use the former to determine the best-fit exponents and statistical errors. For the J - Q_2 model, for which we have the best data, we fit to the function

$$C_Z(r) = \frac{a}{r^{2\Delta_Q}} + \frac{b}{r^{2\Gamma_Q}}, \quad (14)$$

and obtain a good χ^2 value already starting from $r = L/2 = 6$, with $\Delta_Q = 1.417(7)$ and $\Gamma_Q = 2.40(2)$. Here we identify the former value with the scaling dimension Δ_t and have entered the result in Table I. As for Γ_Q , it is very close to $\Delta_t + 1$, but we cannot exclude that this contribution is also mixed in to some extent with that expected from Δ_s .

The results obtained above with the J - Q_2 model at $r = L/2$ are also fully consistent with the r dependence

for $r \ll L$ as well as with analogous results for the $J-Q_3$ model. When fitting these other curves in Fig. 14, we fixed the two decay exponents to the same values as above, to explicitly show the good consistency between all the data sets. As in the case of the order parameter correlations in Sec. IV C 2, here again we do not need any L -dependent scaling corrections beyond the terms in Eq. (14) when fitting the correlations at $r = L/2$. Setting Γ_Q in Eq. (14) to Δ_s from Table I, we can still obtain good fits, though there should also be a component $\propto 1/r^{2\Delta_t+2}$ in this correlation function. In Sec. VI we will also present evidence for the Z operator containing only a very small amplitude of the $SO(5)$ singlet, and we therefore believe that Γ_Q represents a good estimate of $\Delta_t + 1$, which indeed is fully consistent with the fitted value.

Since the transitions in these models are eventually first-order, the algebraic decay seen in Fig. 14 cannot continue for ever but must eventually reflect phase coexistence. Given that the two phases should eventually, when the $SO(5)$ symmetry has broken down, undergo separation in Hilbert space, the correlation function should asymptotically approach a constant, reflecting large fluctuations from the finite system tunneling between the two phases. It is not clear whether such large fluctuations will also be present when the coexistence state still has an approximate $SO(5)$ symmetry. In any case, there are no signs of deviations from the power-law behavior up to the largest distances studied here—not even for much larger distances than in Fig. 14, where the results are too noisy to be useful for extracting the exponents but do not indicate any obvious deviations from the fitted form.

B. Conserved current operator

The W operator illustrated in Fig. 13(d) was studied in Ref. 53 in the context of a helically deformed VBS state. When the entire lattice is modulated in the staircase fashion as in the 5×5 cell depicted, the columnar VBS state acquires a twist that corresponds to helical order, most likely with arbitrary (incommensurate) periodicity in the thermodynamic limit. The staircase modulation of the Heisenberg couplings breaks the square-lattice symmetry, and it was shown that it induces non-zero winding number of the ground state wave function of the $J-Q_3$ model expressed in the valence-bonds basis [53], with the winding number directly related to the wavelength of the helical VBS order.

Many aspects of VBS states in $S = 1/2$ systems can be understood based on their close relationship to classical dimer models; in some cases they can be described by the same kind of height model, with a simple renormalized coupling constant [169, 176]. Winding numbers generally correspond to different topological sectors, which correspond to flux sectors when mapping to an effective electromagnetic theory [175]. The flux sectors are associated with a conserved Noether current, which in the

present case should not only be associated with the emergent $U(1)$ symmetry of the VBS but also with the larger emergent $SO(5)$ symmetry. When applied as a macroscopic perturbation to a critical $J-Q$ model, the W term induces the conserved current, as observed in the form of the helical VBS in Ref. 53.

We note here that the conserved winding number, and associated topological sectors, has been explicitly demonstrated in $J-Q$ models also at the AFM–VBS transition, not only in the ordered VBS phase [177]—where the conservation is essentially trivial, given that the valence bonds are short. Its conservation at criticality, where the bond-length distribution decays as a power law of the length, is directly related to the emergent $U(1)$ symmetry of the VBS.

The CFT current operator that is contained in the W operator must have scaling dimension $\Delta_j = 2$, and a value close to 2 was indeed found in Ref. 53, $\Delta_W = 1.90(2)$, though the identification of W as a current operator was not made. The conserved current was also recently studied using a correlation function in imaginary time [174], but using real-space correlations of the W operator seems an easier route. Though the operator may appear complicated, it is actually not difficult to study its correlation function in QMC simulations. It is also not necessary to use a cell as large as 5×5 spins, but any odd length can be used and results for 3×3 were also presented in Ref. 53. The larger cell has the advantage of producing a correlation function with larger overall amplitude, making it easier to extract the power law. The correlations show an interesting structure in the full 2D space (r_x, r_y) , as discussed in the Supplementary Material of Ref. 53. The strongest signal for extracting the decay exponent is along the line $(x, -x)$, which we also focus on here.

The previous result [53] for Δ_W was five error bars away from the expected result $\Delta_W = \Delta_j = 2$, likely as a result of some remaining finite-size corrections from short-distance data. We now have improved PQMC data and show the results in Fig. 15. Looking at the x dependence on lattices of size $L = 32, 64, 128, \text{ and } 256$, there is a systematic shift upward for r approaching $L/2$, reflecting boundary enhancement of these correlations. The trend for the distances where the finite-size effect becomes significant indicate that $L = 256$ is sufficiently large up to the largest r for which we have results with reasonably small error bars. Fitting to the $x \geq 12$ data, we obtain $\Delta_W = 2.01(3)$, and this value is stable within error bars also when including $L = 10$, which gives $\Delta_W = 2.03(2)$. While the latter fit is also statistically sound, it may be marginally affected by remaining short-distance corrections, noting that Δ_W further increases when additional small system sizes are included (which leads to fits of poor quality).

The data at $x = L/2$ in Fig. 15 still delivers a scaling dimension close to 1.90 [53] when small system sizes are included, even when a scaling correction is included, while the data for larger distances are consistent with

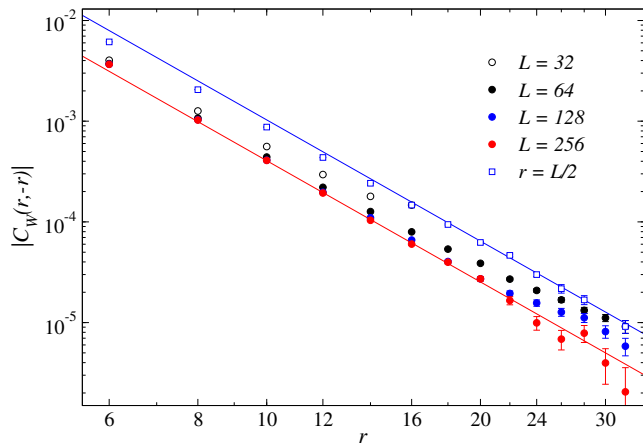


FIG. 15. Correlation function of the W operator defined in Fig. 13(d) along the lattice line $(x, -x)$ on near-critical J - Q_2 lattices of size $L = 32, 64, 128,$ and 256 , and also vs $r = L/2$ for other system sizes up to $L = 56$. The solid lines show the r^{-4} asymptotic decay expected for the conserved current operator ($\Delta_j = 2$). A power-law fit $C_W \propto x^{-2\Delta_W}$ to the $L = 256$ data for $r \geq 12$ gives $\Delta_W = 2.01(3)$.

$\Delta_W = \Delta_j = 2$. The data versus r for $L = 256$ exhibit less scaling corrections and we have entered our result from fitting these data for $r \in [12, 32]$ as Δ_j in Table I (excluding one more short distance than is necessary to obtain a statistically good fit).

C. Pseudo scaling dimension

The Q_n and J operators of the Hamiltonian must also contain both the t and s field operators, but the J - J and Q - Q correlation functions are complicated by the fact that they also contain the VBS order parameter. The dimer correlation function studied in Sec. IV is exactly a correlator of two J terms, though with phases corresponding to the modulation of singlet densities in a columnar state. The symmetric operators should be detectable in the uniform component of the same correlation functions but their contributions are harder to extract because of the faster power law decays (larger scaling dimensions)—we note that the value of $2\Delta_t \approx 2.8$ is not that far from $2\Delta_\phi + 2 \approx 3.2$, the leading correction exponent used in the fits in Fig. 10(b). The lattice arrangement of the spins of the Z operator in the previous section avoids this complication because it does not contain the VBS order parameter.

As first noted in Ref. 81, when the Q - Q plaquette correlations are averaged over the four columnar states in the ordered VBS phase the result vanishes on the line $(r, 0)$ with r odd. The same would be true also for a plaquette-ordered state, and then it will also hold for all fluctuations between the columnar and plaquette patterns that are realized when the critical VBS develops emergent $U(1)$ symmetry. Thus, on the $(r, 0)$ line it

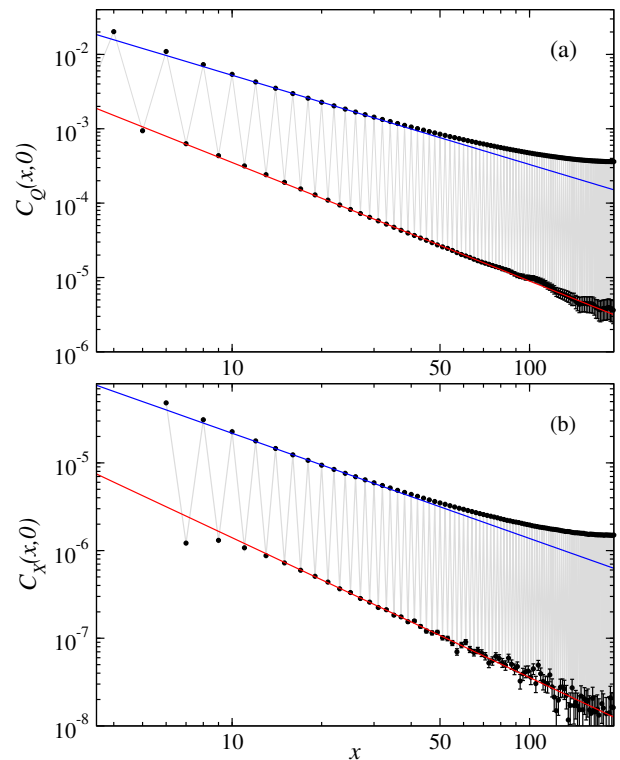


FIG. 16. Correlation function along a lattice axis of the four-spin Q (a) and X (b) operators in the near-critical J - Q_2 model on a lattice of size $L = 384$. The blue lines close to the even- x (upper) branch shows the power-law decay $x^{-2\Delta_\phi}$ of the order parameter, with $\Delta_\phi = 0.607$, while the red curves at the odd (lower) branch has the form $x^{-2\Delta_*}$ with $\Delta_* = 0.80$.

would appear that the uniform component of the Q - Q correlation function can be studied without the complications of eliminating the dominant VBS contributions. Indeed, the power-law decay corresponding to scaling dimension $\Delta_* \approx 0.80$ found in Ref. 81 matched the expected value for a symmetric operator driving a phase transition with correlation-length exponent $\nu_* = (3 - \Delta_*)^{-1} \approx 0.455$. However, we now have a more reliable estimate of ν_* (Sec. VII B), $\nu_* \approx 0.427$, which ruins the above relationship to Δ_* , which still has a value close to that determined previously.

In Fig. 16(a) we show the Q - Q correlation function $C_Q(r)$ computed using PQMC simulations of the J - Q_2 model on an $L = 384$ lattice with a slightly different definition of the Q operator, with just $\mathbf{S}_i \cdot \mathbf{S}_j$ as the individual bond operators instead of the singlet projector $\mathbf{S}_i \cdot \mathbf{S}_j - 1/4$ used in Ref. 81, the latter being more practical in SSE simulations. The even and odd branches clearly show different power-law decays. On the even branch, as shown with the blue line, the decay is consistent with the scaling dimension $\Delta_\phi \approx 0.61$ before the effects of the non-zero ordered moment become significant, similar to Fig. 7. For the odd branch, the red line shows the decay with $\Delta_* = 0.80$, which is the value we determine below by analyzing the decay at $r = L/2 - 1$ for a range of sys-

tem sizes. This value obtained in the ground state with PQMC simulations is very close to the result of Ref. 53, which was obtained with the SSE method with the inverse temperature scaled in proportion to L .

The X operator illustrated Fig. 13(c) consists of a single product of two-spin operators situated on the diagonals of a plaquette. Its correlation function $C_X(r)$ shows a behavior similar to C_Q , with the same scaling dimensions used to draw the lines in Figs. 16(a) and 16(b), but the overall amplitude of C_X is more than two orders of magnitude smaller. It is interesting to note that the odd- r branch does not show any significant enhancement of the correlations close to $r = L/2$, neither in C_Q nor in C_X . Even though this branch, unlike even r , does not sense the order parameter, one might still expect some boundary effect. The deviations from the power law are likely just small in this case.

Our analysis of both the Q - Q and X - X correlations is illustrated in Fig. 17, where we have multiplied the correlation functions by $r^{2\Delta_*}$ in order to make the corrections better visible. In the case of C_Q , we see violations of the scaling behavior for $r \gtrsim 40$, which we interpret as a crossover to the form expected (at some distance) in a first-order coexistence state. In such a state, the C_Q correlation function itself should approach a constant (due to the correlations being different in the AFM and VBS states, between which the system fluctuates) and the multiplier $r^{2\Delta_*}$ then causes the upward trend that is barely statistically significant Fig. 17(a). Such violations are not apparent in C_X , though they may also be present for $r \gtrsim 50$, where the statistical errors are large. We fit the data only up to r where the scaling violations do not seem significant.

From $C_Q(r)$ we obtained the value $\Delta_* = 0.800(3)$ by fitting data for $r \in [9, 39]$ to two power laws. The exponent of the correction is $4.7(2)$, which matches $2\Delta_s$ in Table [?] within the rather large error bar. When a third power law is added with fixed exponent equal to $2\Delta_t$, the amplitude of this term becomes very small. Thus, it seems plausible that the amplitude of the t field is small in the Q operator, while the overlap with the s field is significant. Since Q is the operator driving the AFM-VBS transition, the t field must of course be present to some extent, but there is no contradiction since the t content of the J operator can also be similarly small.

In the case of the X - X correlations, three power laws are required to describe the data. Unconstrained fits deliver exponents with large error bars and we instead fix the corrections to plausible values; the first one at $2\Delta_t$ and the second one in the range $[4.5, 4.8]$, corresponding either to $2\Delta_t + 1$, $2\Delta_s$, or some average of these two values. Such fits have good χ^2 values for $r \in [9, 51]$ and produce $\Delta_* \in [0.599, 0.600]$, fully consistent with the value from C_Q . We therefore have a high confidence in the value of Δ_* . The well defined power law behavior indicates that we are not here dealing merely with some slow gradual crossover to the first-order behavior, but truly a specific pseudocritical behavior governed by an

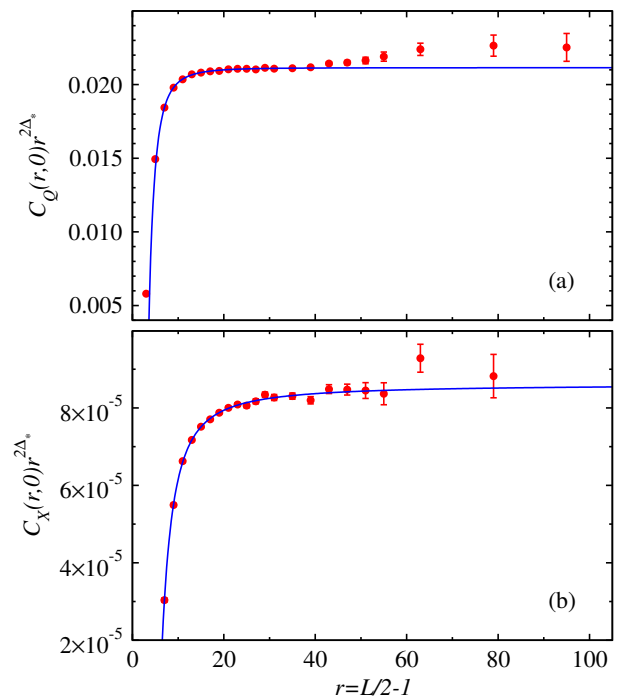


FIG. 17. Correlation function at distance $r = L/2 - 1$ of the Q (a) and X (b) of the J - Q_2 model, multiplied by $r^{2\Delta_*}$ with the best-fit value $\Delta_* = 0.80$. The blue curves show fits with one scaling correction in (a) and two corrections in (b), as discussed in the text.

exponent that does not appear directly in the CFT spectrum (but that we will derive from it in Sec. VIII A). We believe that Δ_* and ν_* must be related in some way, as two manifestations of the weakly perturbed CFT on the first-order line. With $\nu_* = (3 - \Delta_*)^{-1}$ clearly violated, it is not clear what the exact relationship is. A perturbative study of the $SO(5)$ CFT would hopefully give the answer.

In Fig. 18 we show results for the near-critical J - Q_3 model. The same critical decay as in the J - Q_2 model is manifested up to distances $r \approx 50$, but with different sign of the leading correction. In this case it is even more difficult to fit the corrections, and we only show a reference line to highlight a range of distances over which the decay controlled by Δ_* extracted from the J - Q_2 model holds rather well. At large distances there is an even clearer (statistically) upturn of the correlations from the critical form than in the J - Q_2 model. This more prominent precursor to the first-order behavior in the J - Q_3 model should again be a consequence of the slightly stronger first-order nature of its transition. Note that the behavior is very different away from the transition point, as illustrated in Fig. 18(a) with data slightly inside the AFM and VBS phases. In general, energy-type correlators should be expected to decay rapidly inside ordered phases, as we find, though we do not know the exact expected form.

An important aspect of our interpretation of the

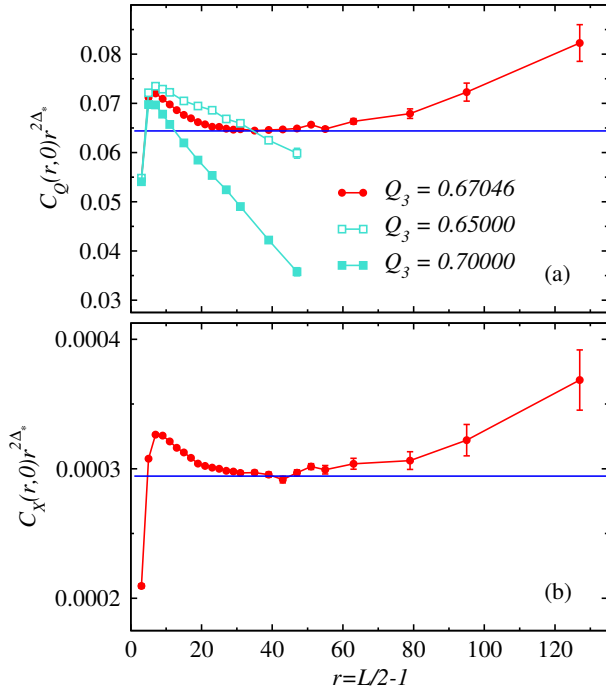


FIG. 18. Correlation function at distance $r = L/2 - 1$ of the Q (a) and X (b) operators in the near-critical J - Q_3 model ($Q_3 = 0.67046$, $J = 1 - Q$) and well as inside the AFM ($Q_3 = 0.65$) and VBS ($Q_3 = 0.67$) phases. The results have been multiplied by $r^{2\Delta_*}$, with $\Delta_* = 0.80$ having the same value as in the J - Q_2 analysis in Fig. 17.

pseudo dimension Δ_* is that it is not a member of the CFT spectrum and therefore cannot be “visible” exactly at the critical point. The natural way in which “fading” can take place upon approach to the critical is that the overall amplitude of contributions to correlation functions from Δ_* diminish gradually when the transition takes place closer to the critical point. Comparing Figs. 17 and 18, it is apparent that the amplitude of both correlations is more than three times larger in the J - Q_3 model, despite the fact that the values on the even- x branch (in Fig. 16 for the J - Q_2 model) differ by only about 10% (results not graphed here). Thus, the amplitude of the Δ_* correlator of the more critical J - Q_2 model has faded off to about 0.3 of its value in the J - Q_3 model. Fading is also manifested in the correlation length crossover schematically illustrated in Fig. 3, which will be demonstrated with data in Sec. VIII.

VI. SCALING ON THE AFM-VBS COEXISTENCE LINE

As we demonstrated in Sec. IV B, the J - Q_n models exhibit increasingly strong first-order discontinuities with n at their AFM–VBS transitions. We here add a third interaction to the J - Q_2 model in order to have two continuous tuning parameters and realize the line of first-order

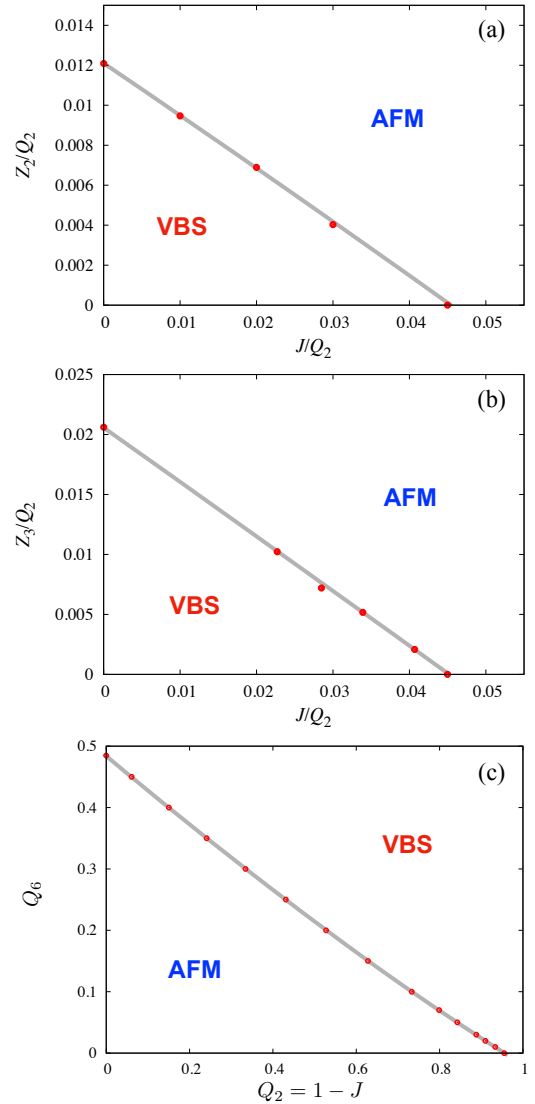


FIG. 19. Phase diagrams of models with two tuning parameters; (a) J - Q_2 - Z_2 , (b) J - Q_2 - Z_3 , and (c) J - Q_2 - Q_6 . Because the Z_n terms enhance the size of the AFM phase, J/Q_2 is used as the horizontal axis in (a) and (b). In (c), $Q_2 = 1 - J$ is used since the Q_6 term enhances the VBS phase.

transitions shown schematically in Fig. 2. We study the evolution of the phase transition extending from that of the pure J - Q_2 model with increasing coupling Z_2 , Z_3 , or Q_6 . The Z_2 and Q_6 interactions are illustrated in Fig. 1(c) and Fig. 1(e), respectively, and Z_3 is a direct generalization of Z_2 with one more singlet projector in the product, forming a staircase with three steps.

All results in this section were obtained using the SSE method, with the inverse temperature taken equal to the system size L . We define both order parameters, M_z (AFM) and $D = (D_x, D_y)$ (VBS), using the diagonal S_i^z

operators,

$$M_z = \frac{2}{N} \sum_{i=1}^N S_i^z (-1)^{x_i+y_i}, \quad (15a)$$

$$D_e = \frac{1}{N} \sum_{i=1}^N S_i^z S_{e(i)}^z (-1)^{e_i}, \quad e \in \{x, y\}, \quad (15b)$$

where $e(i)$ in Eq. (15b) denotes the neighbor of site i in the positive $e \in \{x, y\}$ direction and $e_i \in \{x_i, y_i\}$ are the site coordinates. A factor 2 is included in the definition of M_z in Eq. (15a) because the two order parameters are then of similar magnitude in their respective ordered phases. While this normalization is not crucial, when analyzing finite-size crossing points of the squared order parameters versus a tuning parameter, the L dependence is expected to benefit from a roughly equal scale of the two order parameters. We here denote the expectation values of the squared order parameters by $m_z^2 = \langle M_z^2 \rangle$ and $m_d^2 = \langle D^2 \rangle$.

We have used both the criterion $m_z^2 = m_d^2$ and analogous Binder cumulant (defined below) crossing points to extract the phase diagrams shown in Fig. 19, with the two criteria producing compatible results. We use J/Q_2 as the parameter on the horizontal axis for the J - Q_2 - Z_n models, switching to $Q_2 = 1 - J$ for the J - Q_2 - Q_6 model. In all three cases, we then have a phase boundary starting on the vertical axis and dropping down to zero versus the horizontal tuning parameter.

Like any generic lattice operator obeying all the symmetries of the Hamiltonian (when summed over all lattice translations), the added interactions can be expected to contain both the s and t fields of the CFT. Thus, we expect the introduction of Z_2 , Z_3 , or Q_6 into the J - Q_2 model to affect the way in which the phase transition is crossed, which corresponds to moving the dashed line in the schematic phase diagrams in Fig. 2. With the two generic tuning parameters g and k introduced in Fig. 3, as opposed to the orthogonal CFT scaling fields s and t , we can take $g \in \{J, Q_2\}$ and $k \in \{Z_2, Z_3, Q_6\}$ in the models studied here. We will here use a generic distance δ along with s and t .

In the case of Q_6 , we know that the transition is first-order for $Q_2 = 0$, continuing the trend of increasingly strong discontinuities found for J - Q_n models with n up to 4 in Sec. IV B. We therefore expect an increasing Q_6 value in the J - Q_2 - Q_6 model to move the system toward larger s values at the AFM–VBS transition, i.e., shifting the dashed line upward in Fig. 2. In the case of the Z_2 and Z_3 interactions, when $Q_2 = 0$ there is no phase transition versus Z_2/J (for the positive values of J and Z_2 that can be accessed with QMC simulations), while increasing Z_3/J eventually leads to a strongly first-order transition into a staggered VBS ground state [172]. When starting from the VBS phase of the J - Q_2 model and turning on one of the Z_n interactions, as on the left side of Figs. 19(a) and 19(b), both Z_3 and Z_2 rapidly destroy the VBS order, bringing the system into the AFM phase.

In the case of Z_3 , further increasing this coupling (beyond the values shown in the phase diagram) also leads to a subsequent transition from the AFM phase into a staggered VBS phase [172]. An extended phase diagram including both columnar and staggered VBS phases, and either a direct transition between the two or an intervening AFM phase, was studied in Ref. [173]. Here we will not consider the staggered VBS phase but observe that both Z_2 and Z_3 suppress the columnar VBS phase, in contrast to the clearly VBS enhancing Q_6 interaction.

To investigate how the AFM–VBS transition evolves on the first-order line, we first consider the J - Q_2 - Q_6 model. Here the changes with increasing Q_6 are very clearly observable because the coexisting order parameters in the J - Q_6 model are robust, much larger than those in the J - Q_2 model. However, as we will see, m_z^2 and m_d^2 still only reach a small fraction of their maximum values deep inside the respective ordered phases.

To test scaling with the exponent $\nu_s = (3 - \Delta_s)^{-1}$, we first study the dimensionless Binder cumulant U . For a system of size L at distance δ from the critical point, U should asymptotically be governed by a scaling function $u(x)$ the argument $x = \delta L^{1/\nu}$,

$$U(\delta, L) = u(\delta L^{1/\nu}), \quad (16)$$

where for a system on the coexistence line, i.e., ($t = 0, \delta = s$), $\nu = \nu_s$ should be expected. Otherwise, on approach to the critical point along some other line where both s and t are non-zero and $\delta = \delta(s, t)$, there should be a second scaling argument in Eq. (16); $U = u(sL^{1/\nu_s}, tL^{1/\nu_t})$. Since $\nu_t < \nu_s$, the behavior for large systems will be governed by this second argument. Scaling of U with $\nu = \nu_s$ can asymptotically be observed only on the first-order line, which is what we are pursuing here.

For scaling purposes, the distance of a system from the critical point on the first-order line can be taken as $\delta = Q_6 - Q_{6c} \propto s$ (close enough to the critical point so that any nonlinear behavior on the field s can be neglected), with some yet to be determined critical strength $Q_{6c} < 0$. The negative value of Q_{6c} follows from our expectation that increasing Q_6 above 0 will bring the system further away from the critical point than the very nearly critical J - Q_2 model. We also implicitly assume that the critical point exists in the real model space (i.e., it corresponds to a unitary CFT), though it is located outside the region $Q_6 \geq 0$ accessible with sign-free QMC simulations.

The most practical way to define a size dependent Binder cumulant at system size L is to use the common value of the AFM and VBS cumulants when they cross each other versus J at fixed Q_6 . To define the crossing point in an optimal way, the symmetry of the order parameters should be properly taken into account. When defining the AFM and VBS cumulants, in the past the symmetries of the individual order parameters have been employed in the standard way in the definitions so that $U_{\text{AFM}} \rightarrow 1$ and $U_{\text{VBS}} \rightarrow 0$ with increasing L in the AFM phase and $U_{\text{AFM}} \rightarrow 0$ and $U_{\text{VBS}} \rightarrow 1$ in the VBS phase. However, on the coexistence line close to the critical point

(up to some large system size), we expect a combined order parameter with emergent SO(5) symmetry (which we will show further support for in Sec. VII B). When studying the transition, it may therefore be better to define the two cumulants under the assumption that the AFM and VBS order parameters represent three and two components, respectively, of a five-component order parameter with SO(5) symmetry, which for our purposes again is no different from O(5).

The Binder ratio is defined as

$$R = \frac{\langle X^4 \rangle}{\langle X^2 \rangle^2}, \quad (17)$$

where X denotes an N -component vector (x_1, \dots, x_N) . In the ordered phase $X \rightarrow 1$ trivially, while in the disordered phase the value is easily obtained using Gaussian integrals. The cumulant with the desired values 0 and 1 in the two ordered phases is of the form $U = a(1 - U/b)$ with a and b depending on N . When it is in practice difficult to compute the full ratio R including all N components of X as in Eq. (17), one can also use some subset of the components—typically those corresponding to diagonal observables in the basis used—which is exactly what we do here. The coefficients a and b then have to be adjusted accordingly.

First consider the standard definitions. We here include only the z component of the 3-component AFM order parameter M and define the ratio

$$R_{\text{AFM}} = \frac{\langle M_z^4 \rangle}{\langle M_z^2 \rangle^2}, \quad (18a)$$

where M_z is defined in Eq. (15a) and is evaluated at a given “time slice” of an SSE configuration. The expectation values can be averaged in the usual way over many slices for better statistics. In the VBS case we use both components of the dimer order parameter defined in Eq. (15b);

$$R_{\text{VBS}} = \frac{\langle (D_x^2 + D_y^2)^2 \rangle}{\langle D_x^2 + D_y^2 \rangle^2}. \quad (18b)$$

The properly normalized cumulants are given by

$$U_{\text{AFM}} = \frac{5}{2} \left(1 - \frac{R_{\text{AFM}}}{3} \right), \quad (19a)$$

$$U_{\text{VBS}} = 2 \left(1 - \frac{R_{\text{VBS}}}{2} \right). \quad (19b)$$

The adjustments necessary under the assumption of SO(5) symmetry again only require trivial Gaussian integrals. In terms of the Binder ratios defined in Eqs. (18a) and (18b), the SO(5) cumulants are

$$U_{\text{AFM,SO(5)}} = \frac{35}{10} \left(1 - \frac{R_{\text{AFM}}}{3} \right), \quad (20a)$$

$$U_{\text{VBS,SO(5)}} = \frac{35}{10} \left(1 - \frac{R_{\text{VBS}}}{2} \right). \quad (20b)$$

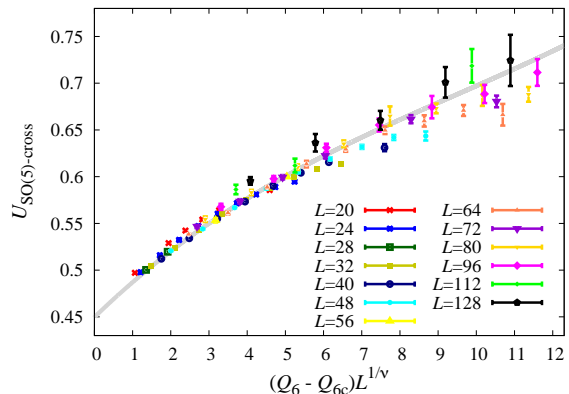


FIG. 20. Data collapse analysis of the common value of the SO(5) variants of the AFM and VBS Binder cumulants, Eqs. (20), at their finite-size crossing points. The SO(5) singlet exponent was fixed at $1/\nu_s = 3 - \Delta_s = 0.727$, corresponding to Δ_s in Table I, and only the critical point was optimized to $Q_{6c} = -0.07$ for best data collapse. The grey curve shows a polynomial fitted to the data points $U(Q_6, L)$ for which the finite size deviations are judged to be mainly statistical (excluding all sizes $L \leq 32$).

Asymptotically, for $L \rightarrow \infty$, the coexistence state does not host the higher symmetry, due to the dangerously irrelevant perturbations discussed in Sec. VII B, which become relevant in the presence of long-range order. Nevertheless, the length scale above which the SO(5) symmetry breaks down will be large, at least for small values of Q_6 . Even after the symmetry has broken down, crossing points of U_{AFM} and U_{VBS} will still represent the phase boundary properly, though likely with some crossover affecting the form of the scaling function.

We here simply test data collapse of the crossing values of the two SO(5) cumulants with our value of Δ_s in Table I, which corresponds to $1/\nu_s = 0.727$ in Eq. (16). For fixed Q_6 , we extract crossing values $U(Q_6, L)$ with error bars from polynomial fits to several (or the order 10) data points in the neighborhood of the transition versus Q_2 , i.e., scanning horizontally in Fig. 19. Results graphed versus the scaled distance to the critical point are shown in Fig. 20, where $Q_{6c} = -0.07(2)$ is the only adjustable parameter for optimizing the data collapse. Though the collapse is not perfect, the deviations from an ideal common scaling function are largely what would be expected from scaling corrections, e.g., the way the data for the smallest sizes shown here, $L = 20$ and $L = 24$, deviate somewhat from the other points for the scaling variable in the range roughly from 1 to 4. There is also a systematic peeling-off of data from the emerging scaling function in the form of a slower growth with the scaling argument as Q_6 increases for given L .

The scaling function to which the data should asymptotically collapse for sufficiently large L is normally analytic in the scaling variable. In Fig. 20 we have therefore fitted a cubic polynomial to the set of points that do

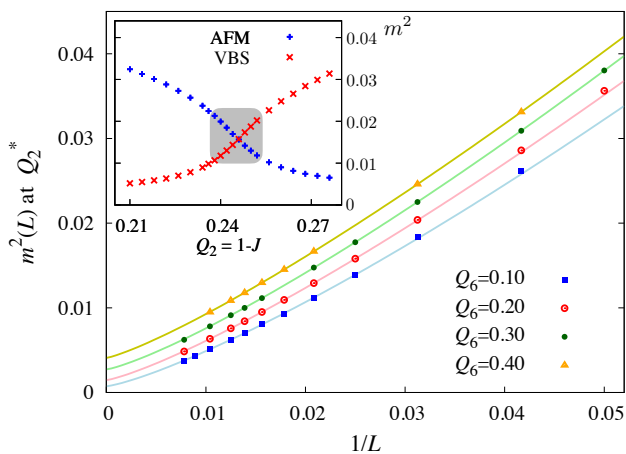


FIG. 21. The common value of the squared AFM and VBS order parameters on the coexistence line for several values of Q_6 . Error bars are much smaller than the symbol sizes in all cases. The definition of the crossing value $m^2(L)$ is illustrated in the inset for $Q_6 = 0.35$, $L = 48$. The crossing point $Q_2^*(L)$ is extracted from polynomials fitted to the data in the crossing region (roughly within the shaded square), where the order parameters are nearly linear. The crossing values are extrapolated in the main graph, using a constant plus a power law, shown with the curves.

not appear to be affected significantly by finite-size corrections. The points for the three largest system sizes deviate somewhat from the fitted scaling function. This flaw is most likely related to the eventual break-down of the emergent $SO(5)$ symmetry, which will take place for any point on the first-order line above some system size that depends on the distance to the critical point (as we will demonstrate explicitly in Sec. VII B). Since the violation of the $SO(5)$ symmetry is shifted to larger system sizes upon moving closer to the critical point, a valid scaling function (one that has the correct asymptotic form on approach to the critical point) can be defined by using only system sizes that are below the scale of $SO(5)$ break-down, as we have done.

Considering the single adjustable parameter and no obvious flaws beyond likely scaling for the smallest and very largest ($L > 100$) systems, these results support the scenario of a critical end point of a first-order transition. It should also be noted again that the exponent ν_s is unusually large, roughly twice the value at 3D $O(N)$ transitions with small N [60]. The good data collapse without adjusting any exponent is therefore a confirmation of a very different universality class.

As a further test, we extrapolate the order parameters to infinite size, first defining a common value m^2 as the crossing value $m_z^2(Q_2, L) = m_d^2(Q_2, L)$ at fixed Q_6 . We have also tried to extrapolate the individual AFM and VBS order parameters to infinite size separately, but such a procedure is very challenging because of the uncertainties in the location of the coexistence line. We can again in principle use the cumulant crossing points,

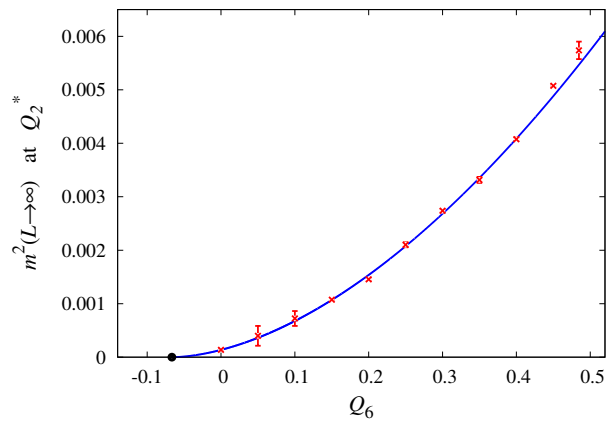


FIG. 22. Infinite-size extrapolated (as illustrated in Fig. 21) common value of the squared AFM and VBS order parameters at their finite-size crossing points, corresponding to the coexistence line in Fig. 19 for several values of Q_6 . The dependence on Q_6 (excluding the two points for largest Q_6) is fitted to the form $m^2 \sim (Q_6 - Q_{6c})^{2\beta}$, resulting in the critical point $Q_{6c} = -0.07(2)$ and exponent $\beta = 0.87(5)$.

but doing so we find that the VBS order parameter some times is non-monotonic in $1/L$, likely for similar reasons as discussed in Sec. IV B (Fig. 6). The crossing values $m^2(L) = m_z^2(L) = m_d^2(L)$ are ideal in this sense, guaranteeing that the coexistence line is followed in a completely systematic way, with the order parameters balanced at a consistent mix as a function of the system size.

It should be noted that the coexistence line is fundamentally broadened in a finite system, in the present case likely representing a window of asymptotic size $\propto L^{-(d+z)}$ with $d = z = 2$ [30]. Moving within this window will change the relative fraction of AFM and VBS order from values close to zero to order one and vice versa. For system sizes where the $SO(5)$ symmetry remains at the transition, this change in order parameters corresponds directly to the deformation of the five-sphere when the field t crosses 0. For larger systems, where the $SO(5)$ symmetry should be violated, the coexistence state realized in QMC simulations will eventually (for very large system sizes that are not reached here) correspond to the fraction of configurations (strictly speaking the fractions of equal-time slices of the spacetime configurations) with either type of order. In both cases, the change in relative fraction of the order parameters with the tuning parameter Q_2 will then be roughly linear around the value where $m^2(L) = m_z^2(L) = m_d^2(L)$.

Thus, the crossing method should provide a good definition of the center of the coexistence line, provided that the two order parameters have roughly the same scale. In practice, it is not possible to perfectly normalize the order parameters for an unambiguous center of the coexistence window, but, as shown in the inset of Fig. 21, our normalizations in Eq. (15) accomplish this balancing well. A good test for balance of the order parameters

close to an idealized mid-point of the transition region is to confirm that the crossing-point is located in the regime of the nearly linear dependence on the tuning parameter, which is the case in the inset of Fig. 21.

As illustrated in the main part of Fig. 21, we find that the common value $m^2(L)$ exhibits monotonic smooth behavior for all Q_6 values studied. All these systems are still nearly critical, i.e., for large system sizes the order parameters tend to very small values relative to their maximum attainable values. To fit the data, we therefore use a constant (representing the infinite-size squared order parameter) plus a power law, representing the near-critical decay of correlations.

As already discussed in the case of $Q_6 = 0$ in Sec. IV (in that case for the correlation functions at $r = L/2$, which also extrapolate to the squared order parameter), this fitting form cannot be asymptotically completely correct. We there focused on distances where the long-range order can be taken into account by only adding a constant to the critical decay form of the correlation functions. Here we instead focus on the way the long range order approaches its asymptotic $L \rightarrow \infty$ value, and the power-law form with optimized exponent (that is smaller than the critical exponent $1 + \eta$ but larger than 1) should be regarded as a way to approximately account for the crossover from the critical form to the asymptotic $1/L$ form [91] for a system with Goldstone modes.

While polynomials including $1/L^2$ and possibly higher-order terms may also seem appropriate, such fitting produces a high level of scattering (beyond the statistical errors) in the results versus Q_6 , which is not the case with the constant plus power law. The polynomial form should work well only when the systems are completely dominated by the Goldstone modes [91, 93], which is not yet true for the accessible system sizes here. Though the eventual crossover to polynomial form implies some errors in our extrapolated m^2 values, if this crossover takes place only for much larger system sizes (which is the case here, judging from the results in Sec. IV B), there is not much room remaining in $1/L$ for any drastic changes in the intercepts, as long as the true m^2 value is also not too small. To be clear, the balancing act here is rather delicate, and it is not a priori guaranteed that the procedure can deliver meaningful results.

The wxtrapolated order parameter in the entire range of QMC accessible Q_6 values are shown in Fig. 22. In the case of $Q_6 = 0$, we have data for much larger system sizes than in the other cases, and the extrapolated value therefore has smaller error bars than the $Q_6 > 0$ points close to 0. For larger Q_6 the extrapolations are more stable, as the corrections to the $L \rightarrow \infty$ constant (Fig. 21) are smaller. However, the simulations also become more demanding for larger Q_6 , and we are then limited to smaller system sizes and have larger statistical errors of the raw data.

The squared order parameter in the thermodynamic limit should grow as $\delta^{2\beta}$, here with $\delta = Q_6 - Q_{6c}$. In Fig. 22 we show a fit with β and Q_{6c} as free parameters,

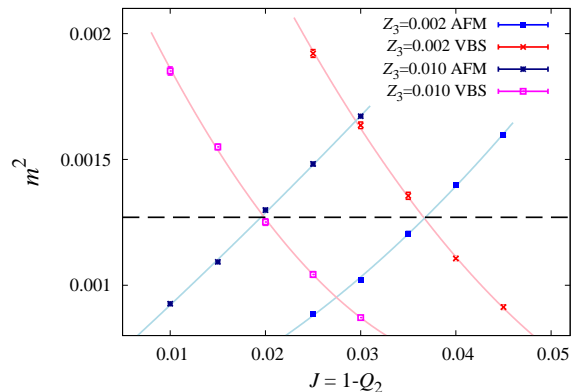


FIG. 23. The two squared order parameters defined in Eqs. (15) graphed vs the coupling J in the $L = 80$ J - Q_2 - Z_3 model at $Z_3 = 0.002$ and 0.01 , the latter value being situated about halfway up to the maximum value on the phase boundary in Fig. 19(b). As shown with the dashed horizontal line, the crossing value of the order parameters does not change appreciably with Z_3 .

leading to $\beta = 0.87(5)$ and $Q_{6c} = -0.07(2)$, the latter value (and error) coinciding with the critical point extracted from the optimized cumulant collapse in Fig. 20. Here we have excluded the two points with largest Q_6 values in Fig. 22. Including one or both of these points, the β value increases somewhat (not beyond the error bars) but the goodness of the fit χ^2 becomes larger than statistically acceptable. In general, the critical form governed by β should only apply in the close neighborhood of the transition. In the case at hand, m^2 is very small throughout the range of QMC accessible Q_6 values, and one may therefore expect the critical form to still apply at the largest Q_6 values. However, it is possible that the curve $m^2(Q_6)$ also has features related to the gradual breakdown of the $SO(5)$ symmetry (i.e., its manifestation on shorter length scales) with increasing Q_6 .

The exponent β is related to scaling dimensions of the critical point according to

$$\beta = \frac{1}{2}(1 + \eta)\nu_s = \frac{\Delta_\phi}{3 - \Delta_s} = 0.836(8), \quad (21)$$

where the numerical value is obtained with our values of Δ_ϕ and Δ_s in Table I. Thus, the fitted form in Fig. 22 agrees within one error bar with what is expected under the multicritical scenario. Using the values of the scaling dimensions from the CFT bootstrap calculation gives $\beta \approx 0.95$.

With Q_6 replaced by one of the Z_n interactions, we also expect to see the same kind of evolution of m^2 and the Binder cumulant on the first-order line. However, as shown in Fig. 23 for the Z_3 case, we observe almost no change in m^2 when Z_3 increases, and this applies also with the Z_2 interaction. This insensitivity of the order parameters even though the phase boundary shifts significantly suggests that there is very little overlap of the

s field of the CFT with the Z_n operators (at least for $n = 2, 3$). In Sec. V A we indeed concluded that the correlation function C_Z can be well fitted without including any contribution from the s field, though the closeness of the scaling dimensions Δ_s and $\Delta_t + 1$ makes it very difficult to discriminate between the contributions from the s field and the descendant of the t field.

It should also be noted that the maximum transition values of Z_2 and Z_3 in Figs. 19(a) and 19(b), i.e., at $J = 0$, are small. Therefore, the impact of the s field is also limited trivially by these small values of Z_n on the first-order lines. In the case of Q_6 , its maximum transition value is above 0.5 in Fig. 19(c), more than an order of magnitude larger than the maximum Z_2 and Z_3 values. The singlet content of the Q_6 operator is presumably much larger as well, due to the large spatial extent of this operator.

As a way to compare with the relatively large dependence on Q_6 in the J - Q_2 - Q_6 model, in Fig. 22 the value of m^2 changes only marginally, in absolute terms, from $Q_6 = 0$ to 0.02 (the maximum value of Z_3), and the changes are most notable for large system sizes (larger than those we have used for the J - Q_2 - Q_6 model with small Q_6). This comparison suggests that the combination of less singlet (likely much less) content in the Z_n operators and the smaller range of the control parameter should be sufficient to explain the differences between the models. It would still be useful to study J - Q_2 - Z_n models more extensively.

VII. EMERGENT SYMMETRIES

The emergence of a symmetry higher than that of the Hamiltonian at a critical point requires that all perturbations of said symmetry are irrelevant, i.e., in the case at hand, have scaling dimensions larger than $d + z = 3$. Scaling dimensions of various perturbations can be computed using correlation functions of corresponding local operators, as in Sec. V. However, if a system already contains an irrelevant perturbation of a given symmetry, as is essentially guaranteed in the case of emergent symmetries (except at some accidentally fine-tuned point), there is a more direct and efficient method: investigating the size dependence of a global (system integrated) quantity V that is zero if the symmetry is exact and non-zero in a finite system because of inherent perturbations. The coarse grained perturbation should decay with increasing size at the rate $L^{-|y_V|}$, where $y_V = 3 - \Delta_V$, which is much more favorable for numerical purposes than analyzing a very fast decaying correlation function $C(r) \propto r^{-2\Delta_V}$ with $2\Delta_V > 6$.

This method of exploiting intrinsic perturbations to extract irrelevant scaling dimensions was applied in Ref. 87 to 3D classical clock models i.e., the XY model with a non-zero \mathbb{Z}_q symmetric field added (for $q \geq 4$), or by restricting the spins to q “clock” angles (for $q \geq 5$). In Sec. VII A we use the same method to study the emergent

$U(1)$ symmetry of the VBS order parameter, determining the scaling dimension $\Delta_4 \approx 3.72$ of the leading lattice-induced \mathbb{Z}_4 perturbation. In this case the perturbation is unavoidable, being truly intrinsic to the model system, in contrast to being added at arbitrary strength to the Hamiltonian as in the clock models.

We also examine the expected relationship between $y_4 = 3 - \Delta_4$ of the deformation of the $U(1)$ symmetry and the exponent μ_4 governing its length scale, $\xi'_t \sim t^{-\mu_4}$, in the near-critical VBS phase. We write this relationship for general number of angles q , with $q = 4$ for the square-lattice VBS:

$$\mu_q = \nu \left(1 + \frac{|y_q|}{p} \right). \quad (22)$$

Here $p = 2$ in the classical q -state clock models [5, 85, 87] while a crossover from $p = 2$ to $p = 3$ was found in a quantum clock model in Ref. [178]. Our results for the J - Q_3 model (which we use in order to reach sufficiently deep into the VBS phase) are also consistent with $p = 3$, though we cannot exclude $p = 2$.

We study the the larger $SO(5)$ symmetry of the combined five-component AFM and VBS order parameters in Sec. VII B. Here a key result is that the most obvious $SO(5)$ perturbation inherent to the model, i.e., the \mathbb{Z}_4 lattice perturbation with scaling dimension Δ_4 , is not causing the same degree of deformation of the entire five-component order parameter as in the (D_x, D_y) plane. The AFM components of course always retain their exact $SO(3)$ symmetry, but the symmetry in the space of one each of the AFM and VBS components is also much less violated than the $U(1)$ symmetry of the VBS components. While the deformation of the VBS corresponds to the scaling dimension $\Delta_4 \approx 3.72$, the asymmetry between AFM and VBS components has the larger dimension $\Delta_{4'} = \Delta_4 + 1$ of a descendant operator of the primary \mathbb{Z}_4 deformation. This fact will be crucial when deriving the pseudocritical exponent ν_* in Sec. VIII. Studying the emergent $SO(5)$ symmetry, we also found a way to extract $1/\nu_*$ in Eq. (1) to high precision, which is what allows us to obtain the rather precise estimate of Δ_s in Table I.

A. \mathbb{Z}_4 perturbation and $U(1)$ crossover

Following Ref. 87, we treat the components (D_x, D_y) of the VBS order parameter in analogy with the magnetization (m_x, m_y) of the 3D q -state clock models. For details of the method and tests of consistency with the conventional approach based on correlation functions, we refer to Ref. 87. We use the J - Q_3 model in the analysis here, because it has a stronger \mathbb{Z}_4 deformation at criticality and can be pushed deeper into the VBS phase. The J - Q_2 model exhibits very similar behaviors but the statistical errors are larger.

Based on instances (D_x, D_y) of the VBS order parameter generated either in the converged ground state in

PQMC simulations or in SSE simulations at $T \propto L^{-1}$, we define an angular order parameter as

$$\phi_q = \langle \cos(q\Theta) \rangle, \quad (23)$$

where the angle (which we can always shift to the $[0, \pi/2]$ quadrant because of lattice symmetries) is

$$\Theta = \cos^{-1}(|D_x|/R), \quad R = (D_x^2 + D_y^2)^{1/2}. \quad (24)$$

This angle is not defined if $D_x = D_y = 0$, but such QMC configurations become extremely rare with increasing system size, and when they do occur we simply do not include them in the averaging. In principle we could avoid this issue altogether by instead of Eq. (23) using, e.g., $\langle R \cos(q\Theta) \rangle / \langle R \rangle$, or with some other power of R . Here we follow Ref. 87 and obtain good results with Eq. (23).

In a system with perfectly U(1) symmetric order parameter, clearly $\phi_q = 0$ for all q . In the 3D classical q -state clock models the clock perturbation is irrelevant for $q \geq 4$, and the scaling dimension Δ_q increases with increasing q . In a quantum magnet on the square lattice, the lattice itself induces a perturbation of a presumed U(1) symmetric coarse-grained VBS order parameter corresponding to $q = 4$ by the fact that the local singlets form on the lattice links with coordination number 4. When the angle Θ is defined for the VBS order parameter on the entire lattice, the coarse-graining scale is the lattice length L , and we therefore expect scaling of the $q = 4$ angular order parameter of the form $\phi_4 \sim L^{-|y_4|}$, with $y_4 = 3 - \Delta_4 < 0$. This is the scaling dimension that we target here.

In our PQMC simulations, we use the definition

$$D_e = \sum_{i=1}^N (-1)^{e_i} \mathbf{S}_i \cdot \mathbf{S}_{e(i)}, \quad e \in \{x, y\} \quad (25)$$

of the components of the VBS order parameter, where $i(e)$ denotes the nearest neighbor of site i in the x or y lattice direction, and e_i is likewise either the x or y coordinate of i . The off-diagonal quantity $\mathbf{S}_i \cdot \mathbf{S}_j$ for any i, j has a simple expression in the valence-bond basis used, being simply $-3/4$ or 0 , for sites i and j being, respectively, in the same loop or different loops in the transition graph representing overlap of the bra and ket states propagated by a sampled string of operators drawn from the Hamiltonian (Sec. III A) [93]. In SSE simulations, we instead use the diagonal definition, Eq. (15b), in the basis of S^z spins, taken at any ‘‘slice’’ in the periodic propagation dimension (which is directly related to imaginary time [185]). The corresponding angle Θ is then extracted in each case, and only the average ϕ_4 is taken over slices.

We can also average all S_i^z over imaginary time first and define (D_x, D_y) using such averages \bar{S}_i^z , which in SSE correspond exactly to imaginary time integrals;

$$\bar{S}_i^z = \frac{1}{\beta} \int_0^\beta d\tau S_i^z(\tau). \quad (26)$$

We then use \bar{S}_i^z in Eq. (15b) to define the instance of the order parameter (D_x, D_y) from which Θ is extracted according to Eq. (24), which corresponds to a full space-time definition of the global angle. The scaling dimension extracted from Eq. (23) should be the same as with the space-only definition.

Yet another way to define Θ in the angular order parameter is to use Q_n operators to define (D_x, D_y) . The Q_n operator summed over space with the appropriate $(\pi, 0)$ or $(0, \pi)$ phase detects the VBS order parameter as discussed in the context of the Q - Q correlation function in Sec. VIII. For the present purpose we use a space-time definition, because of the simplicity within the SSE approach of time integrals of operators in the Hamiltonian—they are simply obtained by counting operators in the sampled operator strings [171, 185]. Thus, for a given SSE configuration, we can compute

$$\bar{O}_i = \frac{1}{\beta} \int_0^\beta d\tau O_i(\tau), \quad (27)$$

where the operators O_i of interest here are the local Q interactions (Q_2, Q_3 , etc., depending on the model considered). Since we here use the J - Q_3 model, we should also take into account the lattice orientation of a given operator. Therefore, to evaluate this definition of D_e , $e \in \{x, y\}$, we count only the set q_e of Q_3 operators with e -oriented singlet projectors;

$$D_e = \sum_{i \in q_e} (-1)^{e_i} \bar{Q}_{3,i}, \quad e \in \{x, y\}. \quad (28)$$

Then again we extract the angle Θ corresponding to (D_x, D_y) and use it in Eq. (23).

1. Scaling dimension Δ_4

Results for the size dependence of ϕ_4 with all four definitions of Θ are shown in Fig. 24. We include PQMC data for three different couplings close to the transition point of the J - Q_3 model, in order to demonstrate the insensitivity of the results to small variations of J close to J_c ; among these, J_c is closest to $J = 0.4015$, which is also the coupling used in the SSE simulations. The PQMC results show very good power law scaling already from $L = 14$, and taking $L = 16$ as the smallest size in a fit we obtain $y_4 = -0.723(11)$, corresponding to the value $\Delta_4 = 3.723(11)$ entered in Table I. The SSE results with the three different Θ definitions are fully consistent with the above value of y_4 , but the finite-size corrections are much larger for the smaller systems. In this case we therefore do not carry out independent fitting but just show consistency, for the larger system sizes, with the same asymptotic power-law form.

Our value of Δ_4 is somewhat smaller than the CFT and fuzzy sphere results in Table I, though here again we point out that the CFT results depend to some extent (unknown in the case of Δ_4) on the exact value of the

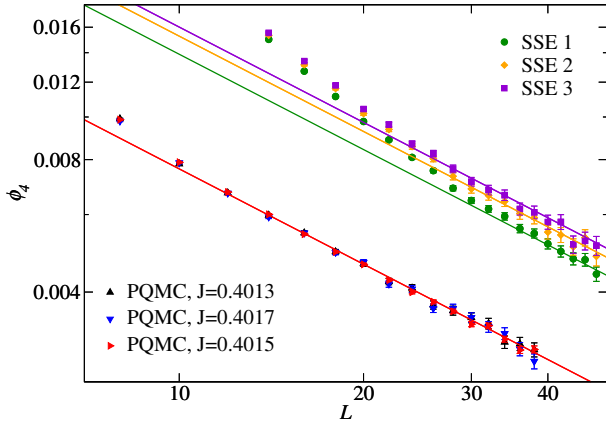


FIG. 24. Size dependence of the critical angular order parameter ϕ_4 of the J - Q_3 model (with $J + Q_3 = 1$). PQMC results based on the off-diagonal definition Eq. (25) of the VBS order parameter are shown for three different couplings close to the AFM–VBS transition. The results are so similar that the $J = 0.4015$ points cover the other results for many of the system sizes, and where the other points are seen they are still statistically indistinguishable. SSE results based on the three different definitions discussed in the text are shown for $J = 0.4015$, with the legends corresponding to: 1) the diagonal definition of the VBS order parameter Eq. (15b), 2) the same with S_i^z replaced by the time average \bar{S}_i^z in Eq. (26), and 3) with the Q_3 operator time average, Eq. (28). The red line is a fit to a power law of the $J = 0.4015$ PQMC data, delivering the exponent $y_4 = -0.723(11)$. The line drawn through the SSE data points have the same slope.

input parameter Δ_ϕ . In the case of the fuzzy sphere, the results are likely not yet fully converged in the number of orbitals included (or possibly the coupling used may not be located exactly at its critical value).

2. Emergent $U(1)$ scale in the VBS phase

While the \mathbb{Z}_4 perturbation is irrelevant at the critical point, it becomes relevant inside the VBS phase; the ground state is a four-fold degenerate columnar pattern with tunneling paths corresponding to \mathbb{Z}_4 symmetry for finite systems (see Ref. 32 for a discussion of the role of tunneling paths between the degenerate states) [25]. Such a perturbation of often referred to as dangerously irrelevant [82].

The length scale on which the emergent $U(1)$ symmetry is manifested inside the VBS phase should diverge faster than the conventional correlation length on approach to the critical point [23–25]. The exponent μ_q governing this $U(1)$ scale has been the subject of much work, and some controversy, in the context of the 3D clock models [83–86]. There is now overwhelming numerical evidence [85, 87] for Eq. (22) with $p = 2$, a relationship first (to our knowledge) derived in Appendix B of Ref. [5]. The derivation of this relationship involves the linearly dispersing gapless Goldstone mode of the $U(1)$

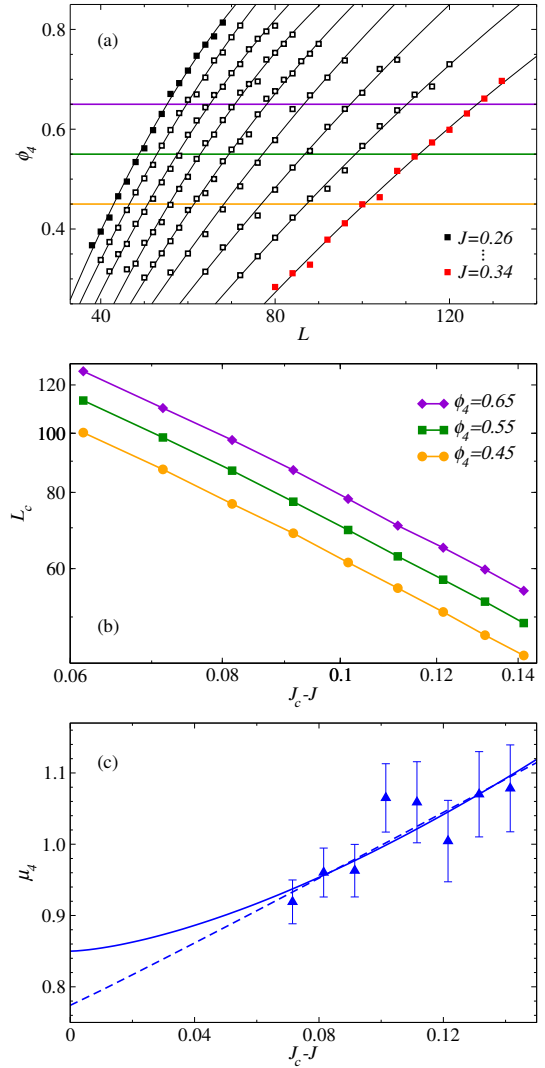


FIG. 25. (a) SSE results ($\beta = L$) for the size dependence of ϕ_4 (using τ -integrated Q operator definition) for several values of J inside the VBS phase of the J - Q_3 model, with $J + Q_3 = 1$. The horizontal lines are used to define crossing sizes $L_c(J)$ for three different values of ϕ_4 . (b) The crossing sizes vs the distance to the critical value $J_c \approx 0.4015$ extracted from the three lines in (a). (c) Local exponent extracted from pairs of points at adjacent J values in (b), using the scaling form $L_c \propto (J - J_c)^{-\mu_4}$. The asymptotic value of μ_4 should be given by Eq. (22) with $\nu_t = (3 - \Delta_t)^{-1}$ from Table I, $|y_4| \approx 0.72$ from the analysis in Fig. 24, and with either $p = 2$ or $p = 3$. The data points have therefore been fitted to $\mu_4(L) = \mu_4(\infty) + (J - J_c)^\omega$ with two values of the asymptotic exponent; $\mu_4(\infty) = 0.85$ and $\mu_4(\infty) = 0.77$, corresponding, respectively, to $p = 2$ and $p = 3$ in Eq. (22). The exponent ω reflects a scaling correction.

phase that the system flows toward (in a RG sense) before the clock perturbation becomes effectively large and brings the system to the ultimately \mathbb{Z}_q breaking fixed point. While $p = 2$ works well for the classical clock models, results for a 2D quantum clock model suggested a crossover from $p = 2$ to $p = 3$ with increasing systems

size [178]. The value $p = 3$ had also previously been argued for in the case of the clock models [84]. In Ref. [178] the crossover to $p = 3$ was also demonstrated in 3D classical clock models on lattices with $L \times L \times L_z$ spins when $L_z \gg L$, which in the quantum to classical mapping corresponds to the ground state of the 2D quantum clock model.

Like in the clock models, we expect Eq. (22) with $\nu \rightarrow \nu_t$ to hold also in the VBS phase of the J - Q_n models close to the critical point (i.e., for values of n for which the VBS–AFM transition is near critical). Thus, there should be an exponent μ_4 related to ν_t (the relevant correlation length exponent when tuning the system into the VBS phase) and $y_4 = 3 - \Delta_4$ according to Eq. (22). We next test this relationship with both $p = 2$ and $p = 3$.

SSE and PQMC calculations again deliver consistent results; here we show SSE results for the definition of the VBS order parameter used to extract Θ based on the τ -integrated Q operators, Eq. (27). Fig. 25(a) shows ϕ_4 versus the system size for several values of the coupling J of the J - Q_3 model in the regime where ϕ_4 is already approaching 1. Its scaling dimension is therefore 0, which is where Eq. (22) should apply [85, 87]. From these data, we can extract a length scale versus J by finding the intersection point with a line at fixed ϕ_4 , with three such lines drawn in Fig. 25(a). The resulting length scales L_c corresponding to the three lines are graphed versus $J - J_c$ in Fig. 25(b). Here the behavior is not yet the ultimately expected pure power law, $L_c \sim L^{-\mu_4}$. To study the evolution of μ_4 systematically, we therefore define a size-dependent exponent by assuming the power-law form to apply between adjacent- J points (which are equally spaced in J) in Fig. 25(b). The result for this floating exponent, where we have averaged results corresponding to all three fixed- ϕ_4 lines, is graphed versus $J - J_c$ in Fig. 25(c).

According to Eq. (22) with $\nu \rightarrow \nu_t \approx 0.63$ from Table I and $|y_4| \approx 0.72$ extracted above, we should have $\mu_4 \approx 0.85$ if $p = 2$ and $\mu_4 \approx 0.77$ if $p = 3$. To check the consistency with these values we simply assume it to be asymptotically correct and fit the data with a single adjustable power law correction in Fig. 25(c). Even without such fits, the results are clearly statistically consistent with Eq. (22) with either $p = 2$ or $p = 3$, given the large error bars. An independent reliable fit to the data with a constant plus power-law correction is not meaningful. The fit is marginally better with $p = 3$ but not enough so to rule out $p = 2$.

The way the data approach μ_4 in the expected range is reassuring, and there is no reason to doubt that emergent U(1) symmetry crossover in the near-critical VBS phase is governed by the same mechanisms as the emergent symmetry in the classical 3D clock models, only with different values of the exponents involved. It would be interesting to improve the results further by going to larger system sizes and reducing the error bars. These calculations are very time consuming, however.

Note that $y_4 \approx -0.11$ in the $q = 4$ clock model [87], i.e.,

this clock perturbation is much closer to being relevant than the lattice deformation of the U(1) symmetry at the AFM–VBS transition. Most of the works on the clock models were done for $q = 6$ [87, 178], where $|y_4|$ is larger and all the crossovers can be studied in greater detail.

Here we also point out that studies of J - Q models on the honeycom lattice, with coordination number and VBS degeneracy $q = 3$, have indicated that there is no emergent U(1) symmetry on this lattice [167, 168]. The quantity ϕ_3 does not decay to zero but appears to approach a constant, which would imply that the perturbation is marginal. It is also possible that the \mathbb{Z}_3 perturbation is weakly relevant, so that larger lattices would be required to observe a clearly growing ϕ_3 . In the presumed SO(5) CFT, the $q = 3$ perturbation is indeed clearly relevant [55, 59, 61].

B. Irrelevant SO(5) perturbations

The U(1) symmetry of the VBS order parameter should be just one aspect of the emergence of the higher SO(5) symmetry. We next study another inherent deformation of the SO(5) sphere, using quantities involving one component each of the AFM and VBS order parameters. We choose the z spin component M_z of the staggered magnetization and one of the components, D_x or D_y , of the VBS order parameters and use these to test for SO(5) symmetry in the full five-component vector $(M_x, M_y, M_z, D_x, D_y)$. Here we can use the fact that the components (M_x, M_y, M_z) obey an exact SO(3) symmetry and (D_x, D_y) transform under \mathbb{Z}_4 that becomes U(1) at the phase transition.

The diagonal M_z AFM order parameter was defined in Eq. (15a). For the VBS order parameter, we again use the definition in Eq. (15b) and Eq. (25) with the PQMC and SSE methods, respectively. We can then extract an angle Θ as in Eq. (24) based on the components (M_z, D_x) or (M_z, D_y) and study the angular order parameters ϕ_q in Eq. (23) for different values of q . However, to stay closer to previous works studying emergent SO(5) symmetry, we will here proceed with alternative quantities.

Nahum et al. [35] considered generalizations of ϕ_q :

$$\phi_{q,a} = \langle r^a \cos(q\Theta) \rangle, \quad (29)$$

where Θ is the angle between an AFM and a VBS component, and r is a normalized length of the vector that in our notation has the components $M_z / \langle M_z^2 \rangle^{-1/2}$ and $D_x / \langle D_x^2 \rangle^{1/2}$. They noted that, for $a = 4$, these expressions can be converted in to simple forms only involving expectation values of powers of the order parameters; specifically, for $q = 2$ and $q = 4$ they used

$$F_2 = \frac{\langle M_z^4 \rangle}{\langle M_z^2 \rangle^2} - \frac{\langle D_x^4 \rangle}{\langle D_x^2 \rangle^2}, \quad (30a)$$

$$F_4 = \frac{\langle M_z^4 \rangle}{\langle M_z^2 \rangle^2} + \frac{\langle D_x^4 \rangle}{\langle D_x^2 \rangle^2} - 6 \frac{\langle M_z^2 D_x^2 \rangle}{\langle M_z^2 \rangle \langle D_x^2 \rangle}, \quad (30b)$$

which are equivalent to $\phi_{4,2}$ and $\phi_{4,4}$, respectively, in Eq. (29). Both these quantities must vanish if the system has exact SO(5) [or O(5)] symmetry, and the non-zero values inside the SO(3) symmetric AFM phase and the \mathbb{Z}_4 or U(1) symmetric (depending on the length scale) VBS phase can also be easily computed.

We will here consider the J - Q_2 , J - Q_3 , and J - Q_4 models only at and very close to their transition points but have also confirmed the correct values of F_2 and F_4 inside the ordered phases. In the expressions above we can substitute D_x for D_y , but when considering a single component of the staggered magnetization we only have diagonal access to M_z in both SSE and PQMC simulations (though we also have access to M^2 and M^4 through loop estimators, which we will not make use of here).

Nahum et al. showed that the 3D loop model has very small F_2 and F_4 values at the transition point—zero within statistical errors that were relatively large for large systems [28]. However, the system size dependences were not studied in detail. Here we will use the size and coupling dependence of these quantities to gain new insights into the emergence and eventual violation of SO(5) symmetry.

Figure 26 shows results for both F_2 and F_4 in the J - Q_2 model for three different lattice sizes. In the AFM phase, asymptotically for $L \rightarrow \infty$ we must have $F_2 \rightarrow -7/5$, while in the VBS phase $F_2 \rightarrow 2$ because of the \mathbb{Z}_4 symmetry of (D_x, D_y) and there is an intermediate scale at which $F_2 \rightarrow 3/2$ because of the emergent U(1) symmetry [35]. Thus, we expect F_2 to change signs close to the transition point, eventually approaching 0 at the transition if there is emergent SO(5) symmetry. The point at which 0 is crossed indeed moves toward the transition point in Fig. 26(a), which is shown in detail in Fig. 27(a) with results for L up to 256. The quantity F_4 is negative inside both phases and, as seen in Fig. 26(b), is positive within a window of couplings that shrinks as L increases, as also demonstrated explicitly in Fig. 27. Note that the $F_4 = 0$ points always bracket the $F_2 = 0$ point. Fig. 27(b) shows how the bracket shrink to zero as a power law with increasing system size; we will discuss the meaning of the corresponding exponent further below.

In analogy with the quantity ϕ_4 studied in Sec. VII A, F_4 at the transition point is a quantitative measure of the violation of the SO(5) symmetry (provided that this symmetry really is emergent) at a scale given by the system size L . Thus, we would expect F_4 at the transition point to scale as $L^{-|y|}$, where $y = 3 - \Delta$, with Δ the smallest of the scaling dimensions of the irrelevant SO(5) perturbations present in the lattice model. One might expect that $y = y_4 \approx -0.72$, the value determined from the decay of ϕ_4 in Fig. 24. However, as shown in Fig. 28, the y value governing F_4 of the J - Q_2 model is much larger in magnitude; $y \approx -1.72$ for system sizes from $L = 6$ to $L \approx 50$ (and deviations for larger L should arise from non-critical effects, as discussed further below). The results in Fig. 28 were all obtained with PQMC simulations very close to the transition point, but SSE results for the J - Q_2 model,

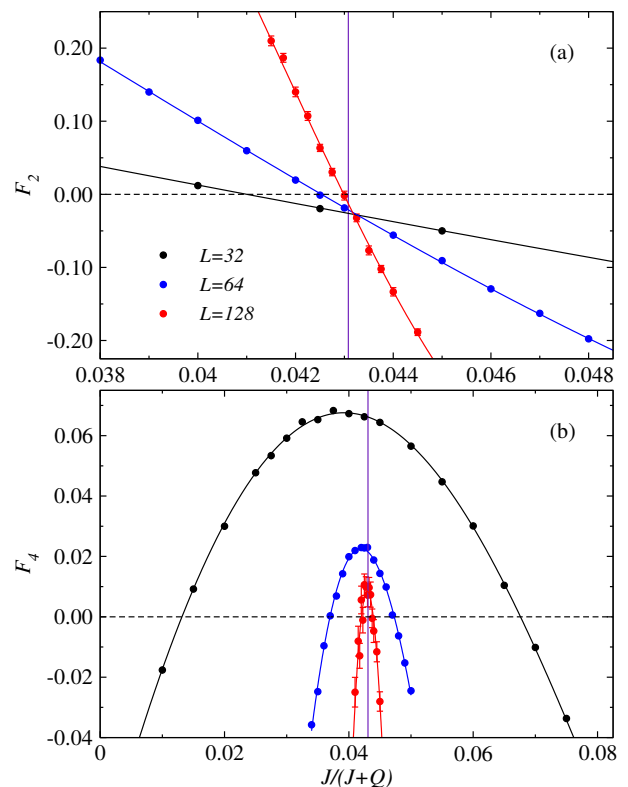


FIG. 26. The SO(5) diagnostic functions F_2 and F_4 computed with SSE simulations ($\beta = L$, $J+Q = 1$) vs the coupling ratio $J/(J+Q)$. Results are shown for three different system sizes to illustrate how F_2 crosses 0 close to the transition while F_4 exhibits a non-monotonic behavior, crossing 0 twice. The curves show polynomial fits. The interpolated J values at which $F_2 = 0$ and $F_4 = 0$ are graphed vs the inverse system size in Fig. 27

like those in Fig 26 interpolated to the transition point, fall almost exactly on top of the PQMC results (with larger error bars).

At first sight this large discrepancy between the irrelevant exponents may appear surprising, but there is a natural explanation that gives us further insights into the nature of the inherent SO(5) perturbations in our models. The value of the exponent from the J - Q_2 results in Fig. 28, $y \approx -1.72$, which we will from now on refer to as $y_{4'}$, is intriguingly close to $y_4 - 1$, with y_4 from the emergent U(1) deformation in Fig. 24. The values cannot be distinguished within statistical errors in the range of L for which the power law holds. This simple relationship would correspond to an operator with scaling dimension $\Delta_{4'} = \Delta_4 + 1$. The most likely explanation for this relationship is that the operator at play here is the first descendant of the primary CFT operator with scaling dimension Δ_4 . What this suggests is that the primary lattice perturbation of the SO(5) symmetry, which is inherent to the model and quantitatively characterized by Δ_4 , only induces a secondary (derivative) perturbation that breaks the symmetry between the AFM and

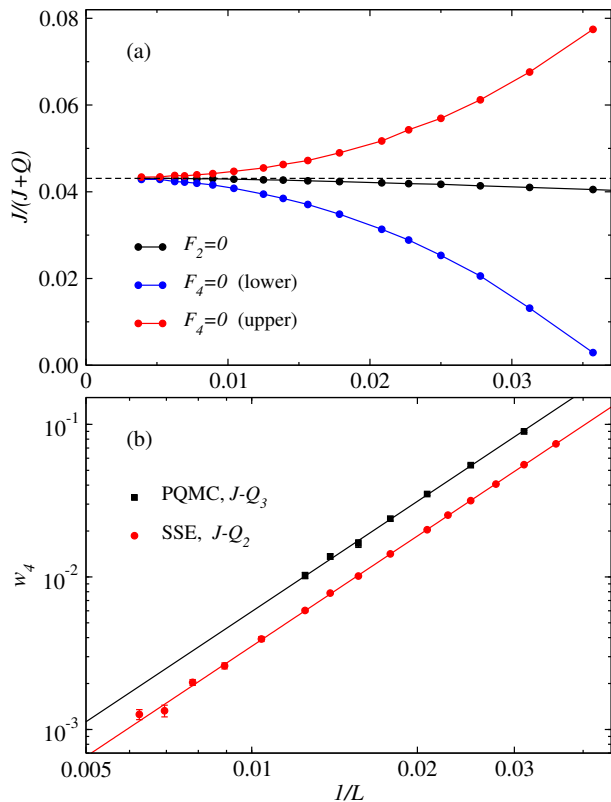


FIG. 27. (a) Zeros of the functions F_2 and F_4 , extracted by fitting polynomials to SSE data such as those in Fig. 26 of the $J-Q_2$ model. The horizontal dashed line shows the location of the extrapolated AFM–VBS transition—at $J_c/Q_2 = 0.04502$, here rescaled to $J_c/(J_c + Q_2)$ pertaining to these simulations carried out with $J + Q = 1$. (b) Log-log plot of the size of the window between the upper and lower $F_4 = 0$ points are shown with red circles for the $J-Q_s$ model in (a). The black squares show analogous results for the $J-Q_3$ model obtained with PQMC simulations. The straight lines shows the scaling form $w_4 \sim L^{-1/\nu_*}$ with $1/\nu_* = 2.402$.

VBS components of the order parameter. Any CFT operator present in the lattice model that directly (not as a secondary effect of the lattice) perturbs this symmetry between the AFM and VBS components must then have a much higher scaling dimension, so that it is essentially invisible in the scaling of F_4 . To our knowledge, this aspect of the emergent $SO(5)$ symmetry has not been discussed before, but we find the scenario intuitively plausible.

There is a further important message conveyed by Fig. 28: While the initial decay of F_4 for the $J-Q_2$ model, up to system sizes $L \approx 50$, is governed by $y_{4'} \approx -1.72$, for larger systems the decay slows down. This behavior could in principle be interpreted as an eventual slower power law decay (smaller scaling dimension Δ'_4). However, the deviations from the fitted $y_{4'}$ line occur for slightly smaller system sizes for the $J-Q_3$ model, and for the $J-Q_4$ model there is no range of L with power-law decay at all, only a gradual flattening out. Knowing that the first-order discontinuities of the AFM–VBS transi-

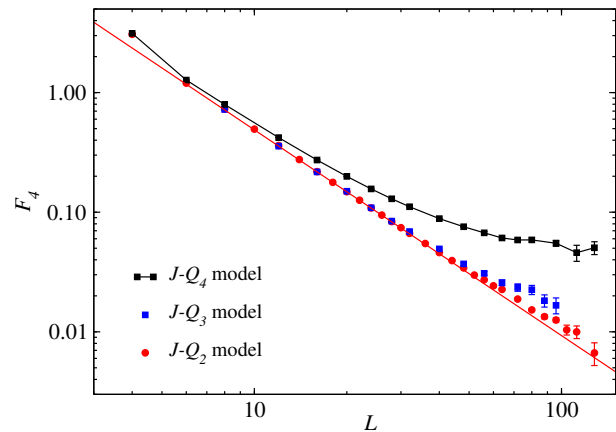


FIG. 28. Size dependence of the function F_4 computed with PQMC simulations in the near-critical $J-Q_2$, $J-Q_3$, and $J-Q_4$ models. The line drawn through the $J-Q_2$ data for $L \lesssim 50$ has slope -1.72 , corresponding to $y_{4'} = y_4 - 1$, with $y_4 \approx -0.72$ determined in Fig. 24. Deviations from the critical form for the largest system sizes (essentially all sizes in the case of the $J-Q_4$ model) indicate the length scale at which the emergence of $SO(5)$ symmetry is affected by the first-order transition. Note that the $J-Q_3$ points completely cover many of the $J-Q_2$ points because of the close coincidence of the values.

tion become stronger for $J-Q_n$ models as n increases, the large- L behaviors of the $J-Q_2$ and $J-Q_2$ data in Fig. 28 are plausibly explained as the initial stage of the breakdown of the $SO(5)$ symmetry, as indeed eventually expected in the coexistence state.

The corresponding length-scale of $SO(5)$ symmetry in the coexistence state should be given by Eq. (22), now with $\nu \rightarrow \nu_s$ and $|y_q| \rightarrow |y_{q'}| = |y_q| + 1$. Using the values of the exponents that we have determined (Table I), we obtain a very large exponent, $\mu_s \approx 2.8$, for the exponent governing the divergence of the $SO(5)$ length scale upon approaching the critical point. In principle we could test this value in the same way as we tested the expected value of μ_4 in Sec. VII A, by monitoring F_4 versus the system size for points on the coexistence line that we determined in the phase diagram of the $J-Q_2$ - Q_6 model in Sec. VI. However, such a program is currently computationally expensive and we have not pursued it.

C. $SO(5)$ finite-size window

Returning to the $J-Q_2$ data in Fig. 26, we next investigate the zeros of the F_2 and F_4 functions in Fig. 27(a) more carefully. Here we observe that the J point where $F_2(J, L) = 0$ moves toward the previously extracted transition point with increasing L , and this point is always (for any L studied) between the two points where $F_4(J, L) = 0$. We have already seen above that $F_4 \rightarrow 0$ at the infinite-size critical point (though in the models, which are not exactly at the critical point, F_4 will eventually flow away from 0 for large system sizes), and we

have also confirmed that F_4 at its L dependent peak coupling exhibits the same scaling governed by the exponent $y_{4'} \approx -1.72$. Thus $F_4 \rightarrow 0$ as L grows in the entire region between the couplings where the function vanishes. This behavior is of course qualitatively necessary for there to be emergent $\text{SO}(5)$ symmetry at the critical point, and the above results reinforces the notion that such a critical point is almost realized in the J - Q models in the QMC accessible part of their phase diagrams.

The region between the zeros of $F_4(J, L)$ can be taken as a practical definition of the finite-size region where the system hosts an emergent $\text{SO}(5)$ symmetry that is gradually violated when moving out from the transition point, which can be taken as the point where $F_2 = 0$ or the peak location of F_4 . An important quantitative question is then how this region shrinks with increasing L . The width w_4 of the $\text{SO}(5)$ region defined by the zeros of F_4 is graphed versus the inverse system size on log-log plot in Fig. 27(b) for both the J - Q_2 and J - Q_3 models. In both models we observe the same kind of decay by a single power law, $w_4 \sim L^{-a}$, with apparently very small corrections. From the J - Q_2 results we can extract the exponent $a = 2.402(6)$, which is a very stable value with respect to the number of points included in the fit. Here we point out that the smallest system size included in Fig. 27(b), $L = 32$, is the first size for which the two zeros of F_4 are both within the QMC accessible region $J \geq 0$ (as is in Fig. 26). The fit to the single power law is of good statistical quality already starting from this L .

The power law forms of $F_4(J_c, L)$ and w_4 suggest that $F_4(J, L)$ obeys the scaling form

$$F_4 = L^{-|y_{4'}|} f(\delta L^a), \quad (31)$$

in the close neighborhood $\delta = J - J_c$ of the transition at $\delta = 0$. In Fig. 29(a) we show PQMC data for the J - Q_3 model over a wide range of the tuning parameter and system sizes, which we replot in Fig. 29(b) in the manner that should lead to data collapse if Eq. (31) holds. Systematic collapse indeed builds up as the system size increases, with $f(x)$, $x = \delta L^a$ forming a close to parabolic shape and with data peeling off from this form at values of $|x|$ that increase with L . As shown in Fig. 29(c), the peeled off data instead exhibit data collapse when the rescaled variable is $x = \delta L^{-1/\nu_t}$, then with no rescaling of the value of F_4 .

The asymptotic value of F_4 inside both ordered phases is negative of order one [28]. Thus, its scaling dimension in the ordered phases should be taken as zero, as we do in Fig. 29(c). It is also natural that the scaling here is controlled by the exponent ν_t corresponding to the tuning parameter, with J largely driving the t field. The different scaling seen very close to the transition in Fig. 29(a) reflects the emergence of the $\text{SO}(5)$ symmetry in the overall decay of F_4 to zero, $F_4 \propto L^{-|y_{4'}|}$, but the scaling variable $x = \delta L^a$ with $a = 2.40$ does not have any apparent explanation from the CFT, matching neither $1/\nu_t$ nor $1/\nu_s$. The value is very close to $1/\nu_\phi = 3 - \Delta_\phi$, with the order parameter scaling dimension Δ_ϕ from Ta-

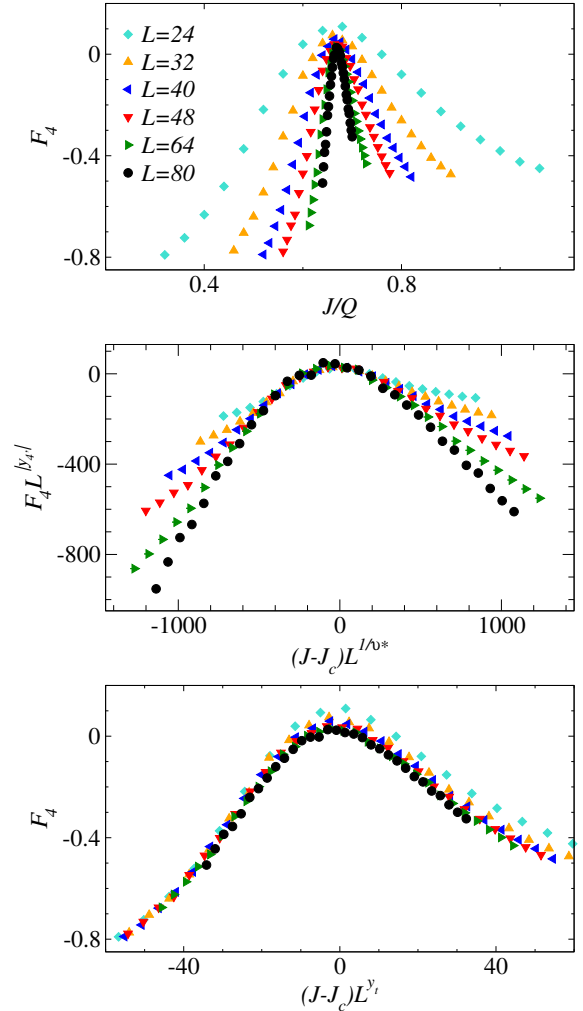


FIG. 29. Scaling analysis of the function F_4 from PQMC simulations of the J - Q_3 model. (a) Raw data in the neighborhood of the VBS–AFM transition vs J ($Q = 1$) for different system sizes. (b) Scaling collapse in the neighborhood of the maximum, where the magnitude of F_4 decays as $L^{-|y_{4'}|}$ with $y_{4'} \approx -1.72$, according to Fig. 28, and its dependence on J is controlled by $1/\nu_* = 2.40$ according to the scaling observed in Fig. 27(b). The data collapse extends to larger values of the scaled coupling $(J - J_c)L^{1/\nu_*}$ with increasing system size. (c) Data sufficiently far from the maximum—the points peeling off from the common scaling function in (b)—are collapsed by scaling $(J - J_c)L^{1/\nu_t}$. Here F_4 is dimensionless, i.e., there is no rescaling of the value of F_4 .

ble I. However, $1/\nu_\phi$ controls the behavior when an order parameter field is added to the Hamiltonian, i.e., breaking its symmetries explicitly. There are no such symmetry breaking terms in the Hamiltonian, and therefore the exponent a cannot be $1/\nu_\phi$.

The only plausible explanation we can find for the value of a is to identify it with the pseudocritical length scale illustrated in Fig. 3. It was previously believed that $1/\nu_* \approx 2.20$ [41, 81], corresponding to the correlation length exponent $\nu \approx 0.45$ in both the J - Q_2 [41, 81] and

the classical loop model [28]. However, the extrapolations of the quantities used to obtain this value of ν are challenging, as large system sizes are required for convergence of, e.g., Binder cumulant slopes, and the statistical errors grow with L . As we will see in Sec. VIII, $1/\nu = 2.40$ also fits high quality data very well. Moreover, in Sec. VIII A we will derive an expression for $1/\nu_*$ by explicitly evoking the dangerously irrelevant operator that is responsible for violations of the SO(5) symmetry on the first-order line. The way F_4 detects the emergence and breakdown of the SO(5) symmetry in the neighborhood of the transition driven by the t field conforms with the picture painted there. Thus, we identify a as $1/\nu_*$.

Beyond Eq. (31), a more complete form of the scaling form of F_4 involves also ν_t and ν_s

$$F_4 = L^{-|y_4|} f(\delta L^{1/\nu_*}, \delta L^{1/\nu_t}, \delta L^{1/\nu_s}). \quad (32)$$

Since $1/\nu_* > 1/\nu_t > 1/\nu_s$, there is a regime where $\delta L^{1/\nu_*}$ is much larger than the other two arguments but still relatively small so that the function f can be Taylor expanded in this argument—this regime corresponds to the near parabolic shape formed by the collapsed data in Fig. 29(b). When also the argument $\delta L^{1/\nu_t}$ becomes large, the function eventually crosses over to a form dominated by this argument; $f \rightarrow f(\delta L^{1/\nu_t})$, as seen in the data collapse plot Fig. 29(c). The third argument $\delta L^{1/\nu_s}$ will also to some extent influence the behavior further away from $\delta = 0$. In Sec. VIII we will present several examples of physical observables that can be described by similar functions of three arguments, and where all of them are needed to fully describe numerical data.

To conclude the discussion of the emergent SO(5) symmetry, in Fig. 30 we show a data collapse analysis for the function F_2 obtained with both PQMC and SSE calculations (using different windows on the x axis). This analysis confirms that F_2 should be regarded as dimensionless, i.e., no scaling of the function values are required to achieve data collapse. This may not be surprising, considering that F_2 in Eq. (30a) is the difference between two Binder ratios, both of which are dimensionless, though in principle the difference very close to the transition point could be a subleading contribution with scaling dimension $\Delta > 3$, of which we see no sign here.

In Fig. 30(b) and the main part of Fig. 30(a) the distance from the transition point is scaled with the conventional correlation length exponent ν_t , which follows from the fact that F_2 measures the violations of the SO(5) symmetry that are “manually” tuned by the parameter J , taking the system between the AFM phase with SO(3) order parameter and the VBS phase with emergent U(1)=O(2) symmetry by effectively deforming the five-sphere defining the order parameter. To effectively cancel a possible scaling correction, we have here used the size dependent distance $J - J_c(L)$ from the critical point, with $J_c(L)$ defined as the point where $F_2(J, L) = 0$, graphed for the J - Q_2 model in Fig. 27(a). The essentially perfect data collapse for system sizes up to $L \approx 100$ of a function manifestly probing the imposed deformation of

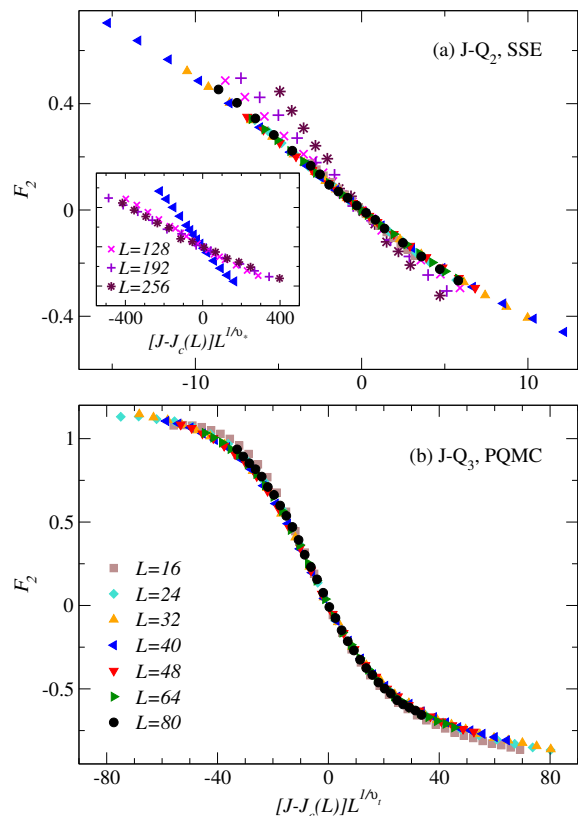


FIG. 30. The function F_2 of the J - Q_2 (a) and J - Q_3 (b) models, obtained with SSE ($Q_2 = 1$, $\beta = L$) and PQMC simulations, respectively. The distance $J - J_c(L)$ to the size-dependent critical point is defined here by $F_2 = 0$ from Fig. 27(a) (and similar PQMC results) and is rescaled by L^{1/ν_t} , with $\nu_t = (3 - \Delta_t)^{-1} = 0.63$ from Table I.

the SO(5) order away from the transition lends further support to the interpretation of the exponent $\nu_t \approx 0.63$ as that of the traceless symmetric tensor.

In Fig. 30(a) we observe clearly that the data for system sizes $L = 128$ and above do not collapse to the common function. As shown in the inset of the figure, for the large system sizes we instead see good data collapse when $J - J_c$ is scaled with L^{1/ν_*} . This crossover between behaviors controlled by ν_t and ν_* is a manifestation of the pseudocriticality illustrated in Fig. 3. In the case of Fig. 30(a), the larger sizes in finite-size scaling translate to systems closer to the transition, i.e., moving to the right on the logarithmic scale in Fig. 3. It is important to note that F_4 , in contrast to F_2 , exhibits scaling with ν_* already from much smaller system sizes in Fig. 29, which shows that the length scale ξ_* exists already further away from the transition but is manifested in many physical observables only closer to the transition, at larger scales.

VIII. PSEUDOCRITICAL SCALING

We have argued that the exponent ν_* describes a novel phenomenology of the weakly first-order AFM–VBS transition, in the form of the crossover of the correlation length illustrated in Fig. 3 and also in finite-size scaling of an important indicator of emergent SO(5) symmetry above in Sec. VII B. No scaling dimension matching ν_* appears in the (approximate) CFT spectrum now available from the CFT bootstrap calculations [55, 62] and the fuzzy sphere model [59]. In light of the CFT results, the initial observation of ν_* in the form of a correlation length with anomalously small growth appears puzzling—reminding us of Rabi’s famous question “Who ordered that?” when pondering Anderson’s 1936 discovery of (as it turned out to be) the muon [?].

The emergent pseudocriticality actually does fit perfectly into the SO(5) multicritical scenario, though it is not directly observable exactly at the critical point, only in its neighborhood. The main manifestations of the pseudocriticality are in the evolution of observables on approach to the critical point. Here we will derive the expression Eq. (1) relating ν_* to conventional scaling dimensions of the underlying CFT, though we will not make explicit use of any CFT formalism, only critical exponents. The derivation first makes a detour to the phase diagram in Fig. 2(c), where the first-order line is replaced by an extended phases, where AFM and VBS orders coexist. Though, as we will see below, we can exclude this scenario, some key results for a coexistence phase [64] can be taken over to the present situation and will form the basis of the arguments that eventually lead us to Eq. (1).

A. Emergent length scale

Bruce and Aharoni [64] considered a system with two ordered parameters, ϕ_A and ϕ_B , in Landau theory including an interaction term $v\phi_A^2\phi_B^2$. They further assumed that the joint order parameter with a total of N components develops an emergent O(N) symmetry at an isolated critical point in the space of a parameter preserving this symmetry and one that violates it; like the s and t field strengths in our phase diagrams in Fig. 2. Within this scenario, a first-order line forms, as in Fig. 2(b), if the two order parameters are mutually repulsive, i.e., $v > 0$. For attractive order parameters, $v < 0$, the coexistence phases forms instead, as in Fig. 2(c).

Though we do not have a coexistence phase in our case, for the moment our discussion will be framed around such a putative phase, in order to derive useful results that also will apply once we have abandoned the extended coexistence phase in favor of a coexistence line. The key result of Ref. 64 for our purpose here is that the shape of the phase boundaries of the coexistence phase is given

by

$$s_c(t) \sim |t|^{1/\psi}, \quad (33)$$

where the exponent ψ depends on the crossover exponent as well as the scaling dimension of the leading irrelevant perturbation of the O(N) symmetry. According to Eq. (5,11) of Ref. 64, $\psi = \phi_g - \phi_v$, where translating to the situation at hand here, $\phi_g \rightarrow y_t = 1/\nu_t = 3 - \Delta_t$ and $\phi_v \rightarrow y_{4'} = y_4 - 1 = 2 - \Delta_4$. Here it is important to note that $y_{4'}$ appears, not y_4 itself, because we are dealing with the inherent perturbation discriminating between the VBS and AFM components of the SO(5) order parameter. Thus, the exponent of the phase boundaries (if they were to exist) would be

$$\psi = y_t - y_{4'} = 1 + \Delta_4 - \Delta_t. \quad (34)$$

Using Eq. (33), we can also obtain the width w_{co} of the coexistence phase in the t field direction as a function of the s field:

$$w_{co}(s) \sim s^\psi. \quad (35)$$

From this expression we can obtain an effective finite-size width of the coexistence phase at the critical point, $s \rightarrow 0$, in the standard way by expressing s using the correlation length $\xi_s \sim s^{-\nu_s}$ and replacing ξ_s by L :

$$w_{co}(L) = L^{-\psi/\nu_s}, \quad (36)$$

which of course vanishes for $L \rightarrow \infty$. If a length scale diverges as $t^{-\nu}$ with some $\nu > 0$, then the value of t for which this length reaches the system length L scales as $L^{-1/\nu}$. Applying these arguments in the reverse, from Eq. (36) we can identify an exponent

$$\nu_* = \frac{\nu_s}{\psi} \quad (37)$$

governing a divergent length scale $\xi_* \sim t^{-\nu_*}$, which, when using the form of ψ in Eq. (34), can be written as Eq. (1).

Another way to arrive at the same result is to consider the conventional s correlation length $\xi_s \sim s^{-\nu_s}$ in combination with a proposed new length scale $\xi_* \sim |t|^{-\nu_*}$. If there is a singular boundary in the (s, t) plane given by Eq. (33), then its functional form should correspond $\xi_* \sim \xi_s$, i.e., $s_c(t) = |t|^{\nu_*/\nu_s} = |t|^{1/\psi}$, so that $\psi = \nu_s/\nu_*$. Such an argument applies generally to the shape of a transition line emerging from a critical point when a relevant perturbation is turned on, which would correspond to ν_s and ν_t being known and the exponent ψ is the one sought. Here instead the general form of ψ in Eq. (34) is known, and we propose a related length scale controlled by ν_* , which according to the above steps is given by Eq. (37). The unusual aspect here is that ψ in Eq. (34) involves not only Δ_t but also $\Delta_4 + 1$, because of the emergent symmetry with its dangerously irrelevant perturbation.

Note that, with the form of ψ in Eq (34), the coexistence phase shrinks when Δ_4 increases, i.e., when the

SO(5) perturbation becomes more irrelevant. This has to be the case, because if the symmetry is exact there will be no coexistence phase, only a line with exact SO(5) symmetry. For reasonable values of the scaling dimensions, the coexistence phase is extremely narrow in the t direction for small $s > 0$, and, as pointed out already in Ref. 64, it can easily be mistaken for a direct first-order transition.

We would expect the emergent length scale $\xi_* \sim |t|^{-\nu_*}$ to apply when $|t|$ is not too close to the coexistence boundary, i.e., outside the narrow range of t values defined by Eq. (35). However, in our present case we do not have a coexistence phase. This conclusion follows from the study of the quantity F_4 in Sec. VII B, where the results in Fig. 28 show that F_4 stays positive for system sizes above the crossover from the critical decay—this is very clear for the $J-Q_4$ model, and the trends for the $J-Q_2$ and $J-Q_3$ models suggest the same. Inspecting the definition of F_4 in Eq. (30b) and considering the fact that its denominators do not decay to zero with increasing system size in the coexistence state (since both order parameters are non-zero by definition), we see that $F_4 < 0$ would imply positively correlated order parameters, i.e., effectively attractive interactions between them. Since actually $F_4 > 0$ when the SO(5) symmetry breaks down, we conclude that the interactions must be repulsive, which implies [64] a first-order line, as in Fig. 2(b) instead of the extended coexistence phase in Fig. 2(c).

Why then are the above results relevant to our case? The reason is that the scaling forms do not rely on the sign of the interactions between the order parameters; only the physical interpretation does. For repulsive interactions, the form of s_c versus t in Eq. (33) should not be interpreted as a phase boundary, but as a crossover value of s above which the repulsive interactions become important. Similarly, the key result in Eq. (36) should be interpreted as the window of t values around $t = 0$ in which the order parameter repulsion is important. Clearly, for large $|t|$ the system has stabilized in one of the phases by the explicit enforcement of anisotropy by t , and any repulsive interactions are then completely irrelevant. But when the transition point is approached and the fluctuations increase, the repulsive interactions will eventually affect the order parameters and, for a finite system, the size of that window is given by Eq. (36). Thus, all the above arguments that lead to Eq. (1) still apply.

In the repulsive case, the exponent ν_* describes the growth of a correlation length ξ_* (whose meaning we will further elaborate on below) when the repulsive interactions affect the defects in the long-range ordered phase, AFM or VBS, that the system is in. An important question now is what the length scales ξ_t and ξ_* represent, and whether they exist simultaneously in a system close to the transition point, or whether there is only one type of defect of size ξ (as Fig. 3 may suggest) and it is only the nature of the defect that changes in the crossover. The simultaneous existence of two length scales is supported by the fact that F_4 in Figs. 27 and 29 scales with

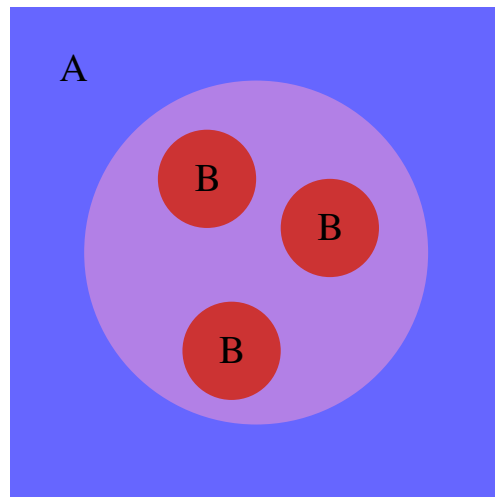


FIG. 31. Illustration of a defect in one of the ordered phases A (blue square). The purple circular region corresponds to a fluctuation of the A order partially into the direction corresponding to phase B. Actual bubbles of phase B can form inside this “bag”, because of the lowered cost of domain walls as compared to the nucleation of bubbles directly in phase A.

ν_* already for small system sizes, where ν_t at the same scale governs other quantities, like F_2 in Fig. 30 or the correlation length that we will discuss in the next section.

We have not investigated the defects of the $J-Q$ models directly, and will here only present a reasonable but speculative scenario. Figure 31 illustrates a system in one of the phases, called A, in which a domain has formed that is not fully in phase B but has fluctuated in its direction through the emergent SO(5) symmetry that is manifested on a length scale set by ν_t . Inside this “bag”, we indicate bubbles of the other phase B, which have been able to nucleate more easily here than directly from the undisturbed part of phase A because the domain wall energy is already lowered inside the bag. The bubble size is controlled by ν_* . The repulsive A-B interactions make the direct domain wall between the phases more expensive, because the phases must coexist in the domain wall. In principle, this kind of mechanism could just lead to smaller bubbles, without any need for the bag holding the bubbles, but if two length scales coexist, then the bubbles in a bag scenario seems at least plausible.

The reason why the observed correlation length is not affected by the bubbles in a bag mechanism until a crossover length is reached in Fig. 3 could be that the nucleation of the bubbles cannot take place until the bag is sufficiently “softened” when the transition is approached. Depending on how the correlation length is measured (in a real system or in a numerical simulation), it is also possible that the two lengths cannot be completely separated even though they are already manifested in some way.

A practically useful aspect of the exponent ν_* is that its numerical estimate from the finite-size scaling of the SO(5) indicator F_4 in Fig. 29 has rather small statistical errors. If correct, the form Eq. (1) can therefore be used

to obtain a good estimate of $1/\nu_*$, which we were not able to extract from the correlation function that gave us Δ_t in Sec. V A. The resulting value of Δ_s has been entered in Table I and it also is consistent with the value of the critical exponent β governing the growth of the coexisting order parameters on the first order line, Fig. 22.

B. Scaling crossover

We now consider tuning a system on a line where the s and t fields are parametrized by g as in Fig. 3; $s = s(g)$ $t = t(g)$. A scaling function governing a dimensionless observable when the line crosses the multicritical point should be of the form $f(gL^{y_s}, gL^{y_t})$, while for dimensionfull quantity a power of L also multiplies f . Eventually for $g \rightarrow 0$, the larger of the two arguments will dominate the scaling behavior, which in our case means $f(gL^{y_s}, gL^{y_t}) \rightarrow f(gL^{y_t})$, except on the coexistence line ($t = 0$) where $f(sL^{y_s})$ applies. If instead the first-order line is crossed at a small value of $s = s_0$ ($k > 0$ in Fig. 3), the scaling function also will depend on y_* ;

$$f = f(sL^{y_s}, tL^{y_t}, ts_0^b L^{y_*}), \quad (38)$$

where we keep s and t in the scaling arguments and the factor s_0^b with $b > 0$ has been introduced to account for the diminished effects of the pseudocritical scaling when $s_0 \rightarrow 0$. While we do not know the value of the exponent b , we can obtain a bound from the fact that pseudocriticality has been observed on rather larger length scales [28, 41, 81], as we will also show with improved numerical results below in Sec. VIII C.

We would like to know the range of length scales over which the bubble size dominates, i.e., in the thermodynamic limit the range $[\xi(g_1), \xi(g_2)]$ in Fig. 3. We consider a corresponding finite-size version first and cross the transition versus t at some small $s > 0$. For the three inverse correlation length exponents we have $y_s < y_t < y_*$, and there will therefore be an (s, t) region where the correlation length is controlled by t and the first argument of the scaling function in Eq. (38) is unimportant (effectively s can be taken as 0). Further, since $y_* \approx 2.4$ is significantly larger than $y_t \approx 1.6$, above some large L the function crosses over to effectively one of a single argument, $f \rightarrow f(ts^b L^{y_*})$, disregarding for now the fact that this scaling form must break down when L becomes sufficiently large for the first-order transition to be sensed (i.e., where s cannot be neglected). However, when s^b is small, there will also be some range of smaller system sizes for which tL^{y_t} dominates in Eq. (38). Balancing the two arguments, in a scaling sense, produces the crossover length scale. From $L^{y_t} \sim s_0^b L^{y_*}$ we obtain the finite-size crossover length, and by replacing L by the generic correlation length ξ in the thermodynamic limit we can write the first crossover length in Fig. 3 as

$$\xi(g_1) \sim s_0^{-b/(y_* - y_t)}. \quad (39)$$

The upper crossover length $\xi(g_2)$ in Fig. 3 will roughly correspond to the saturation length—the bubble size at the first-order transition, which is given by $\xi_s \sim s^{-\nu_s}$. Thus, the second crossover length is given by

$$\xi(g_2) \sim s_0^{-\nu_s} = s_0^{-1/y_s}, \quad (40)$$

and the entire window in which the scaling is governed by the pseudo operator is therefore

$$\xi \in [s_0^{-b/(y_* - y_t)}, s_0^{-1/y_s}]. \quad (41)$$

Provided that $y_s < (y_* - y_t)/b$, the range diverges when $s \rightarrow 0$, and it is in this sense that ξ_* can be a truly divergent length scale even if it is completely invisible exactly at the multicritical point, where the first crossover never takes place. The fact that we can observe the crossover suggests that the above condition holds, i.e., that the unknown “fading exponent” b in Eq. (38) satisfies $0 < b < (y_* - y_t)/y_s$, or, using the numerical values of the scaling dimensions, $0 < b \lesssim 0.1.12$.

C. Tests of the correlation length

A common way to extract a generic correlation length exponent ν is to consider the finite-size scaling form of a dimensionless singular quantity. The dependence of such a quantity on the distance δ to the critical point is exemplified in the case of the Binder cumulant in Eq. (16). This form is often used to collapse data for a range of δ values and system sizes, as we did in the coexistence state with the predicted value of $\nu = \nu_s$ in Fig. 17. If the exponent is not known, it can be determined by adjusting the value of ν for optimal collapse onto a scaling function when L is sufficiently large for scaling corrections to be negligible. We have already seen above that a scaling function with three arguments is in principle needed in the present case when crossing the first-order transition, Eq. (38), but that this function crosses over into the form in Eq. (16) with a single argument for large L , with ν_s replaced by $\nu_* = 1/y_* \approx 0.42$. For smaller L , the function will instead be dominated by the argument controlled by $\nu_t = 1/y_t \approx 0.63$.

Instead of performing a full data collapse analysis, the presence of two scaling regimes, separated by a smooth crossover, can be tested more systematically (without having to make choices on what data points will be included) by analyzing the derivative of the cumulant with respect to the tuning parameter. Using J as the tuning parameter in the J - Q models, $\delta J - J_c$, the scaling form Eq. (16) of the cumulant implies that its derivative with respect to J scales as

$$\frac{dU(J)}{dJ} \Big|_{\delta=0} \propto L^{1/\nu}, \quad (42)$$

at the critical point. This way of extracting ν from the derivative was used in Refs. 28, 41, and 81.

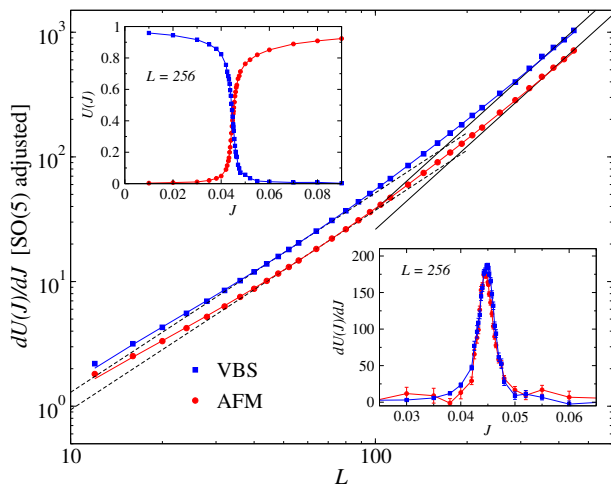


FIG. 32. System size dependence of the SO(5) adjusted derivatives of the AFM and VBS Binder cumulants of the near-critical J - Q_2 model ($Q_2 = 1$) obtained with SSE simulations at inverse temperature $\beta = 0.42L$. The curves closely reproducing the data points are fits to Eq. (43) including $L \geq 16$ data. The dashed lines show the predicted form when the growth of the correlation length is governed purely by the exponent ν_t (slope $y_t = 1.60$) and the solid lines where ν_* fully dominates (slope $y_* = 2.20$). The top-left inset shows raw data for the SO(3) (AFM) and U(1) (VBS) definitions of the cumulants, Eqs. (19). The derivatives in the main figures have been interpolated to the size-dependent point where the two SO(5) adjusted cumulants cross each other. The bottom-right inset shows the derivatives obtained directly from an estimator in the simulations.

We now generalize the above conventional form of the cumulant slope U' to multiple length scales. Using the scaling form of a generic dimensionless quantity in Eq. (38), where the fields s and t depend linearly on the tuning parameter J , we expect

$$U'(J_c) = aL^{1/\nu_*} + bL^{1/\nu_t} + cL^{1/\nu_s}. \quad (43)$$

We will test this three-length scaling form with data for the J - Q_2 and J - Q_2 - Q_6 models.

Here we use the SO(5) versions of the cumulants defined in Eqs. (20). The derivatives can either be obtained from a set of closely spaced numerical values of the cumulants fitted to polynomials, by taking the derivative of the polynomials, or directly from an estimator in the SSE simulations. Typically, we find the latter to produce results with smaller statistical errors. In either case, results are interpolated at the crossing point of the AFM and VBS cumulants, or at the infinite-size critical point if its known to sufficient precision. Alternatively, the maximum slopes (which occurs at slightly different J values for the two cumulants) can be analyzed and should scale in the same way. Here we use the derivatives at the cumulant crossing point.

Fig. 32 shows results for the J - Q_2 model, with insets showing raw data for the cumulants and the derivatives directly produced by the SSE simulations for each

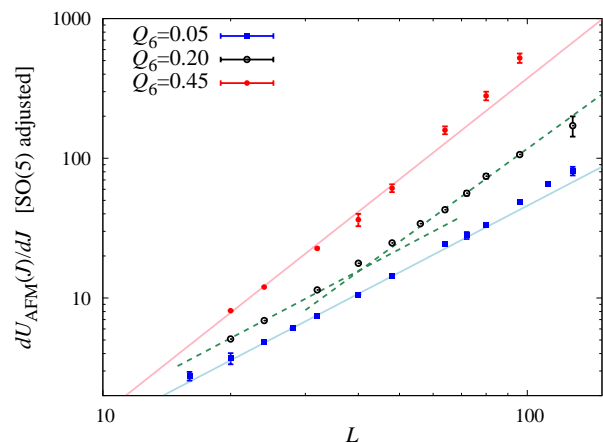


FIG. 33. Size dependence of the derivatives of the SO(5) AFM and VBS cumulants of the J - Q_2 - Q_6 model at the points where the two cumulants cross each other vs Q_2 . Results are shown close to the critical point ($Q_6 = 0.05$), near the maximal Q_6 value accessible without QMC sign problems ($Q_6 = 0.45$), and one point in between ($Q_6 = 0.20$). The lines have slopes corresponding to Δ_t ($1/\nu_t = 1.58$) and Δ_* ($1/\nu_* = 2.40$), where, according to the scenario of the pseudo operator, the former should have a larger range of applicability for small Q_6 and the latter should describe the slopes in the scaling regime before the crossover to asymptotic first-order behavior with much larger slope [30].

value of J . In practice, we find no significant differences between results obtained with the conventional cumulant definitions in Eqs. (19) and the SO(5) versions in Eq. (20), beyond some small shifts of the size dependent transition points and the values of the cumulants and their derivatives. The data presented below are for the SO(5) definitions, with the derivatives evaluated at the L dependent point at which the two cumulants cross each other. We have also analyzed data at the estimated infinite-size transition point $J/Q_2 = 0.4502$ and in addition studied the size behavior of the maximum slope (peak values in the right-bottom inset of Fig. 32). Both these definitions produce only small overall shifts of the data points relative to those in Fig. 32.

For system sizes roughly in the range $L = 30$ to 100 , the results in Fig. 32 are well described by the exponent ν_t , while for larger sizes the behavior crosses over to a significantly faster growth with L . Though the expected form with $1/\nu \approx 2.40$ is not yet quite reached for these system sizes (up to $L = 448$), the predicted form Eq. (43) describes the data well for all system sizes $L \in [16, 448]$. This good fit is not trivial, since only the three factors a, b, c in Eq. (43) are adjustable.

Next we study the cumulant derivatives in the J - Q_2 - Q_6 model, in order to examine the expected shift of the crossover from ν_t to ν_* scaling as we move deeper into the first-order line, as schematically illustrated in Fig. 3, where the generic parameter k now corresponds to Q_6 . Fig. 33 shows results for three values of Q_6 , with the

slopes extracted at the cumulant crossing points as before in Fig. 32 at $Q_6 = 0$. In this case we only show results obtained from the AFM cumulants, but the VBS results look very similar. The expected shift of the crossover is seen clearly. At $Q_6 = 0.05$, the behavior is still similar to the case $Q_6 = 0$ in Fig. 32, with the data points up to $L \approx 80$ falling close to the line corresponding to ν_t scaling. We do not have data for much larger L here, but the early stage of crossover to ν_* scaling is seen at a scale $L \approx 100$, somewhat smaller than at $Q_6 = 0$ in Fig. 32. At the point furthest inside the first-order line, $Q_6 = 0.45$, there is no regime for smaller sizes where the scaling is governed cleanly by ν_t ; instead, for $L \gtrsim 30$ the behavior is already well described by ν_* . Thus, when moving further into the first-order line, the influence of the pseudo operator is larger and significant already on smaller length scales, as in Fig. 3 for increasing k . Finally, at a point between these extremes, $Q_6 = 0.2$, we explicitly see the crossover taking place at $L \approx 40$.

The physical bubble size at the first-order transition will eventually saturate at a value set by the scaling field s , as schematically illustrated in Fig. 3, and its observation would necessitate observables not considered here. This robustness of the emergent scaling on the first-order line should be a reflection of the unusually large correlation length exponent governing the coexistence line, $\nu_s \approx 1.40$, which sets the length scale at which the scaling finally crosses over to the saturation value at the transition. In finite-size scaling, the correlation length, as typically estimated, instead grows faster, in the case at hand likely $\xi \sim L^4$. There are clear signs of the onset of this faster growth for the largest system sizes at $Q_6 = 0.45$ in Fig. 33.

The divergent correlation length measured at first-order transitions in finite-size scaling reflects two different phases occupying different parts of the Hilbert space. Since a finite system can still tunnel between these subspaces, through the formation of system spanning domain walls, there are apparent fluctuations on the length scale L that are not present in the thermodynamic limit. It is well known from the classical literature that the finite-size fluctuations result in an effective exponent $1/\nu = d$ [182–184]. In the quantum case we should have $1/\nu = d + z$, with $z = 2$ when at least one of the coexisting phases has gapless Goldstone modes [30], here from the SO(3) AFM order. For the J - Q_2 model this final stage of the transition cannot be observed with systems of practical size (Fig. 32), and even for the J - Q_2 - Q_6 at $Q_6 = 0.40$ (Fig. 33) the slope taken with the largest 2-3 points corresponds to $1/\nu \approx 3$. Values as large as $1/\nu \approx 3.5$ were observed in a different model with emergent O(4) symmetry [30], where the first-order tendency is larger.

Here we have focused on the manifestation of the crossover in finite-size scaling of the exponent governing the correlation length, which should be directly related to how the correlation length crosses over when the transition point is approached in the thermodynamic limit.

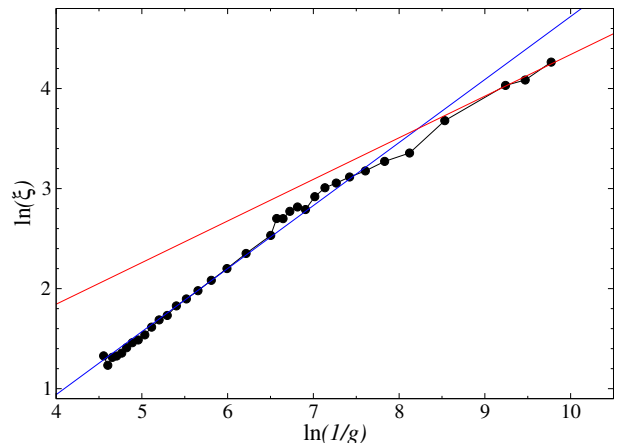


FIG. 34. Dependence of the logarithm of the correlation length on the logarithmic distance to the phase transition in the 3D loop model [28], with $g = |J - J_c|$. The circles are data reproduced by digitizing Fig. 18 of Ref. 28 (for error bars we refer to the original article) and the blue and red lines show, respectively, the predicted scaling behavior with the our exponent values $\nu_t = 0.632$ and $\nu_* = 0.417$.

We have not computed the correlation length itself under the condition $\xi \ll L$, but exactly such a calculation for the 3D loop was presented by Nahum et al., in Fig. 18 of Ref. 28. For convenience, we have re-graphed their data in Fig. 34 along with lines showing the predicted scaling with the inverse distance $g = |J - J_c|$ to the critical point. The behaviors $\xi \sim g^{1/\nu_*}$ and $\xi \sim g^{1/\nu_t}$ are matched well for systems close to and far away, respectively, from the transition. Like in Fig. 32, the largest length scale here is barely enough to clearly follow the behavior $\xi \sim g^{-\nu_*}$ without any influence from ν_t , but the crossover to the slower growth is still compelling. The behavior conforms with our assertion in Fig. 3, apart from the missing crossover to the eventual first-order behavior, which just means that the saturation value has not yet been reached at the minimum value of g . This previously unexplained behavior serves as further confirmation of the pseudocritical crossover, as well the close similarity of the J - Q and loop models.

D. Crossover scaling of the transition point

We conclude this section by again considering the location of the critical point of the J - Q_2 model—the model for which we have data up to the largest system sizes. Based on the long-distance correlation functions in Fig. 4, the transition should be located somewhere between $J/Q = 0.04500$ and $J/Q = 0.04505$, which is slightly smaller than the value $J_c/Q = 0.04510(2)$ obtained by extrapolating the conventional cumulant crossings in Ref. 81. Results based on the SO(5) crossing points and improved SSE data are shown in Fig. 35. At first sight, it again looks like the $L \rightarrow \infty$ crossing point

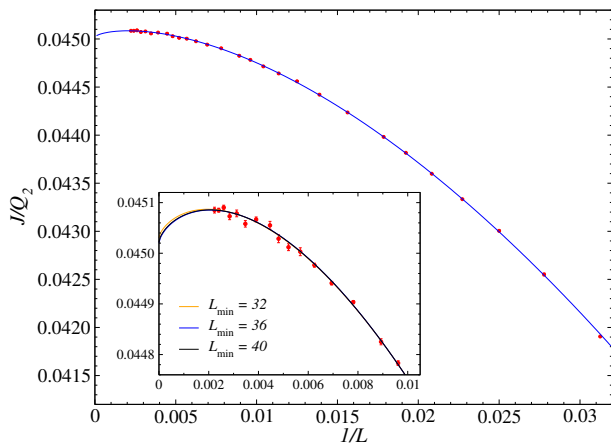


FIG. 35. Crossing values J/Q of the SO(5) versions of the AFM and VBS Binder cumulants defined in Eqs. (20) for the J - Q_2 model, obtained from the same data sets as in Fig. 32. The curve is a fit to the form Eq. (44). The inset zooms in on the data for $L > 100$, with the three barely distinguishable curves corresponding to different minimum system sizes included in the fit.

tends to about $J_c/Q = 0.04510$, at odds with the results in Fig. 4, which indicates that the system at that coupling ratio is marginally inside the AFM phase. We therefore analyze the cumulant crossing points in more detail next.

Instead of fitting the data versus $x = 1/L$ to the form $f(x) = f_0 + ax^b + cx^d$ with five adjustable parameters (as was done in Ref. 81), we here use a constrained form that should be expected in the presence of the three length scales governed by the exponents ν_s , ν_t , and ν_* :

$$J_c(L) = J_c(\infty) + aL^{-1/\nu_s} + bL^{-1/\nu_t} + cL^{-1/\nu_*}, \quad (44)$$

with only $J_c(\infty)$ and the coefficients a, b, c taken as fitting parameters. This form can be motivated by first considering a system approaching the critical point exactly, where ν_* does not come into play. On the line $t = 0$, the condition of the two cumulants being equal to each other corresponds to some function $h(x) = h(sL^{1/\nu_s}) = 0$, which has some solution $x = x_0$. Thus, the size dependent critical point scales as $s_c \sim L^{-1/\nu_s}$. Similarly, on the line $s = 0$ we have $t_c \sim L^{-1/\nu_t}$. For a system tuned to the critical point on some line δ such that $s = d_s\delta$ and $t = d_t\delta$, with d_s, d_t arbitrary non-zero coefficients, we assume that both powers come into play for a finite-size shift of the form $\delta_c \sim aL^{-1/\nu_s} + bL^{-1/\nu_t}$. In Eq. (44) we have assumed that a similar term originating from the pseudo operator appears when approaching the weak first-order line with small $s \neq 0$.

Since $1/\nu_s \approx 0.73$ is much smaller than the other exponents, it will eventually control the behavior for large sizes. In fact, we find that the coefficients a and b have different signs, leading to non-monotonic behavior not yet obvious with the SSE data at hand with $L \leq 448$ but is a very stable feature of the fit. As shown in the inset of Fig. 35, for three data sets including different minimum

system sizes, the fitted function consistently has a maximum at $L \approx 500$. The extrapolated value is also stable (also when excluding additional small systems) and now agrees very well with the previous conclusion that the critical coupling ratio should be between $J/Q_2 = 0.04500$ and $J/Q_2 = 0.04505$. Based on the statistical quality of the fits and the variations among different L_{\min} , we conclude that the critical point is at $J_c/Q = 0.04502(1)$. The third correction in Eq. (44) is actually not very important for system size $L \gtrsim 50$, since the exponent $1/\nu_*$ is much larger than the other two. Leaving out this term still produces a statistically good non-monotonic fit and critical point consistent with the value stated above.

It should be noted that fitting two independent power laws does not produce the same exponents as the known ones imposed above. In fact, the best fit has two exponents very close to each other, both around 1.9, and with opposite signs of their coefficients. This behavior in itself indicates that the best fit mimics a different form. While the fit with fixed exponents $1/\nu_s$ and $1/\nu_t$ is not completely optimal (since other exponents give marginally lower χ^2 values), it is still statistically good, as can even be judged visually in the inset of Fig. 35. The known exponents seemingly provide a good approximation to the non-monotonic crossover behavior that can be inferred from our other indications of a transition between $J/Q_2 = 0.04500$ and $J/Q_2 = 0.04505$.

IX. ANOMALOUS FINITE-SIZE SCALING

The crossover behavior of the correlation length will impact also other physical observables—those that are directly related to the correlation length, in a way that will be made more precise in this section. In Ref. 41 it was already realized that a scaling form involving two length scales could explain some of the anomalous behaviors that had been observed in the lattice models. While those insights remain technically valid, the physical interpretation of the roles of the different length scales have to be revised in light of our current understanding of the exponent ν_* . Previously this exponent was just called ν , as it was assumed to be associated with the single relevant operator within the DQCP scenario. Another exponent $\nu' > \nu$ was extracted that appeared to fit within the conventional DQCP scenario and its larger U(1) scale in the near-critical VBS phase, which was predicted [23–25] to also set the scale of spinon deconfinement. The numerical values of the exponents determined in Ref. 41 were $\nu = 0.446(8)$, extracted from cumulant slopes, and $\nu' = 0.585(18)$, from the scaling of the critical VBS domain wall energy density as well as an observable explicitly probing the size of a bound state of two spinons. These values agree reasonably well with our improved results.

The quantitatively most important result of Ref. 41 was that the finite-size scaling forms for many physical observables depend on the ratio ν/ν' . As we will see be-

low, this ratio, now identified as ν_*/ν_t , is indeed of crucial importance in finite-size scaling of a broad class of observables, but with ν_* governing the bubble scale and ν_t the conventional correlation length. If indeed $\nu' \equiv \nu_t$, as it appears, the scale of spinon deconfinement is actually the correlation length and should then, presumably, exhibit crossover between ν_t and ν_* scaling when approaching the weak first-order line. Since it is hard to extract the size of a bound state for large systems—only lattices of size up to $L = 64$ were used in Ref. 41—the crossover scale was likely not reached (though some weak tendencies are seen in Fig. 1 of Ref. 41). We will not revisit the spinon scale directly here, but will discuss our updated view of the extended scaling hypothesis where ν_*/ν_t appears, formulating an extended finite-size scaling ansatz for certain observables in Sec. IX B and presenting three illustrative examples in Sec. IX A; the spin stiffness, the order parameters, and the energy of a critical VBS domain wall.

A. Extended finite-size scaling hypothesis

In standard finite-size scaling [179–181], a physical observable A with scaling behavior $A \sim \delta^\kappa$ (with κ denoting a generic critical exponent) in the thermodynamic limit is first rewritten using the correlation length $\xi \sim \delta^{-\nu}$, i.e., $A \sim \xi^{\kappa/\nu}$. Then at criticality ξ is simply replaced by the system size L . Thus, $A(L) \sim L^{-\kappa/\nu}$, which is valid in a window of size $L^{-1/\nu}$, where the correlation length exceeds L . Finite-size scaling effectively corresponds to the flow of observables with the length scale on which they are probed, motivating the some times used term “phenomenological renormalization” [179].

The easiest way [41] to construct a modified finite-size behavior in the presence of the bubble scale ξ_* is to posit that it should be used in place of ξ above, i.e., $A \sim \xi_*^{\kappa/\nu}$. Here we have only changed the relevant length scale that appears, without changing κ/ν (which is related to the scaling dimension of A exactly at the critical point). Since $\xi_* \sim \xi^{\nu_*/\nu}$, we can also write $A \sim \xi^{(\kappa/\nu)(\nu_*/\nu)}$. If we now replace ξ by L we obtain $A(L) \sim L^{-(\kappa/\nu)(\nu_*/\nu)}$, or, more specifically when the AFM–VBS transition is crossed by tuning the t field and ν corresponds to ν_t ,

$$A(L) \sim L^{-(\kappa/\nu)(\nu_*/\nu_t)}, \quad (45)$$

Here the exponent indeed differs by a factor ν_*/ν_t from the conventional finite-size exponent κ/ν_t . The form should be valid at the transition point roughly in the range of system sizes corresponding to the window $[g_1(k), g_2(k)]$ of a tuning parameters g in the schematic drawing of the crossover behavior in Fig. 3.

The physical interpretation of the steps leading to Eq. (45) was [41] that the shorter length scale ξ_* ceases to grow when the larger scale ξ reaches L . If that is so, then it would appear that the two length scales are present at the same time (with the longer scale ξ_t having been replaced by L in finite-size scaling), which is not

clear from just the crossover behavior illustrated in Fig. 3 and the actual calculation of ξ versus the distance to the transition by Nahum et al. [28] (data reproduced here in Fig. 34). One way in which this simultaneous presence of the length scales could be realized is with the “bag of bubbles scenario” illustrated in Fig. 31. A typical calculation may only probe only one of the scales or some combination of them.

A key question is to what observables anomalous scaling involving ν_* applies. Clearly, a form like Eq. (45) cannot apply to all operators, because the exponent κ/ν_t is the scaling dimension of the operator A and we have presented numerous examples in the previous sections of scaling dimensions extracted from the system sizes dependence. For instance, in Sec. V A we extracted the relevant scaling dimensions Δ_t from the correlation function of the Z operator at distance $r = L/2$. If this correlation function $C_Z(L)$ takes the form where the exponent $2\Delta_t$ is modified by the factor ν_*/ν_t , then we would have to compensate by multiplying the exponent from the fit by the inverse ratio to obtain the true values of the two scaling dimensions. This would completely ruin the good agreement in Table I between the AFM–VBS transition and the SO(5) CFT and the fuzzy sphere model. Moreover, we considered both $r = L/2$ and $r \ll L$ in Fig. 17, with full agreement between the decay exponents. A very strong confirmation of the correctness of the procedure is that the scaling dimension of the conserved current comes out very close to $\Delta_j = 2$ in Fig. 15.

What we are asserting is that the anomalous behavior is an effect of finite size, with no modified exponents for $r \ll L$ as long as we are in the distance regime where criticality can be observed (before the crossover to the asymptotic first-order behavior). Thus, the good agreement between the $r = L/2$ and $r \ll L$ correlations suggest that they are not affected by anomalous scaling.

The bubble size governed ν_* is of course at the heart of the matter, and we propose that only those quantities are affected that relate explicitly to the order parameters so that their standard scaling forms include ξ_t or ξ_s . Such quantities can either involve integration over the entire lattice or distances approaching the system length, likely for distances beyond some radius L^c with c an unknown exponent. For such quantities, there should also be similar anomalous scaling behaviors away from the transition point in the thermodynamic limit, related to the crossover of the correlation length illustrated in Fig. 3.

Quantities that in some way involve the order parameter integrated over the lattice typically have a scaling form in the thermodynamic limit that explicitly depends on the correlation length. For example, a squared order parameter (here VBS or AFM) scales with the distance to the critical point as $m^2 = \delta^{2\beta}$, where $2\beta = 2\Delta_\phi\nu$, where $\nu = \nu_t$ if only the field t is tuned at $s = 0$ and $\nu = \nu_s$ if s is tuned with $t = 0$. Thus, m^2 depends explicitly on an inverse correlation length, ξ_s or ξ_t . Another example is the spin stiffness ρ_s , which scales as

$\rho_s \sim \delta^{z\nu}$. This quantity as well is directly related to the (AFM) long-range order (as a response to a twist of the order parameter); since $z = 1$ here, the scaling should be identical (in terms of exponents, not the shape of the full scaling function) to that of the inverse correlation length. Then it is also plausibly affected by the crossover behavior. We will study both m^2 and ρ_s below, in addition to the critical domain wall energy considered in Refs. 177 and 41. Its scaling form also contains the inverse correlation length, in a product with the inverse emergent U(1) length scale.

The inverse correlation length of a system with a single tuned relevant field can be written as

$$\xi^{-1} = \delta^\nu f(\delta L^{1/\nu}), \quad (46)$$

where δ^ν is the form for $L \rightarrow \infty$ and the function $f(x)$, $x = \delta L^{1/\nu}$, accounts for the finite-size cut-off. The finite-size form $\xi^{-1} \sim L^{-1}$ is obtained from the necessary condition (to eliminate δ at criticality) that $f(x) \rightarrow x^{-\nu}$ when $x \rightarrow \infty$, i.e., for $L \rightarrow \infty$ at $x \neq 0$. An alternative, more common form of Eq. (46) for finite-size scaling including $\delta \neq 0$ is

$$\xi^{-1} = L^{-1} f(\delta L^{1/\nu}), \quad (47)$$

with a different form of the scaling function $f(x)$. In practice, this form holds up to some value of x , beyond which there is a finite-size peel-off from the scaling function, with that peel-off value increasing with L . Here we will start from a generalized form of Eq. (46) with more than one scaling argument and derive a corresponding critical form with more than one power of L .

Generalizing Eq. (46) to the case at hand, we have already argued that scaling function depending on all the exponents ν_s , ν_t , and ν_* is needed; Eq. (38). Further, we have in mind a situation where the bubble scale dominates the behavior for small values of s in the thermodynamic limit and therefore start from the form

$$\xi^{-1} = \delta^{\nu_*} f(\delta L^{1/\nu_*}, \delta L^{1/\nu_t}, \delta L^{1/\nu_s}). \quad (48)$$

Here we have replaced all the factors in front of L by just δ , but it should be kept in mind that different arguments will dominate the behavior depending on how s and t are tuned by δ . The last scaling argument should really be $(\delta + s_0)L^{1/\nu_s}$, with s_0 the value of s when we cross $t = 0$ ($\delta = 0$). Then the system will eventually cross over to a first-order form that we do not consider here. The question is whether there is some range of system sizes where Eq. (48) can describe the finite-size behavior when the transition is weakly first-order, i.e., when s_c is very small and there is a large range of length-scales governed by ξ_* in the thermodynamic limit, as in Fig. 3 for small k .

In the example of the cumulant derivative U' in Sec. VIII C we already saw how the scaling function in Eq. (38) can, effectively, produce three different power laws. Since U is a dimensionless quantity, there is no power of δ in front of the scaling function and Eq. (43)

is produced by the derivative. Such a form was able to reproduce the data in Fig. 32 very well from small to large systems. For the inverse correlation length of interest now, the asymptotic power of the arguments in Eq. (48) must be $-1/\nu_*$ in order to eliminate the overall δ dependence, thus producing the form

$$\xi^{-1}(L) = aL^{-1} + bL^{-\nu_*/\nu_t} + cL^{-\nu_*/\nu_s}. \quad (49)$$

This form is valid under the assumption that each argument, when large, produces its own power law to remove the δ dependence at criticality. While we have not proved this property, Eqs. (48) and (49) are certainly mutually consistent. We will also see below that Eq. (49) is sufficient to describe numerical data without any cross terms or even more complicated crossover behavior.

According to Eq. (49), a conventional finite-size scaling term L^{-1} will be produced in addition to the anomalous $L^{-\nu_*/\nu_t}$ term of the original two-length proposal [41]. The anomalous term decays slower and may dominate the behavior for large system sizes. In the last term, $L^{-\nu_*/\nu_s}$ decays even slower but here the coefficient c should be small if the crossing value s_0 of the s field is small. Thus, it may only become important for very large system sizes, where the other terms have essentially decayed away. When the last term does become important, we also expect the first-order behavior to take over. In practice, only the L^{-1} and $L^{-\nu_*/\nu_s}$ terms will likely reflect critical scaling.

We will next test the extended anomalous scaling form with the tree observables mentioned, for which the above form on the right-hand side will acquire an additional common factor in all the exponents, except in the case of ρ_s . However, in that case and the squared order parameters we further have to add a constant to account for the weak long-range long-range order.

B. Spin stiffness

The spin stiffness ρ_s provided the first hint of anomalous scaling in the J - Q_2 model [33] and has frequently been used to argue for a first-order transition [33, 45]. It is computed in SSE (and other QMC) simulations in terms of winding number fluctuations [186, 187]. The conventional critical form when $z = 1$ is $\rho_s \sim L^{-1}$, arising from $\rho_s \sim \delta^{\nu_t}$ when crossing the transition by tuning t at $s = 0$ in the thermodynamic limit. Thus, the L dependent scaling form is identical to that for ξ^{-1} in Eq. (49),

$$\rho_s(L) = \rho_s(\infty) + aL^{-1} + bL^{-\nu_*/\nu_t} + cL^{-\nu_*/\nu_s}, \quad (50)$$

except for the added constant $\rho_s(\infty)$, which reflects an expected non-zero value for $L \rightarrow \infty$ because of the weak AFM order in the coexistence state. While the contribution originating from the s field close to criticality may play some role, the crossover to the ultimate constant form for $L \rightarrow \infty$ at the transition (or to other forms away

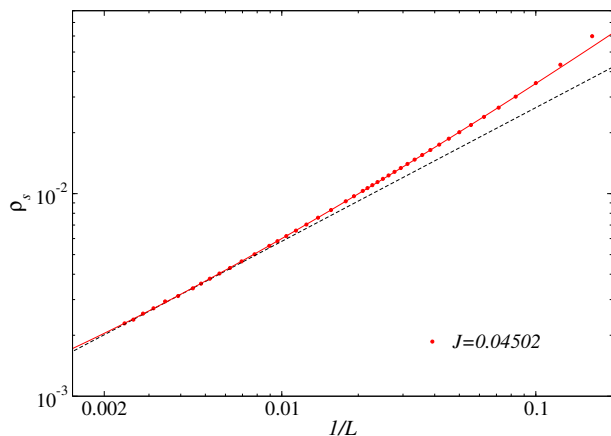


FIG. 36. Spin stiffness of the J - Q_2 model at the transition point, taken as $J = 0.04502$ ($Q_2 = 1$). The red curve shows a fit to Eq. (50) with $c = 0$ and the exponent $\nu_*/\nu_t = 0.66$ fixed at our improved value. The dashed line shows the single power law $\propto L^{-\nu_*/\nu_t}$, with the factor adjusted for best fit to the large- L data.

from the transition) is likely more intricate. Moreover, even with high precision data it is not possible to reliably extract the relative contributions of the constant and the $L^{-\nu_*/\nu_s}$ term. We therefore leave out the s contribution here.

We fit to SSE data for the J - Q_2 model generated at inverse temperature $\beta = 0.42L$, where the factor 0.42 being approximately the inverse of the critical spin wave velocity [142], thus representing cubic space-time geometry (which is not a prerequisite for scaling but may reduce some corrections). We have data for large systems, up to $L = 448$, at two coupling ratios, $J = 0.0450$ and $J = 0.0451$ ($Q = 1$), and interpolated in those data sets to the estimated transition point $J = 0.04502$.

The data are graphed versus $1/L$ in Fig. 36 and have been fitted to the expected form for $L \geq 12$, shown with the red curve. The dashed black line shows the form $L^{-\nu_*/\nu_t} = L^{-0.63}$, where the exponent is slightly smaller than in Ref. [41] (≈ 0.715). While this term indeed governs the large- L data very well, the L^{-1} is important to match the results for the smaller systems and also to improve the fit overall before the asymptotic behavior sets in. The L^{-1} term corresponds almost exactly to a correction term with optimized exponent used in Ref. [41]. Thus, the results of the two fits are almost the same (but here we also have data for larger systems), with the main difference being the added constant $\rho_s(\infty)$ in Eq. (50), which has a value ≈ 0.0003 in our fit and plays only a minor role in the available range of system sizes. There are still, not unexpectedly, further corrections for the smaller system sizes that are not included in Eq. (50). Overall, the extended scaling ansatz work well here.

X. DISCUSSION

The many past efforts to elucidate the nature of the DQCP and its adjacent phases can be likened to the ancient Indian parable of a group of blind men examining an elephant, an entity that they have never before encountered. Feeling different parts of the animal without access to the whole, they present their individual findings and theories but, given the conflicting observations, they cannot come to any consensus on what they are dealing with. In the case of the putative DQCP, many models and methods have been applied to study the AFM–VBS transition in different ways. Individually, most of these studies present plausible and coherent scenarios for exotic critical phenomena, but, taken together, no consistent unified picture has emerged.

Here we have reconstructed the entire elephant—a multicritical point at the end of a line of weak first-order transitions—which explains previously irreconcilable observations and scenarios. Using our own results and insights from CFT studies, we conclude that, in a space of two tunable model parameters, there is a $SO(5)$ symmetric multicritical point with scaling dimensions compatible with results for an $SO(5)$ CFT. The CFT results of main interest here [55, 62] are strictly speaking only boundaries of allowed values in the space of scaling dimensions. However, it is believed that the true exponents should fall at or very close to the boundaries, as is the case for $O(N)$ models [60]. Our relevant scaling dimensions listed in Table I fall within about 1-2% from the boundaries, read off of graphs available for the combinations (Δ_ϕ, Δ_s) and (Δ_ϕ, Δ_t) [62]. While Δ_4 , as well as the other dimensions, is in less good agreement with Ref. [55], the discrepancies can likely be explained by the input value $\Delta_\phi = 0.63$ used in that calculation. Our value is lower, $\Delta_\phi = 0.607(4)$, and once this is taken into account the agreement is improved for all scaling dimensions [63]. Overall, the remarkable agreement between two very different calculations represent strong support for the multicritical $SO(5)$ CFT.

The multicritical point is inaccessible (with our current models) in QMC simulations, because of sign problems (e.g., a negative Q_6 interaction would be needed, according to Fig. 22). However, the point is not fundamentally inaccessible, in contrast to the complex CFT scenario [47, 59]. In principle methods such as DMRG and machine learning approaches can be used to study models like the J_1 - J_2 - Q_2 Hamiltonian, but on much smaller lattices than those accessed here. Useful results may still be obtained, because the scaling behavior will not be contaminated by the effects from the weak first-order transition. Based on previous results for frustrated spin models, which can be continuously deformed into the J - Q model studied here, there is also most likely a gapless QSL phase adjacent to the parameter regime accessible to efficient (sign problem free) QMC simulations. The simplest scenario then is that the phase diagram is of the type in Fig. 2(b), where the multicritical point (which

then is bicritical) is also the tip of the QSL phase. If there is also a line of generic DQCPs, as in Fig. 2(a), its endpoint at the spin liquid would be a bicritical point at which the QSL phase opens.

Beyond the nature of the critical point that we have now resolved, we have also demonstrated that the emergent $SO(5)$ symmetry leads to previously not anticipated pseudo critical scaling behaviors when the weak first-order transition is approached. The practically most important manifestation of this emergent phenomenon is the crossover of the correlation length to a power law form governed by an exponent ν_* , which is related to CFT exponents according to Eq. (1). All our numerical results conform very well with this expression. As far as we know, this type of pseudocriticality has not been discussed previously in the literature.

The pseudocriticality is also a “beyond Landau” phenomenon, in the sense that it relies on the emergent $SO(5)$ symmetry. Classical spin models cannot have emergent $O(N > 2)$ (unless a relevant perturbation is tuned away, which would make such a critical point an even higher-order multicritical point). Thus, the proposed topological θ term is likely needed in the field theory, which in the most well known incarnation would be the 2+1 dimensional WZW $k = 1$ theory with $SO(5)$ symmetry. It has been believed that this theory has no relevant singlet, contrary to what we have found here at the AFM–VBS transition.

It is also possible to study J - Q type models with emergent $O(4)$ symmetry, either by having a two-fold degenerate plaquette-singlet (PS) phases transitioning into an $SO(3)$ breaking AFM state, or by four-fold degenerate VBS transitioning into an $O(2)$ AFM state [189]. Previous work on a “checker-board” J - Q model with AFM–

PS transition showed emergent $O(4)$ symmetry up to the largest system sizes studied ($L = 96$) even though the transition was rather obviously first-order [30] (a related classical loop model found similar behaviors [31]). A J - Q model with $O(2)$ deformed AFM state has also been studied [42, 188]. It also has a first-order transition but signatures of deconfined spinons were seen in the dynamic spectral functions [42]. These models should be further studied in light of our results presented here. It will also be interesting to further study $SU(N)$ lattice models with $N \geq 3$ [37–40, 106, 156], where there should be no emergent $SO(5)$ symmetry and for sufficiently large N the original DQCP scenario should hold, i.e., there will only be one relevant operator with the symmetries of the Hamiltonian.

ACKNOWLEDGMENTS

Acknowledgments.—We would like to thank Shai Chester, Yin-Chen He, Ribhu Kaul, Zi Yang Meng, Masaki Oshikawa, Slava Rychkov, Subir Sachdev, T. Senthil, Ning Su, and Cenke Xu for valuable discussions. This work was supported by the National Science Foundation Grant No. PHY-2116246 (J.T.) by the National Natural Science Foundation of China under Grants No. 12122502 and No. 12175015, and by National Key Projects for Research and Development of China under Grant No. 2021YFA1400400 (H.S. and W.G.), and by the Simons Foundation under Grant No. 511064 (A.W.S.). Many of the numerical calculations were carried out on the Shared Computing Cluster managed by Boston University’s Research Computing Services.

[†] These two authors contributed equally to this work.

-
- [1] P. W. Anderson, *Science* **235**, 1196 (1987).
 - [2] S. Chakravarty, B. I. Halperin, and D. R. Nelson, Two-dimensional quantum Heisenberg antiferromagnet at low temperatures, *Phys. Rev. B* **39**, 2344 (1989).
 - [3] E. Dagotto and A. Moreo, The spin-1/2 Heisenberg antiferromagnet on a square lattice and its application to the cuprous oxides *Phys. Rev. Lett.* **63**, 2148 (1989).
 - [4] E. Manousakis, *Rev. Mod. Phys.* **63**, 1 (1991).
 - [5] A. V. Chubukov, S. Sachdev, and J. Ye, Theory of two-dimensional quantum Heisenberg antiferromagnets with a nearly critical ground state, *Phys. Rev. B* **49**, 11919 (1994).
 - [6] H. T. Diep (Editor), *Frustrated Spin Systems* (World Scientific, Singapore, 2004).
 - [7] P. Fazekas and P. W. Anderson, *Philos. Mag.* **30**, 23 (1974).
 - [8] X. G. Wen, Mean-field theory of spin-liquid states with finite energy gap and topological orders. *Phys. Rev. B* **44**, 2664 (1991).
 - [9] L. Savary and L. Balents, Quantum Spin Liquids, *Rep. Prog. Phys.* **80**, 016502 (2017).
 - [10] N. Read and S. Sachdev, Valence-Bond and Spin-Peierls Ground States of Low-Dimensional Quantum Antiferromagnets, *Phys. Rev. Lett.* **62**, 1694 (1989).
 - [11] N. Read and S. Sachdev, Spin-Peierls, valence-bond solid, and Néel ground states of low-dimensional quantum antiferromagnets, *Phys. Rev. B* **42**, 4568 (1990).
 - [12] S. Sachdev, Quantum magnetism and criticality, *Nat. Phys.* **4**, 173 (2008).
 - [13] M. Hermele, T. Senthil, M. P. A. Fisher, P. A. Lee, N. Nagaosa, and X.-G. Wen, Stability of $U(1)$ spin liquids in two dimensions, *Phys. Rev. B* **70**, 214437 (2004).
 - [14] M. Hermele, T. Senthil, and M. P. A. Fisher, Algebraic spin liquid as the mother of many competing orders, *Phys. Rev. B* **72**, 104404 (2005).
 - [15] M. Hermele, Y. Ran, P. A. Lee, and X.-G. Wen, Properties of an algebraic spin liquid on the kagome lattice *Phys. Rev. B* **77**, 224413 (2008).
 - [16] C. Xu and S. Sachdev, Global phase diagrams of frustrated quantum antiferromagnets in two dimensions: doubled Chern-Simons theory, *Phys. Rev. B* **79**, 064405 (2009).

- [17] A. Thomson and S. Sachdev, Fermionic spinon theory of square lattice spin liquids near the Néel state, *Phys. Rev. X* **8**, 021048 (2018).
- [18] X.-Y. Song, C. Wang, A. Vishwanath, and Y.-C. He, Unifying description of competing orders in two-dimensional quantum magnets, *Nat. Comm.* **10**, 4254 (2019).
- [19] Y. Yu and S. A. Kivelson, Phases of frustrated quantum antiferromagnets on the square and triangular lattices, *Phys. Rev. B* **101**, 214404 (2020).
- [20] L. Zou, Y.-C. He, and C. Wang, Stiefel liquids: Possible non-lagrangian quantum criticality from intertwined orders, *Phys. Rev. X* **11**, 031043 (2021).
- [21] H. Shackleton, A. Thomson, and S. Sachdev, Deconfined criticality and a gapless Z_2 spin liquid in the square lattice antiferromagnet, *Phys. Rev. B* **104**, 045110 (2021).
- [22] H. Shackleton and S. Sachdev, Anisotropic deconfined criticality in Dirac spin liquids, *J. High Energy Phys.* **2022** 141 (2022).
- [23] T. Senthil, A. Vishwanath, L. Balents, S. Sachdev, and M. P. A. Fisher, *Science* **303**, 1490 (2004).
- [24] T. Senthil, L. Balents, S. Sachdev, A. Vishwanath, and M. P. A. Fisher, *Phys. Rev. B* **70**, 144407 (2004).
- [25] M. Levin and T. Senthil, *Phys. Rev. B* **70**, 220403 (2004).
- [26] T. Senthil and M. P. A. Fisher, Competing orders, nonlinear sigma models, and topological terms in quantum magnets, *Phys. Rev. B* **74**, 064405 (2006).
- [27] A. W. Sandvik, Evidence for Deconfined Quantum Criticality in a Two-Dimensional Heisenberg Model with Four-Spin Interactions, *Phys. Rev. Lett.* **98**, 227202 (2007).
- [28] A. Nahum, J. T. Chalker, P. Serna, M. Ortuño, and A. M. Somoza, *Phys. Rev. X* **5**, 041048 (2015).
- [29] G. J. Sreejith, S. Powell, and A. Nahum, Emergent $SO(5)$ Symmetry at the Columnar Ordering Transition in the Classical Cubic Dimer Model, *Phys. Rev. Lett.* **122**, 080601 (2019).
- [30] B. Zhao, P. Weinberg, and A. W. Sandvik, Symmetry-enhanced discontinuous phase transition in a two-dimensional quantum magnet, *Nat. Phys.* **15**, 678 (2019).
- [31] P. Serna and A. Nahum, Emergence and spontaneous breaking of approximate $O(4)$ symmetry at a weakly first-order deconfined phase transition, *Phys. Rev. B* **99**, 195110 (2019).
- [32] J. Takahashi and A. W. Sandvik, Valence-bond solids, vestigial order, and emergent $SO(5)$ symmetry in a two-dimensional quantum magnet, *Phys. Rev. Research* **2**, 033459 (2020).
- [33] F.-J. Jiang, M. Nyfeler, S. Chandrasekharan, and U.-J. Wiese, From an antiferromagnet to a valence bond solid: Evidence for a first-order phase transition, *J. Stat. Mech.* **2008** P02009 (2008).
- [34] J. Lou, A. W. Sandvik, and N. Kawashima, Antiferromagnetic to valence-bond-solid transitions in two-dimensional $SU(N)$ Heisenberg models with multispin interactions, *Phys. Rev. B* **80**, 180414(R) (2009).
- [35] A. Nahum, P. Serna, J. T. Chalker, M. Ortuño, and A. M. Somoza, Emergent $SO(5)$ Symmetry at the Néel to Valence-Bond-Solid Transition, *Phys. Rev. Lett.* **115**, 267203 (2015).
- [36] R. G. Melko and R. K. Kaul, Scaling in the Fan of an Unconventional Quantum Critical Point, *Phys. Rev. Lett.* **100**, 017203 (2008).
- [37] R. K. Kaul and R. G. Melko, Large- N estimates of universal amplitudes of the CP^{N-1} theory and comparison with a $S = 1/2$ square-lattice model with competing four-spin interactions, *Phys. Rev. B* **78**, 014417 (2008).
- [38] R. K. Kaul and A. W. Sandvik, Lattice Model for the $SU(N)$ Néel to Valence-Bond Solid Quantum Phase-Transition at Large N , *Phys. Rev. Lett.* **108**, 137201 (2012).
- [39] M. S. Block, R. G. Melko, and R. K. Kaul, Fate of CP^{N-1} Fixed Points with g , *Phys. Rev. Lett.* **111**, 137202 (2013).
- [40] E. Dyer, M. Mezei, S. S. Pufu, and S. Sachdev, Scaling dimensions of monopole operators in the CP^{N_b-1} theory in $2 + 1$ dimensions, *J. High Energy Phys.* **2015**, 37 (2015); *erratum* **2016**, 111 (2016).
- [41] H. Shao, W. Guo, and A. W. Sandvik, Quantum criticality with two length scales, *Science* **352**, 213 (2016).
- [42] N. Ma, G.-Y. Sun, Y.-Z. You, C. Xu, A. Vishwanath, A. W. Sandvik, and Z. Y. Meng, Dynamical signature of fractionalization at a deconfined quantum critical point *Phys. Rev. B* **98**, 174421 (2018).
- [43] A. B. Kuklov, M. Matsumoto, N. V. Prokof'ev, B. V. Svistunov, and M. Troyer, Deconfined Criticality: Generic First-Order Transition in the $SU(2)$ Symmetry Case, *Phys. Rev. Lett.* **101**, 050405 (2008).
- [44] A. B. Kuklov, M. Matsumoto, N.V. Prokof'ev, B.V. Svistunov, M. Troyer, Search for Deconfined Criticality: $SU(2)$ Déjà Vu, arXiv:0805.4334.
- [45] K. Chen, Y. Huang, Y. Deng, A. B. Kuklov, N. V. Prokof'ev, and B. V. Svistunov, Deconfined Criticality Flow in the Heisenberg Model with Ring-Exchange Interactions, *Phys. Rev. Lett.* **110**, 185701 (2013).
- [46] A. W. Sandvik, Continuous Quantum Phase Transition between an Antiferromagnet and a Valence-Bond Solid in Two Dimensions: Evidence for Logarithmic Corrections to Scaling, *Phys. Rev. Lett.* **104**, 177201 (2010).
- [47] C. Wang, A. Nahum, M. A. Metlitski, C. Xu, and T. Senthil, Deconfined Quantum Critical Points: Symmetries and Dualities, *Phys. Rev. X* **7**, 031051 (2017).
- [48] V. Gorbenko, S. Rychkov, and B. Zan, Walking, weak first-order transitions, and complex CFTs, *J. High Energy Phys.* **10**, 108 (2018).
- [49] V. Gorbenko, S. Rychkov, and B. Zan, Walking, Weak first-order transitions, and Complex CFTs II. Two-dimensional Potts model at $Q > 4$, *SciPost Phys.* **5**, 50 (2018).
- [50] R. Ma and C. Wang, A theory of deconfined pseudocriticality, *Phys. Rev. B* **102**, 020407(R) (2020).
- [51] A. Nahum, Note on Wess-Zumino-Witten models and quasi-universality in $2+1$ dimensions, *Phys. Rev. B* **102**, 201116(R) (2020).
- [52] Y.-C. He, J. Rong, and N. Su, Non-Wilson-Fisher kinks of $O(N)$ numerical bootstrap: from the deconfined phase transition to a putative new family of CFTs, *SciPost Phys.* **10**, 115 (2021).
- [53] B. Zhao, J. Takahashi, and A. W. Sandvik, Multicritical Deconfined Quantum Criticality and Lifshitz Point of a Helical Valence-Bond Phase, *Phys. Rev. Lett.* **125**, 257204 (2020).
- [54] D.-C. Lu, C. Xu, and Y.-Z. You, Self-duality protected multi-criticality in deconfined quantum phase transitions, *Phys. Rev. B* **104**, 205142 (2021).

- [55] S. M. Chester and N. Su, Bootstrapping Deconfined Quantum Tricriticality, *Phys. Rev. Lett.* **132**, 111601 (2024).
- [56] M. E. Zayed, et al., *Nat. Phys.* **13**, 962 (2017).
- [57] J. Guo, et al., *Phys. Rev. Lett.* **124**, 206602 (2020).
- [58] Y. Cui et al., Proximate deconfined quantum critical point in $\text{SrCu}_2(\text{BO}_3)_2$, *Science* **380**, 1179 (2023).
- [59] Z. Zhou, L. Hu, W. Zhu, Y.-C. He, The $\text{SO}(5)$ Deconfined Phase Transition under the Fuzzy Sphere Microscope: Approximate Conformal Symmetry, Pseudo-Criticality, and Operator Spectrum, arXiv:2306.16435.
- [60] D. Poland, S. Rychkov, and A. Vichi, The Conformal Bootstrap: Theory, Numerical Techniques, and Applications, *Rev. Mod. Phys.* **91**, 15002 (2019).
- [61] Y. Nakayama and T. Ohtsuki, Necessary Condition for Emergent Symmetry from the Conformal Bootstrap *Phys. Rev. Lett.* **117**, 131601 (2016).
- [62] Z. Li, Bootstrapping conformal QED3 and deconfined quantum critical point, arXiv:1812.09281.
- [63] S. M. Chester and N. Su (private communication).
- [64] A. D. Bruce and A. Aharony, Coupled order parameters, symmetry-breaking irrelevant scaling fields, and tetracritical points, *Phys. Rev. B* **11**, 478 (1975).
- [65] S.-S. Gong, W. Zhu, D. N. Sheng, O. I. Motrunich, and M. P. A. Fisher, Plaquette Ordered Phase and Quantum Phase Diagram in the Spin-1/2 J_1 - J_2 Square Heisenberg Model, *Phys. Rev. Lett.* **113**, 027201 (2014).
- [66] S. Morita, R. Kaneko, and M. Imada, Quantum spin liquid in spin 1/2 J_1 - J_2 Heisenberg model on square lattice: Many-variable variational Monte Carlo study combined with quantum-number projections, *J. Phys. Soc. Jpn.* **84**, 024720 (2015).
- [67] L. Wang and A. W. Sandvik, Critical Level Crossings and Gapless Spin Liquid in the Square-Lattice Spin-1/2 J_1 - J_2 Heisenberg Antiferromagnet, *Phys. Rev. Lett.* **121**, 107202 (2018).
- [68] F. Ferrari and F. Becca, Gapless spin liquid and valence-bond solid in the J_1 - J_2 Heisenberg model on the square lattice: Insights from singlet and triplet excitations, *Phys. Rev. B* **102**, 014417 (2020).
- [69] Y. Nomura and M. Imada, Dirac-Type Nodal Spin Liquid Revealed by Machine Learning, *Phys. Rev. X* **11**, 031034 (2021).
- [70] L. Wang, Y. Zhang, and A. W. Sandvik, Quantum Spin Liquid Phase in the Shastry-Sutherland Model Detected by an Improved Level Spectroscopic Method, *Chin. Phys. Lett.* **39**, 077502 (2022).
- [71] J. Yang, A. W. Sandvik, and L. Wang, Quantum criticality and spin liquid phase in the Shastry-Sutherland model *Phys. Rev. B* **105**, L060409 (2022).
- [72] W.-Y. Liu, J. Hasik, S.-S. Gong, D. Poilblanc, W.-Q. Chen, and Z.-C. Gu, Emergence of Gapless Quantum Spin Liquid from Deconfined Quantum Critical Point, *Phys. Rev. X* **12**, 031039 (2022).
- [73] W.-Y. Liu, D. Poilblanc, S.-S. Gong, W.-Q. Chen, and Z.-C. Gu, Tensor network study of the spin-1/2 square-lattice J_1 - J_2 - J_3 model: incommensurate spiral order, mixed valence-bond solids, and multicritical points, arXiv:2309.13301.
- [74] A. Pelissetto and E. Vicari, Critical Phenomena and Renormalization-Group Theory, *Phys. Rep.* **368**, 549 (2002).
- [75] A. Eichhorn, D. Mesterházy, and M. M. Scherer, Multicritical behavior in models with two competing order parameters, *Phys. Rev. E* **88**, 042141 (2013)
- [76] A. Tanaka and X. Hu, Many-Body Spin Berry Phases Emerging from the π -Flux State: Competition between Antiferromagnetism and the Valence-Bond-Solid State, *Phys. Rev. Lett.* **95**, 036402 (2005).
- [77] J. Lee and S. Sachdev, Wess-Zumino-Witten Terms in Graphene Landau Levels, *Phys. Rev. Lett.* **114**, 226801 (2015)
- [78] Z. Wang, M. P. Zaletel, R. S. K. Mong, and F. F. Assaad, Phases of the (2+1) Dimensional $\text{SO}(5)$ Nonlinear Sigma Model with Topological Term, *Phys. Rev. Lett.* **126**, 045701 (2021).
- [79] B.-B. Chen, X. Zhang, Y. Wang, K. Sun, and Z. Y. Meng, Phases of (2+1)D $\text{SO}(5)$ non-linear sigma model with a topological term on a sphere: multicritical point and disorder phase, arXiv:2307.05307.
- [80] M. E. Fisher, Renormalization group in the theory of critical behavior, *Rev. Mod. Phys.* **46**, 597 (1974).
- [81] A. W. Sandvik and B. Zhao, Consistent scaling exponents at the deconfined quantum-critical point, *Chin. Phys. Lett.* **37**, 057502 (2020).
- [82] D. J. Amit and L. Peliti, On dangerously irrelevant operators, *Ann. Phys. (N.Y.)* **140**, 207 (1982).
- [83] M. Oshikawa, Ordered phase and scaling in Z_n models and the three-state antiferromagnetic Potts model in three dimensions, *Phys. Rev. B* **61**, 3430 (2000).
- [84] J. Lou, A. W. Sandvik, and L. Balents, Emergence of $U(1)$ Symmetry in the 3D XY Model with Z_q Anisotropy, *Phys. Rev. Lett.* **99**, 207203 (2007).
- [85] T. Okubo, K. Oshikawa, H. Watanabe, and N. Kawashima, Scaling relation for dangerously irrelevant symmetry-breaking fields, *Phys. Rev. B* **91**, 174417 (2015).
- [86] F. Léonard and B. Delamotte, Critical Exponents Can Be Different on the Two Sides of a Transition: A Generic Mechanism, *Phys. Rev. Lett.* **115**, 200601 (2015).
- [87] H. Shao, W. Guo, and A. W. Sandvik, Monte Carlo Renormalization Flows in the Space of Relevant and Irrelevant Operators: Application to Three-Dimensional Clock Models, *Phys. Rev. Lett.* **124**, 080602 (2020).
- [88] P. W. Anderson, An Approximate Quantum Theory of the Antiferromagnetic Ground State, *Phys. Rev.* **86**, 694 (1952).
- [89] E. J. Neves and J. F. Peres, *Phys. Lett.* **114A**, 331 (1986).
- [90] F. J. Dyson, E. H. Lieb, and B. Simon, *J. Stat. Phys.* **18**, 335 (1987).
- [91] J. D. Reger and A. P. Young, Monte Carlo simulations of the spin-1/2 Heisenberg antiferromagnet on a square lattice, *Phys. Rev. B* **37**, 5978 (1988).
- [92] S. Liang, Existence of Néel order at $T=0$ in the spin-1/2 antiferromagnetic Heisenberg model on a square lattice, *Phys. Rev. B* **42**, 6555 (1990).
- [93] A. W. Sandvik and H. G. Evertz, Loop updates for variational and projector quantum Monte Carlo simulations in the valence-bond basis, *Phys. Rev. B* **82**, 024407 (2010).
- [94] F.-J. Jiang and U.-J. Wiese, High-precision determination of low-energy effective parameters for a two-dimensional Heisenberg quantum antiferromagnet, *Phys. Rev. B* **83**, 155120 (2011).
- [95] A. V. Chubukov and D. K. Morr, Phase transition, longitudinal spin fluctuations, and scaling in a two-layer

- antiferromagnet, Phys. Rev. B **52**, 3521 (1995).
- [96] A. W. Sandvik and D. J. Scalapino, Order-disorder transition in a two-layer quantum antiferromagnet, Phys. Rev. Lett. **72**, 2777 (1994).
- [97] M. Troyer, H. Kontani, and K. Ueda, Phase Diagram of Depleted Heisenberg Model for CaV_4O_9 , Phys. Rev. Lett. **76**, 3822 (1996).
- [98] M. Matsumoto, C. Yasuda, S. Todo, and H. Takayama, Ground-state phase diagram of quantum Heisenberg antiferromagnets on the anisotropic dimerized square lattice, Phys. Rev. B **65**, 014407 (2001).
- [99] M. Lohöfer, T. Coletta, D. G. Joshi, F. F. Assaad, M. Vojta, S. Wessel, and F. Mila, Dynamical structure factors and excitation modes of the bilayer Heisenberg model, Phys. Rev. B **92**, 245137 (2015).
- [100] N. Ma, P. Weinberg, H. Shao, W. Guo, D.-X. Yao, and A. W. Sandvik, Anomalous Quantum-Critical Scaling Corrections in Two-Dimensional Antiferromagnets Phys. Rev. Lett. **121**, 117202 (2018).
- [101] F. D. M. Haldane, $O(3)$ Nonlinear Model and the Topological Distinction between Integer- and Half-Integer-Spin Antiferromagnets in Two Dimensions, Phys. Rev. Lett. **61**, 1029 (1988).
- [102] G. Murthy and S. Sachdev, Action of hedgehog instantons in the disordered phase of the $(2+1)$ -dimensional CP^{N-1} model, Nucl. Phys. B **344**, 557 (1990).
- [103] Y. Tang and A. W. Sandvik, Method to Characterize Spinons as Emergent Elementary Particles, Phys. Rev. Lett. **107**, 157201 (2011).
- [104] Y. Tang and A. W. Sandvik, Method to Characterize Spinons as Emergent Elementary Particles, Phys. Rev. Lett. **110**, 217213 (2013).
- [105] K. Harada, N. Kawashima, and M. Troyer, Néel and Spin-Peierls Ground States of Two-Dimensional $\text{SU}(N)$ Quantum Antiferromagnets, Phys. Rev. Lett. **90**, 117203 (2003).
- [106] K. S. D. Beach, F. Alet, M. Mambrini, and S. Capponi, $\text{SU}(N)$ Heisenberg model on the square lattice: A continuous- N quantum Monte Carlo study, Phys. Rev. B **80**, 184401 (2009).
- [107] S. Chandrasekharan and U.-J. Wiese, Meron-Cluster Solution of Fermion Sign Problems, Phys. Rev. Lett. **83**, 3116 (1999).
- [108] P. Henelius and A. W. Sandvik, Sign problem in Monte Carlo simulations of frustrated quantum spin systems, Phys. Rev. B **62**, 1102 (2000).
- [109] H. J. Schulz and T. A. L. Ziman, Finite-size scaling for the two-dimensional frustrated quantum Heisenberg antiferromagnet, Europhys. Lett. **18**, 355 (1992).
- [110] T. Einarsson and H. J. Schulz, Direct calculation of the spin stiffness in the J_1 - J_2 Heisenberg antiferromagnet, Phys. Rev. B **51**, 6151 (1995).
- [111] G. Misguich, C. Lhuillier, B. Bernu, and C. Waldtmann, Spin-liquid phase of the multiple-spin exchange Hamiltonian on the triangular lattice, Phys. Rev. B **60**, 1064 (1999).
- [112] M. Mambrini, A. Läuchli, D. Poilblanc, and Frédéric Mila, Plaquette valence-bond crystal in the frustrated Heisenberg quantum antiferromagnet on the square lattice Phys. Rev. B **74**, 144422 (2006)
- [113] R. R. P. Singh, Z. Weihong, C. J. Hamer, and J. Oitmaa, Dimer order with striped correlations in the J_1 - J_2 Heisenberg model, Phys. Rev. B **60**, 7278 (1999).
- [114] S. R. White, Density matrix formulation for quantum renormalization groups, Phys. Rev. Lett. **69**, 2863 (1992).
- [115] Y.-C. He, M. P. Zaletel, M. Oshikawa, and F. Pollmann, Signatures of Dirac cones in a DMRG study of the Kagome Heisenberg model, Phys. Rev. X **7**, 031020 (2017).
- [116] L. Loris Viteritti, R. Rende, A. Parola, S. Goldt, and F. Becca, Transformer Wave Function for the Shastry-Sutherland Model: emergence of a Spin-Liquid Phase, arXiv:2311.16889.
- [117] O. I. Motrunich and A. Vishwanath, Emergent photons and transitions in the $O(3)$ sigma model with hedgehog suppression, Phys. Rev. B **70**, 075104 (2004).
- [118] S. Liang, B. Doucot, and P. W. Anderson, Some New Variational Resonating-Valence-Bond-Type Wave Functions for the Spin- $\frac{1}{2}$ Antiferromagnetic Heisenberg Model on a Square Lattice, Phys. Rev. Lett. **61**, 365 (1988).
- [119] J. Lou and A. W. Sandvik, Variational ground states of two-dimensional antiferromagnets in the valence bond basis, Phys. Rev. B **76**, 104432 (2007).
- [120] K. S. D. Beach, Master equation approach to computing RVB bond amplitudes, Phys. Rev. B **79**, 224431 (2009).
- [121] F. F. Assaad, M. Imada, and D. J. Scalapino, Charge and spin structures of a $d_{x^2-y^2}$ superconductor in the proximity of an antiferromagnetic Mott insulator, Phys. Rev. B **56**, 15001 (1997).
- [122] A. W. Sandvik, S. Daul, R. R. P. Singh, and D. J. Scalapino, Striped Phase in a Quantum XY Model with Ring Exchange, Phys. Rev. Lett. **89**, 247201 (2002).
- [123] I. Affleck and F. D. M. Haldane, Critical theory of quantum spin chains, Phys. Rev. B **36**, 5291 (1987).
- [124] N. Seiberg, T. Senthil, C. Wang, E. Witten, A Duality Web in 2+1 Dimensions and Condensed Matter Physics Ann. Phys. **374**, 395 (2016).
- [125] B. Roberts, S. Jiang, and O. I. Motrunich, Deconfined quantum critical point in one dimension, Phys. Rev. B **99**, 165143 (2019).
- [126] Z. Bi and T. Senthil, An Adventure in Topological Phase Transitions in 3 + 1-D: Non-abelian Deconfined Quantum Criticalities and a Possible Duality, Phys. Rev. X **9**, 021034 (2019).
- [127] H.-C. Jiang, S. A. Kivelson, and D.-H. Lee, Superconducting valence bond fluid in lightly doped eight-leg t-J cylinders, Phys. Rev. B **108**, 054505 (2023).
- [128] M. Christos, Z.-X. Luo, H. Shackleton, Y.-H. Zhang, M. Scheurer, and S. Sachdev, A model of d-wave superconductivity, antiferromagnetism, and charge order on the square lattice, Proc. Natl. Acad. Sci. **120**, e2302701120 (2023).
- [129] M. Christos, H. Shackleton, S. Sachdev, Z.-X. Luo, Deconfined quantum criticality of nodal d-wave superconductivity, Néel order and charge order on the square lattice at half-filling, arXiv:2402.09502.
- [130] K. Harada, T. Suzuki, T. Okubo, H. Matsuo, J. Lou, H. Watanabe, S. Todo, and N. Kawashima, Possibility of deconfined criticality in $\text{SU}(N)$ Heisenberg models at small N , Phys. Rev. B **88**, 220408(R) (2013).
- [131] O. I. Motrunich and A. Vishwanath, Comparative study of Higgs transition in one-component and two-component lattice superconductor models, arXiv:0805.1494
- [132] S. Powell and J. T. Chalker, $\text{SU}(2)$ -Invariant Continuum Theory for an Unconventional Phase Transition in

- a Three-Dimensional Classical Dimer Model, *Phys. Rev. Lett.* **101**, 155702 (2008)
- [133] S. Powell and J. T. Chalker, Classical to quantum mapping for an unconventional phase transition in a three-dimensional classical dimer model, *Phys. Rev. B* **80**, 134413 (2009).
- [134] D. Charrier, F. Alet, and P. Pujol, Gauge Theory Picture of an Ordering Transition in a Dimer Model, *Phys. Rev. Lett.* **101**, 167205 (2008).
- [135] G. Chen, J. Gukelberger, S. Trebst, F. Alet, and L. Balents, Coulomb gas transitions in three-dimensional classical dimer models, *Phys. Rev. B* **80**, 045112 (2009).
- [136] G. J. Sreejith and S. Powell, Critical behavior in the cubic dimer model at nonzero monomer density, *Phys. Rev. B* **89**, 014404 (2014).
- [137] F. F. Assaad and T. Grover, Simple Fermionic Model of Deconfined Phases and Phase Transitions, *Phys. Rev. X* **6**, 041049 (2016).
- [138] S. Gazit, F. F. Assaad, S. Sachdev, A. Vishwanath, and Chong Wang, Confinement transition of Z_2 gauge theories coupled to massless fermions: emergent QCD3 and $SO(5)$ symmetry, *Proc. Natl. Acad. Sci.* **115**, E6987 (2018).
- [139] Z.-X. Li, S.-K. Jian, and H. Yao, Deconfined quantum criticality and emergent $SO(5)$ symmetry in fermionic systems, arXiv:1904.10975.
- [140] A. Götz, S. Beyl, M. Hohenadler, and F. F. Assaad, Valence-bond solid to antiferromagnet transition in the two-dimensional Su-Schrieffer-Heeger model by Langevin dynamics, *Phys. Rev. B* **105**, 085151 (2022).
- [141] T. Sato, Z. Wang, Y. Liu, D. Hou, M. Hohenadler, W. Guo, and F. F. Assaad, Simulation of fermionic and bosonic critical points with emergent $SO(5)$ symmetry, *Phys. Rev. B* **108**, L121111 (2023)
- [142] H. Suwa, A. Sen, and A. W. Sandvik, Level spectroscopy in a two-dimensional quantum magnet: Linearly dispersing spinons at the deconfined quantum critical point, *Phys. Rev. B* **94**, 144416 (2016).
- [143] Z. Deng, L. Liu, W. Guo, and H.Q. Lin, Diagnosing $SO(5)$ Symmetry and First-Order Transition in the $J-Q_3$ Model via Entanglement Entropy, arXiv:2401.12838.
- [144] J. D’Emidio and A. W. Sandvik, Entanglement entropy and deconfined criticality: emergent $SO(5)$ symmetry and proper lattice bipartition, arXiv:2401.14396.
- [145] A. W. Sandvik, *AIP Conf. Proc.* **1297**, 135 (2010).
- [146] H. G. Evertz, G. Lana, and M. Marcu, Cluster algorithm for vertex models, *Phys. Rev. Lett.* **70**, 875 (1993).
- [147] A. W. Sandvik, Stochastic series expansion method with operator-loop update, *Phys. Rev. B* **59**, R11457 (1999).
- [148] H. G. Evertz, The Loop Algorithm, *Adv. Phys.* **52**, 1, (2003).
- [149] K. S. D. Beach and A. W. Sandvik, Some formal results for the valence bond basis, *Nucl. Phys. B* **750**, 142 (2006).
- [150] A. W. Sandvik, Finite-size scaling and boundary effects in two-dimensional valence-bond solids, *Phys. Rev. B* **85**, 134407 (2012).
- [151] A. W. Sandvik, V. N. Kotov, and O. P. Sushkov, Thermodynamics of a Gas of Deconfined Bosonic Spinons in Two Dimensions, *Phys. Rev. Lett.* **106**, 207203 (2011).
- [152] J. D’Emidio, A. A. Eberharter, and A. M. Läuchli, Diagnosing weakly first-order phase transitions by coupling to order parameters, *SciPost Phys.* **15**, 061 (2023).
- [153] J. Zhao, Y.-C. Wang, Z. Yan, M. Cheng, and Z. Y. Meng, Scaling of Entanglement Entropy at Deconfined Quantum Criticality, *Phys. Rev. Lett.* **128**, 010601 (2022).
- [154] Y. D. Liao, G. Pan, W. Jiang, Y. Qi, and Z. Y. Meng, The teaching from entanglement: 2D $SU(2)$ antiferromagnet to valence bond solid deconfined quantum critical points are not conformal, arXiv:2302.11742.
- [155] M. Song, J. Zhao, Z. Y. Meng, C. Xu, and M. Cheng, Extracting subleading corrections in entanglement entropy at quantum phase transitions, arXiv:2312.13498.
- [156] M. Song, J. Zhao, L. Janssen, M. M. Scherer, and Z. Y. Meng, Deconfined quantum criticality lost, arXiv:2307.02547.
- [157] H. Shao and A. W. Sandvik, Progress on stochastic analytic continuation of quantum Monte Carlo data, *Phys. Rep.* **1003**, 1 (2023).
- [158] R. Rattazzi, V. S. Rychkov, E. Tonni, and Alessandro Vichi, Bounding scalar operator dimensions in 4D CFT, *J. High. Ener. Phys.* **2008**, 31 (2008).
- [159] F. Kos, D. Poland, D. Simmons-Duffin, and A. Vichi, Precision Islands in the Ising and $O(N)$ Models, *J. High. Ener. Phys.* **2016**, 36, (2016).
- [160] E. Buffenoir and S. Wallon, The Correlation Length of the Potts Model at the First-Order Transition Point, *J. Phys. A* **26**, 3045 (1993).
- [161] H. Ma and Y.-C. He, Shadow of complex fixed point: Approximate conformality of $Q > 4$ Potts model, *Phys. Rev. B* **99**, 195130 (2019).
- [162] F. D. M. Haldane, Fractional quantization of the hall effect: A hierarchy of incompressible quantum uid states, *Phys. Rev. Lett.* **51**, 605 (1983).
- [163] W. Zhu, C. Han, E. Huffman, J. S. Hofmann, and Y.-C. He, Uncovering Conformal Symmetry in the 3D Ising Transition: State-Operator Correspondence from a Quantum Fuzzy Sphere Regularization, *Phys. Rev. X* **13**, 021009 (2023).
- [164] M. Hasenbusch, Finite size scaling study of lattice models in the three-dimensional Ising universality class, *Phys. Rev. B* **82**, 174433 (2010).
- [165] A. W. Sandvik and R. G. Melko, Ground-state phases and quantum phase transitions in a two-dimensional spin-1/2 XY model with four-spin interactions, *Annals of Physics* **321**, 1651 (2006).
- [166] E. Domany and M. E. Fisher, Equations of state for bicritical points. III. Cubic anisotropy and tetracriticality, *Phys. Rev. B* **15**, 3510 (1975).
- [167] S. Pujari, K. Damle, and F. Alet, Néel-State to Valence-Bond-Solid Transition on the Honeycomb Lattice: Evidence for Deconfined Criticality *Phys. Rev. Lett.* **111**, 087203 (2013).
- [168] S. Pujari, F. Alet, and K. Damle, Transitions to valence-bond solid order in a honeycomb lattice antiferromagnet, *Phys. Rev. B* **91**, 104411 (2015).
- [169] Y. Tang, A. W. Sandvik, and C. L. Henley, Properties of resonating-valence-bond spin liquids and critical dimer models, *Phys. Rev. B* **84**, 174427 (2011).
- [170] A. W. Sandvik, A generalization of Handscomb’s quantum Monte Carlo scheme—Application to the 1-D Hubbard model, *J. Phys. A* **25**, 3667 (1992).
- [171] A. W. Sandvik, R. R. P. Singh, and D. K. Campbell, Quantum Monte Carlo in the interaction representation—Application to a spin-Peierls model, *Phys. Rev. B* **56**, 14510 (1997).
- [172] A. Sen and A. W. Sandvik, Example of a first-order

- Néel to valence-bond-solid transition in two dimensions, *Phys. Rev. B* **82**, 174428 (2010).
- [173] B. Zhao, J. Takahashi, and A. W. Sandvik, Tunable deconfined quantum criticality and interplay of different valence-bond solid phases, *Chin. Phys. B* **29**, 057506 (2020).
- [174] N. Ma, Y.-Z. You, and Z. Y. Meng, Role of Noether's Theorem at the Deconfined Quantum Critical Point, *Phys. Rev. Lett.* **122**, 175701 (2019),
- [175] J. T. Chalker, Spin liquids and frustrated magnetism, in *Topological Aspects of Condensed Matter Physics: Lecture Notes of the Les Houches Summer School: Volume 103*, edited by Claudio Chamon et al. (Oxford University Press, 2017).
- [176] P. Patil, I. Dasgupta, and K. Damle, Resonating valence-bond physics on the honeycomb lattice, *Phys. Rev. B* **90**, 245121 (2014).
- [177] H. Shao, W. Guo, and A. W. Sandvik, Emergent topological excitations in a two-dimensional quantum spin system, *Phys. Rev. B* **91**, 094426 (2015)
- [178] P. Patil, H. Shao, and A. W. Sandvik, Unconventional $U(1)$ to Z_q crossover in quantum and classical q-state clock models, *Phys. Rev. B* **103**, 054418 (2021).
- [179] M. E. Fisher and M. B. Barber, Scaling Theory for Finite-Size Effects in the Critical Region, *Phys. Rev. Lett.* **28**, 1516 (1972).
- [180] K. Binder, Critical Properties from Monte Carlo Coarse Graining and Renormalization, *Phys. Rev. Lett.* **47**, 693 (1981).
- [181] M. N. Barber, in *Phase Transitions and Critical Phenomena*, edited by C. Domb and J. Lebowitz, Vol. 8 (Academic, London, 1983).
- [182] K. Binder, Finite size scaling analysis of ising model block distribution functions, *Z. Phys. B* **43**, 119 (1981).
- [183] K. Vollmayr, J. D. Reger, M. Scheucher, and K. Binder, Finite size effects at thermally-driven first order phase transitions: A phenomenological theory of the order parameter distribution, *Z. Phys. B* **91**, 113 (1993).
- [184] S. Iino, S. Morita, N. Kawashima, and A. W. Sandvik, Detecting Signals of Weakly First-order Phase Transitions in Two-dimensional Potts Models, *J. Phys. Soc. Jpn.* **88**, 034006 (2019).
- [185] A. W. Sandvik, A generalization of Handscomb's quantum Monte Carlo scheme-application to the 1D Hubbard model, *J. Phys. A: Math. General*, **25**, 3667 (1992).
- [186] E. L. Pollock and D. M. Ceperley, Path-integral computation of superfluid densities, *Phys. Rev. B* **36**, 8343 (1987).
- [187] A. W. Sandvik, Finite-size scaling of the ground-state parameters of the two-dimensional Heisenberg model, *Phys. Rev. B* **56**, 11678 (1997).
- [188] Y. Q. Qin, Y.-Y. He, Y.-Z. You, Z.-Y. Lu, A. Sen, A. W. Sandvik, C. Xu, and Z. Y. Meng, Duality between the Deconfined Quantum-Critical Point and the Bosonic Topological Transition, *Phys. Rev. X* **7**, 031052 (2017)
- [189] J. Y. Lee, Y.-Z. You, S. Sachdev, and A. Vishwanath, Signatures of a Deconfined Phase Transition on the Shastry-Sutherland Lattice: Applications to Quantum Critical $\text{SrCu}_2(\text{BO}_3)_2$, *Phys. Rev. X* **9**, 041037 (2019).